Université d'Ottawa · University of Ottawa

PERMISSION DE REPRODUIRE ET DE DISTRIBUER LA THÈSE

PERMISSION TO REPRODUCE AND DISTRIBUTE THE THESIS

NOM DE L'AUTEUR / NAME OF AUTHOR:	Feras HAMAD
ADRESSE POSTALE / MAILING ADDRESS:	509 - 42 Bédard Street Hull QC J8Y 6A1
GRADE / DEGREE:	**ANNÉE D'OBTENTION / YEAR GRANTED**
Ph.D.(Chemical Engineering)	2003
TITRE DE LA THÈSE / TITLE OF THESIS:	
Formation, Characterization, and Performance Testing of Poly (Phenylene Oxide) and Modified Poly (Phenylene Oxide) Membranes for Gas Separation	

L'auteur permet, par la présente, la consultation et le prêt de cette thèse en conformité avec les règlements établis par le bibliothécaire en chef de l'Université d'Ottawa. L'auteur autorise aussi l'Université d'Ottawa, ses successeurs et cessionnaires, à reproduire cet exemplaire par photograhie ou photocopie pour fins de prêt ou de vente au prix coûtant aux bibliothèques ou aux chercheurs qui en feront la demande.

Les droits de publication par tout autre moyen et pour vente au public demeureront la propriété de l'auteur de la thèse sous réserve des règlements de l'Université d'Ottawa en matière de publication de thèses.

The author hereby permits the consultation and the lending of this thesis pursuant to the regulations established by the Chief Librarian of the University of Ottawa. The author also authorizes the University of Ottawa, its successors and assignees, to make reproductions of this copy by photographic means or by photocopying and to lend or sell such reproductions at cost to libraries and to scholars requesting them.

The right to publish the thesis by other means and to sell it to the public is reserved to the author, subject to the regulations of the University of Ottawa governing the publication of theses.

N.B. LE MASCULIN COMPREND ÉGALEMENT LE FÉMININ

29/05/2003
DATE

Feras A Hamad
(AUTEUR) SIGNATURE (AUTHOR)

Université d'Ottawa · University of Ottawa

Université d'Ottawa · University of Ottawa

FACULTÉ DES ÉTUDES SUPÉRIEURES ET POSTDOCTORALES

FACULTY OF GRADUATE AND POSTDOCTORAL STUDIES

HAMAD, Feras

AUTEUR DE LA THÈSE - AUTHOR OF THESIS

Ph. D. (Chemical Engineering)

GRADE - DEGREE

Chemical Engineering

FACULTÉ, ÉCOLE, DÉPARTEMENT - FACULTY, SCHOOL, DEPARTMENT

TITRE DE LA THÈSE - TITLE OF THE THESIS

Formation, Characterization, and Performance Testing of Poly (Phenylene Oxide) and Modified Poly (Phenylene Oxide) Membranes for Gas Separation

T. Matsuura

DIRECTEUR DE LA THÈSE - THESIS SUPERVISOR

EXAMINATEURS DE LA THÈSE - THESIS EXAMINERS

J. Dickson

Z. Duvnjak

A. Macchi

J. Thibault

J.-M. De Koninck, Ph.D.

LE DOYEN DE LA FACULTÉ DES ÉTUDES SUPÉRIEURES ET POSTDOCTORALES

SIGNATURE

DEAN OF THE FACULTY OF GRADUATE AND POSTDOCTORAL STUDIES

Formation, Characterization, and Performance Testing of Poly (Phenylene Oxide) and Modified Poly (Phenylene Oxide) Membranes for Gas Separation

by

Feras Hamad

A thesis submitted to the Faculty of Graduate and Postdoctoral Studies
in partial fulfillment of the requirements for the degree of
Doctor of Philosophy
in the Department of Chemical Engineering
University of Ottawa

June 27, 2003.

Abstract

This work was focused on gas separation membranes made from high molecular weight poly (2,6-dimethyl-1,4-phenyl oxide) (PPO) and its chemically modified derivatives. The molecular weight of the polymer was calculated to be 316400 g/mol corresponding to 1.57 dL/g intrinsic viscosity in chloroform. The research objectives are to (i) study the effect of chemical modification of PPO on the gas separation performance of membranes made from the resulting polymers; (ii) study and compare the formation of dense and composite membranes based on PPO, and correlate the formation of these membranes to their performance and morphology; (iii) put forward a model to predict and evaluate the performance of composite membranes based on the intrinsic properties of the individual polymeric layers forming the composite membrane. The objectives of the research covered the following topics of membrane science: (i) material development and modification, (ii) membrane-gas penetrant interaction, (iii) membrane morphology and formation, and (iv) mathematical modeling of transport phenomena in porous and thin film composite membranes. The gas separation performance of the membranes was tested based on the permeation of CO_2, CH_4, O_2, and N_2 gases. The membrane selectivity was mainly judged by CO_2/CH_4 and O_2/N_2 permeability ratios. These gases are of relevant industrial and/or environmental interest.

The chemical modification of PPO was carried out via sulfonation, bromination, and simultaneous sulfonation and bromination. The gas permeability in 20% and 37.4% brominated PPO membranes increased slightly, while it increased significantly in 60% brominated PPO, in comparison to that of the parent polymer. The permeability ratio of PPO was maintained in the resulting brominated PPO. Infrared study showed that bromination resulted in stiffening the torsional motion of the phenyl ring around the ether link, and at moderate and high bromination levels, the interference of the bromine group

with neighboring methyl groups became significant. This conformed to the postulation that high bromination level is needed to produce significant increase in the length of a diffusional jump segment, hence the diffusional jumps rate.

The effect of sulfonation of PPO, and the effect of replacing the proton of the sulfonic groups with: mono-valent, di-valent, and tri-valent metal cations, was investigated. Generally, membranes made from sulfonated PPO, in either hydrogen or metal cation form, had lower gas permeability, but higher permeability ratios, when compared with PPO membranes performance. Altering the metal cation form would alter: hindrance effects due to the cation size, the SO_3-metal group polarity due to the metal electronegativity, and the cross linking forces. Therefore, the performance of sulfonated PPO membranes, in the different cation forms, was found to correlate with the location of the metal in the universal periodic table of chemical elements.

The main effects of simultaneous sulfonation and bromination of PPO were to: (i) increase the gas permeability, while decreasing the permeability ratio, in comparison to sulfonated-only PPO; (ii) decrease the gas permeability, while increasing the permeability ratio, in comparison to brominated-only PPO. An interesting trend noticed in the permeability of sulfonated brominated PPO membranes, with increasing the degree of bromination while maintaining the same degree of sulfonation, was that the gas permeability would pass through a minimum at moderate bromination levels.

The effects produced by sulfonation and bromination are believed to be the direct result of the manipulation in the polymer backbone stiffness, membrane packing and free volume fraction, and gas membrane interaction.

Infrared study showed that PPO molecules interact physically with gaseous hydrocarbons permeating through the membrane. Gaseous CH_4, C_2H_6, C_2H_4, and C_2H_2 were used to study the effect of different hydrocarbon groups. CH_4 and C_2H_2 affected the PPO IR spectra in the same position. C_2H_6 and C_2H_4 affected the PPO IR spectra in the same

position, however, different to the former pair. The interaction between the gaseous hydrocarbons and PPO membrane molecules was found to be reversible and dependent on the molecular weight of PPO and the boiling point of the solvent used to prepare the membrane. The interaction between PPO and CH_4 showed to follow dynamics similar to that of a first order dynamic system.

Composite membranes prepared by coating PPO on top of porous polyethersulfone (PES) ultrafiltration (UF) membranes (Osmonics-HO51), showed enhanced gas separation factor and gas permeability ratio for CO_2/CH_4 system, with a slight drop in the permeability of CO_2, in comparison to the homogeneous PPO membranes. It is postulated that the coated layer polymer adjacent to the support membrane is highly densified and compacted. This was the result of the migration of the solvent toward the support, and the partial draw of the solvent into the support membrane.

The gas transport through thin film composite (TFC) PPO membranes, prepared by coating PPO on top of PES UF membrane (Osmonics-HW31), was simulated based on the intrinsic transport properties of the gases in the support membrane and the coating layer polymers, and the morphological parameters that characterized the support membrane, which were the total number of pores, the pores size distribution, and the dense layer thickness. This study compared the experimental performance of the TFC membranes with the simulation results based on three scenarios: (i) the support membrane pores were totally plugged by the coated polymer, (ii) partially plugged, and (iii) totally unplugged. The experimental TFC membranes performance was presented best by the partially plugged pores model at low and medium PPO concentration (less than 0.5% in the coating solution). On the other hand, the totally unplugged model presented best the experimental TFC membranes performance at higher PPO concentration in coating solution (1% and more).

Résumé

Ce travail s'est concentré sur des membranes de séparation de gaz faites à partir du poids poly (oxyde du 2.6-diméthylique-1.4-phényle) (PPO) et de ses dérivés chimiquement modifiés. Le poids moléculaire du polymère a été estimé à 316400 g/mol correspondant à 1.57 dL/g viscosité intrinsèque dans le chloroforme. La recherche objective est de (i) étudier de modification chimique du PPO sur la performance de séparation des gaz pour les membranes fabriquées du Polymère résultant ; (i) étudier et comparer la formation des membranes denses et composées basées sur du PPO, et lier réciproquement la formation de ces membranes à leur performances et morphologies ; (iii) proposer un model pour prédire et évaluer la performance des membranes composées selon les propriétés intrinsèques des couches polymères qui forment les membranes composées. Les objectifs de la recherche ont couvert les champs suivants de la science des membranes: (i) développement et modification des matériaux, (ii) interaction pénétrante de membrane-gaz, (iii) morphologie et formation des membranes, et (iv) modélisation mathématique des phénomènes de transport dans des membranes composées de couche poreuse et mince. L'efficacité de séparation des gaz par les membranes a été évaluée en mesurant la perméation des gaz CO2, CH4, O2, et N2. Ces gaz ont un intérêt industriel et/ou environnemental important.

La modification chimique du PPO a été effectuée par l'intermédiaire de la sulfonation, de la bromination, et de la combinaison des deux. La perméabilité des gaz dans les membranes bromées de PPO de 20% et de 37,4% a augmenté, cependant, la perméabilité des gaz a augmenté dramatiquement au degré de bromination à 60%, par rapport au polymère parent. Le rapport de perméabilité a été maintenu dans le PPO bromé résultant. L'étude infrarouge a prouvé que la bromination a raidi le mouvement de torsion de l'anneau

phénylique autour du lien d'éther, et l'interférence du groupe de brome avec les groupes méthyliques voisins est devenue significative aux niveaux modérés et élevés de bromination. Ceci se conforme à l'hypothèse que un niveau élevé de bromination est nécessaire pour produire une augmentation significative de la longueur d'un segment de sursaut diffusionniste, par conséquent le taux du sursaut diffusionniste.

L'effet de la sulfonation du PPO, et l'effet de remplacer le proton des groupes sulfoniques par: des cations de métal monovalents, bivalents, et trivalents, ont été étudiés. D'une façon générale, les membranes faites à partir de PPO transformé en acide sulfone, dans l'hydrogène ou forme de cation de métal, ont eu une perméabilité inférieure de gaz, mais les rapports plus élevés de perméabilité, en comparaison avec le comportement des membranes du PPO. Le changement de la forme de cation de métal changerait: les effets d'obstacle dus à la taille de cation, la polarité de groupe du métal SO_3 due à l'électronégativité du métal, et les forces de liaison. Par conséquent, l'efficacité des membranes du PPO transformé en acide sulfone, sous les différentes formes de cation, s'est avérée liée réciproquement avec l'endroit du métal dans la table périodique universelle des éléments chimiques.

Les effets principaux de la sulfonation et de la bromination simultanées du PPO étaient de: (i) augmenter la perméabilité du gaz, tout en diminuant le rapport de perméabilité, par rapport à PPO seulement transformé en acide sulfone; (ii) diminuer la perméabilité du gaz, tout en augmentant le rapport de perméabilité, par rapport à PPO bromé-seulement. Une tendance intéressante dans la perméabilité des membranes du PPO brominées transformé en acide sulfone a été notée avec l'augmentation du degré de bromination tout en maintenant le même degré de sulfonation, était que la perméabilité du gaz traverserait un

minimum aux niveaux modérés de bromination.

Les effets produits par la sulfonation et la bromation serait le résultat direct de la manipulation dans la rigidité de l'épine dorsale du polymère, l'emballage de la membrane et la fraction libre de volume, et l'interaction de la membrane de gaz.

L'étude infrarouge a prouvé que les molécules de PPO agissent les uns sur les autres physiquement avec des hydrocarbures gazeux qui ont passé à travers la membrane. Les gaz CH4, C2H6, C2H4, et C2H2 ont été employés pour ressembler à différents groupes d'hydrocarbure. CH4 et C2H2 ont affecté les spectres infrarouges de PPO en même position. C2H6 et C2H4 ont affecté les spectres IRS de PPO dans la même position, toutefois, différemment de la paire antérieure. L'interaction entre les molécules gazeuses d'hydrocarbure et de membrane de PPO est avérée réversible et dépendante du pois moléculaire du PPO et du point d'ébullition de dissolvant employé pour préparer la membrane. L'interaction entre PPO et CH_4 semble suivre une dynamique semblable à celle d'un système dynamique du premier ordre.

Les membranes composées préparées en ajoutant une fine couche de PPO sur les membranes d'ultrafiltration (UF) de l'éthersulfone poly poreux (PES) ont montré un facteur de séparation du gaz et du rapport de perméabilité au gaz pour le système CO_2/CH_4, et une légère baisse dans la perméabilité au CO_2, e comparaison avec les membranes homogènes de PPO. On estime que le polymère enduit de couche adjacent à la membrane de soutien est fortement densifié et compact. C'était le résultat de la migration du dissolvant vers le support, et l'aspiration partielle du dissolvant dans la membrane de support.

Le transport du gaz à travers les membranes PPO de composite de couche mince (TFC), préparées en enduisant PPO sur la membrane de PES UF (Osmonics-HW31), a été simulé

sachant les propriétés intrinsèques de transport des gaz dans la membrane de support et les polymères de couche enduisant, et les paramètres morphologiques qui caractérisent la membrane de support, qui sont le nombre total de pores, la distribution de grandeurs de pores, et l'épaisseur de la couche dense. Cette étude a comparé la performance expérimentale des membranes de TFC aux résultats de simulation selon trois scénarios: (i) branchement complet des pores de membrane de soutien par le polymère enduisant, (ii) branchement partiel, et (iii) aucun branchement des pores de membrane de soutien. Le comportement des membranes expérimental de TFC a été présenté mieux par le modèle branchement partiel de pores à basse et moyenne concentration de PPO (moins de 0,5% dans la solution enduisant). D'autre part, à une concentration plus élevée de PPO dans la solution enduisant (1% et plus).

Acknowledgements

I would like to express my great appreciation and gratitude to Prof. T. Matsuura for his guidance, supervision, and support.

I would like to express my deepest gratitude and appreciation to my wife, Kholoud Ismail, my parents and the family, for their encouragement and endless support.

I would like to thank all of IMRI colleagues, the chemical engineering department, and the workshop staff, for their assistance and cooperation.

I would like to extend my appreciation to Mr. Fadi Albatal for preparing the French abstract. Special thanks go to Dr. K.C. Khulbe and Mr. P. Harlick for their continuous encouragement.

Finally, the author would like to acknowledge the financial support of Osmonics Inc.

Statement of Contribution of Collaborators

The author would like to acknowledge the contribution of Dr. K.C. Khulbe to part of the scientific material presented in this thesis. In Chapters 3 and 5, Dr. Khulbe assisted in the IR frequency assignment for PPO and brominated PPO bands and contributed to the discussion presented within. Three papers were published based on the material presented in Chapters 3 and 5. Dr. Khulbe assisted in taking the AFM images appearing in Chapter 7.

List of Tables

List of Figures

Chapter 1

Introduction

Over the past decades, membranes have entered many territories that were dominated by more traditional separation technologies such as adsorption, absorption and cryogenic distillation. However, in many cases, hybrid membrane processes with other traditional processes are still found as an attractive choice. This fast expansion of membrane applications is attributed to many reasons in which the economic consideration is a determinant factor, and as well, to the increasing environmental awareness in the world that the need for a cleaner industry is essential for the well being of the globe. Having membranes as the core of the process or being a part of a hybrid process serves both reasons.

1.1 Membrane Gas Separation

Generally, gas separation using membranes can be performed based on one of the following mechanisms [1]:

1. **Porous flow**: where separation relies on the size of the membrane pores relative to the mean free path of the penetrant molecules. Knudsen flow dominates when the ratio of the pore radius to the mean free path of the gas is less than 0.05. When this size ratio is between 0.05 and 50, slip flow mechanism dominates. In both mechanisms, gas selectivity is inversely proportional to the square root of the molecular weight ratio of the two gases. Viscous flow, where no separation is achieved, occurs when the ratio of pore radius to the mean free path of the gas molecules is greater than 50 [1,2].
2. **Solution-diffusion**: this is the basic mechanism that prevails in selective layers of commercial membranes. Effective solution-diffusion membranes have no continuous passages but the gas transport relies on thermally agitated motion of chain segments

comprising the polymer matrix to generate penetrant-scale transient gaps in the matrix, thereby allowing diffusion of penetrants from the upstream face of the membrane to the downstream face of the membrane. Penetrants undergo random diffusional jumps that are eventually directed to the downstream as the result of concentration gradient [3].

The rate of permeation of a gas through a membrane is simply described by the following equation,

$$Q_A = \frac{p_A}{\delta} \Delta P_A \qquad (1)$$

Where Q_A is the gas flux for gas A, p_A is the permeability of the membrane for gas A, δ is the membrane thickness, and ΔP_A is the transmembrane partial pressure difference of gas A. Since it is difficult to know δ for many practical membranes, p_A/δ is called permeance and used as a combined form. Units of gas permeability, p_A, and gas permeance p_A/δ, are Barrer and GPU, respectively, where:

$$1\ \text{GPU} = 10^{-6} \frac{\text{cm}^3(\text{STP})}{\text{cm}^2\ \text{s cmHg}} = 3.345\times10^{-10} \frac{\text{mol}}{\text{m}^2\ \text{s Pa}} = 7.50\times10^{-12} \frac{\text{m}^3}{\text{m}^2\ \text{s Pa}}$$

$$1\ \text{Barrer} = 10^{-10} \frac{\text{cm}^3(\text{STP})\ \text{cm}}{\text{cm}^2\ \text{s cmHg}} = 3.345\times10^{-16} \frac{\text{mol m}}{\text{m}^2\ \text{s Pa}} = 7.50\times10^{-18} \frac{\text{m}^3\ \text{m}}{\text{m}^2\ \text{s Pa}}$$

The membrane permeability of a gas can be further factored,

$$p_A = S_A D_A \qquad (2)$$

where S_A and D_A are the solubility (m^3(STP)/(Pa m^3)) and the diffusivity (m^2/s) of gas A in the polymeric membrane matrix. The ideal selectivity of a membrane, or the permselectivity, is defined as the permeability ratio of two gases (A and B):

$$\alpha_{AB} = {p_A}/{p_B} \tag{3}$$

By definition, the separation factor of two gases is as follows,

$$F_{AB} = \left(\frac{X_A}{X_B}\right)_p \Big/ \left(\frac{X_A}{X_B}\right)_f \tag{4}$$

where X denotes the mole fraction and subscripts p and f denote the permeate and feed side, respectively. By inserting equations (1) and (2) into equation (4), the separation factor can be rewritten as follows,

$$F_{AB} = \left[\frac{D_A}{D_B}\right]\left[\frac{S_A}{S_B}\right]\left[\frac{\left(\Delta P_A / P_{A_f}\right)}{\left(\Delta P_B / P_{B_f}\right)}\right] \tag{5}$$

where ΔP_A and ΔP_B are the transmembrane partial pressures differences of gas A and gas B, respectively; P_{Af} and P_{Bf} are the partial pressures of gas A and B in the feed side.

Equation (5) relates the selectivity of a membrane to kinetic and thermodynamic parameters as well as to operating parameters. In actual application, the ideal selectivity, where the pressures term is unity, is very difficult to obtain unless the downstream pressure is maintained at zero absolute pressure. The diffusivities ratio is called the mobility selectivity while the solubilities ratio is called the solubility selectivity.

The trend in material development for better gas separation performance is mainly toward improving the properties of existing polymers, which is concerned with chemical and/or physical modification of the polymers to favor the transport properties of the gases of interest. Solubility selectivity is largely determined by the relative condensability of the gases. The critical temperature of gases is a strong indication for their condensability and their relative solubility. For example, O_2 and N_2 have a critical temperature of 154 K and

126 K respectively, which indicates that O_2 is more condensable and hence is more soluble than N_2. Typical range of solubility selectivity of O_2/N_2 system is 1.35-1.89 [4]. This is not sufficient for effective separation without the contribution of mobility selectivity. For CO_2/CH_4 systems, solubility selectivity is typically in the range 3-4 at ambient temperature. Mobility selectivity is determined by the ability of gas penetrants to diffuse through the polymeric membrane matrix and perform diffusional jumps. Diffusion and diffusional jumps are two processes occurring in series and controlled by the diffusional jumps where a penetrant needs to jump into a different intersegmental gap when it is faced by a blocking polymeric segment or other sterric factors that can not be overcome. Observed rates of diffusional jumps are lower by three orders of magnitude than diffusion processes. The diffusion path and the diffusional jump opening size between intersegmental gaps impose the sieving effect of the membrane. Mobility selectivity in some instances is difficult to increase when penetrant sizes are similar as in the case of O_2/N_2 system, where the difference in their sizes is only 0.18 ^{o}A. As a result, mobility selectivity can not become larger than 5. While, on the other hand, for CO_2/CH_4 system mobility selectivity can reach as high as 20. Table 1.1 summarizes sieving diameter for some gases [1,2]. Generally, the selectivity of super critical gases is dominated by their mobility selectivity.

Table 1.1: Kinetic (sieving) diameters of some gases.

Gas	CO_2	CH_4	O_2	N_2
Kinetic diameter (^{o}A)	3.3	3.8	3.46	3.64

Although there are no truly quantitative relationships to guide membrane structure-performance optimization, simple rules have emerged that offer currently the most

reliable guide for understanding membrane structure-performance relation. One of such is "changing the structure within a family of polymers, inhibiting intersegmental packing, while simultaneously hindering the backbone mobility tends to produce a desirable trade off between productivity and permselectivity" [1,5]. Increasing packing inhibition is detected by increased free volume fraction in the polymer matrix not occupied by the electron clouds comprising the atoms of the polymer. Introducing polar groups is useful for inducing intersegmental motion inhibition.

In the following, the properties of poly (phenylene oxide), PPO, as well as the performance of membranes which are made from chemically modified PPO polymers are briefly presented to give some insight about the motivation of this work.

1.2 PPO Polymer and PPO Membranes

Poly (2,6-dimethyl-1,4-phenylene oxide) or Poly (2,6-dimethyl-1,4-phenyl ether) (PPO) is produced by oxidative coupling of 2,6-dimethyl phenol at positions 1 and 4 according to the following reaction.

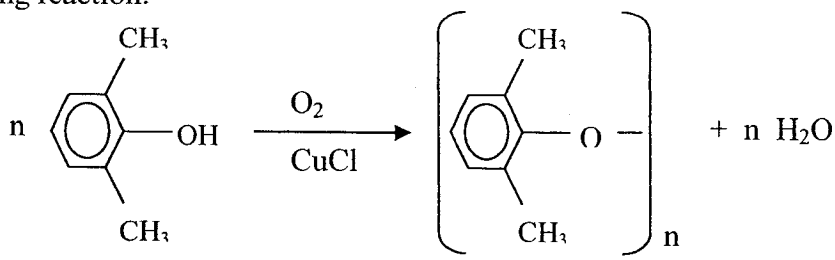

PPO possesses a linear structure with very low transition temperature assigned to the rotational motion of its phenyl ring. This has given PPO polymer excellent mechanical properties at impact and ductility at low temperatures [6]. PPO has the highest gas permeability among the high glass transition temperature aromatic polymers [7]. This stems from the large diffusion coefficients. The presence of ether linkages and the

absence of polar groups suppress chain packing and densification. The methyl groups attached on both sides of phenyl ring hinder the free rotation of the phenyl ring resulting in moderate selectivity of PPO membranes. Permeability of CO_2 and permselectivity of CO_2/CH_4 published in some works are listed in Table 1.2.

Table 1.2: PPO permeability data.

CO_2 Permeability (Barrer)	Permeability ratio CO_2/CH_4	Reference
64.0	16.4	[7]
50	17	[8]
42	15.1	[9]
45	15	[10]

The scatter in CO_2 permeability data is attributed to the lack of details about the degree of crystallinity of PPO membranes [11]. Even though PPO permeation to gases is high, permselectivity is considered a more important property a membrane should possess since permeability deficiency may be overcome by manufacturing thin defect free layers of membranes [11]. Therefore, PPO as a parent polymer is an attractive option for further chemical modification.

1.3 Chemically Modified PPO Membranes

Chemical modification of PPO is accomplished by introducing different groups to the backbone of the phenyl ring or by attaching to the methyl group on either side of the phenyl ring [7-12]. Percec and Li [7] modified PPO via bromination and sulfonylation. A complete substitution of the phenyl ring upon sulfonylation was not possible as a result of decreasing nucleophilicity of the unsubstituted position due to the strong electron withdrawing character of the sulfonyl group. Therefore disubstitution of sulfonyl group on the same phenyl ring was not detected. As well, sulfonylation was limited to 80% of

the phenyl rings because of the steric interference of neighboring substituted phenyl rings [13]. Percec and Li [7] used a gas mixture of CO_2:CH_4:N_2 in molar proportions 3.1:33.6:63.3, to evaluate the performance of the sulfonylated and brominated PPO membranes. The attachment of benzenesulfonyl, which gave the best performance among all bulky sulfonyl groups, resulted in almost 55% increase in CO_2 permeability over that of PPO, which was 64 Barrer, and almost 67% increase in the CO_2/CH_4 separation factor over that of PPO, which was 16.4. When -SO_3H group was attached to the backbone of the PPO polymer, the separation factor increased by 100% while CO_2 permeability dropped by a factor of three. This was attributed to the role of hydrogen bonding in hindering segmental mobility, which was induced by the attachment of the sulfonic group, that as well induced discrimination against methane as a result of increasing the polymer polarity [7]. Bromination of PPO showed no significant effect on permeability or separation factor at bromination degrees less than 46%. At 46% bromination level and higher, permeation of CO_2 increased without sacrificing the separation efficiency of PPO. At 100% bromination level, CO_2 permeability was higher by 250% over that of PPO with only 25% increase in separation factor [7]. Almost the exact performance was obtained by Story and Koros [9] who reported the same enhancement of CO_2 permeability without sacrificing the CO_2/CH_4 selectivity upon 100% PPO bromination. The large increase in diffusivity of CO_2 was attributed to the steric hindrance imparted by the bromine substituents that resulted in increasing the segment length involved in torsional motions. The increase in the glass transition temperature was indicative of the segment mobility hindrance, while the increase in the diffusion rate and the increased stiffness of the segments indicated the enhancement of the rate of diffusional jumps as a result of

increased diffusional jump length. Story and Koros [9] referred to the data of Chern et al. regarding the diffusivity in 36% brominated PPO that was not different from PPO [14]. In order to have a significant increase in the rate of diffusion by brominating PPO, the degree of bromination should be high enough so that it stiffens the chains to the point that more than one repeat unit becomes involved in the chain rotation. The decrease in d-spacing and free volume resulted from bromination is offset by an increase in segmental diffusional jump. The same conclusion can be drawn from the results of Percec and Li [7], where permeability of brominated PPO started to increase at bromination levels higher than 46%. Chern et al. [8] also observed a trend that at levels of bromination higher than 36.0%, diffusivities of CO_2 and CH_4 gases were enhanced and the resultant permeability at 106% bromination level was double that of PPO while the overall permselectivity was maintained. They related their results to the bromine group that hindered the rotational motion of phenyl rings. The conclusion of Story and Koros [9] was in accordance with the results obtained by Chern et al [8].

Carboxylation of the methyl group on either side of the phenyl ring resulted in more dense membranes without changing the d-spacing, which indicated that the added carboxylic groups were occupying a part of the intersegmental spacing. The addition of carboxylic groups resulted in an increase in the solubility of CO_2 and as well the CO_2/CH_4 solubility selectivity. On the other hand, diffusivity of CO_2 and CH_4 dropped due to the presence of additional carboxylic groups in the intersegmental spacing [7].

Fu et al. [12] studied some of the properties of sulfonated PPO (SPPO). Density of SPPO polymers increased almost linearly with the degree of sulfonation. SPPO polymer was soluble in polar solvents in which PPO did not dissolve. PPO was thermally stable. First

decomposition temperature was noticed at 470°C upon heating in thermal gravimetric analysis (TGA) [12]. Three stages or ranges were observed in TGA of SPPO. The first stage started at 100°C that was attributed to the loss of water or moisture absorbed. The second started at about 200 °C, this was attributed to splitting of the $-SO_3H$ group from the phenyl ring. The third stage started at a temperature close to the decomposition temperature of PPO. This was attributed to the decomposition of PPO backbone. Replacing the hydrogen cation of the sulfonic group with a metal cation shifted the splitting temperature of the sulfonate group, $-SO_3$-Me, to 250 °C [12,14]. Fu et al. [12] studied the gas separation performance of SPPO membranes. The permeability of O_2 and N_2 dropped as the degree of sulfonation increased. Permselectivity of the SPPO membranes increased as the degree of sulfonation increased. The sodium form of SPPO, SPPO-Na, showed the same trend as the hydrogen form of SPPO, but the attachment of sodium to the sulfonate group, $-SO_3^-$, enhanced the permeability of O_2 and N_2, while their permselectivity dropped slightly from that of the hydrogen form at the same degree of sulfonation. X-ray diffraction showed no change in the d-spacing while the glass transition temperature and the density of the membrane increased as the degree of sulfonation increased. Density of the membranes increased linearly with the degree of sulfonation. The drop in permeability was attributed to the increased packing of the membrane structure and the hindered segmental motion as the number of sulfonic groups increased [12]. Kruczek [15] reported the same trend for CO_2, CH_4, O_2 and N_2 gases. Permeability of gases decreased upon increasing the degree of PPO sulfonation. CO_2/CH_4 and O_2/N_2 permselectivities increased with an increase in the degree of PPO sulfonation. As well, the proton of the sulfonic group was exchanged with metal cations such as Na^+,

Mg^{2+}, Al^{3+}. Membranes in the metal form were prepared in two methods; the first was by exchanging the proton of the sulfonic group of the sulfonated PPO before preparing the membranes. The second method was by exchanging the proton of the sulfonic groups after preparing membranes. The effect was not significant except that membranes exchanged with Mg^{2+} by the second method were defective and needed to be laminated with silicon rubber. Exchanging the proton of the sulfonic group with a metal cation increased the permeability of the membranes compared to the corresponding hydrogen form of sulfonated PPO. Permeability of the sodium form of SPPO membranes decreased in the following order with the change in sulfonation degree, 18.5% > 13.2% >25.2%. Permeability of gases in the sodium form of SPPO membranes passed a maximum at 18.5% sulfonation degree. Permselectivity of SPPO membranes in the metal form maintained the same trend of the hydrogen form upon increasing the degree of sulfonation. The trend of permselectivity among different metal forms of SPPO membranes was, $Mg^{2+}>H^{+}>Na^{+}$. Kruczek [15] explained, in part, the behavior of Na^{+} form of SPPO based on the observations and conclusions of Koros [9], i.e. the increased stiffness of segments would enhance the diffusional jumps. The average length of diffusional jumps in the case of 18.5% sulfonation degree was estimated to be equivalent to four unsulfonated phenylene rings, while it was equivalent to three phenylene rings in case of 25.2% sulfonation degree. However, the rotation of a segment of four or three repeat units would need higher activation energy, therefore, these stiffed segments would form more opened molecular scale passages where selectivity would be controlled more by the ultramicroporous molecular sieving. The higher selectivity of Mg-form was explained by the fact that Mg^{2+} cation would crosslink two sulfonate groups, therefore,

Mg-form membranes would have tighter structure, resulting in more efficient sieving.

1.4 Thin Film Composite (TFC) Membranes

TFC membranes are bi- or tri-layered membranes consisting of a thin dense film, which is mainly responsible for the permeability and selectivity of the TFC membrane, and a thick porous support structure that acts mainly as a mechanical support to the thin dense layer. A third layer, a gutter layer, may be used as intermediate layer between the support and the thin dense layer which serves only as a funnel for gas molecules penetrating the thin dense layer into the pores of the porous structure [2]. TFC membrane formation is achievable in three approaches:

1. Formation of a thin dense film and a support layer separately, and then laminating the thin film on the support layer.
2. Dip or transfer coating of a dilute polymer solution onto the porous support or gutter layer followed by removal of solvent.
3. Interfacial and plasma polymerization.

The first approach is very difficult and not practical in handling the thin film prior to and during lamination to the support since thin dense films tend to wrap and wrinkle. They are also fragile and can easily tear upon adhering them to the support. The second approach is mostly used, as it is a practical and usually the most economical method.

What is appealing about TFC membranes is their potential of minimizing the cost of material associated with the usage of the expensive selective polymer. Selecting a low cost and solvent resistant support, the selective layer can be chosen in the optimum way for a specific application. A suboptimal support can undermine the effective selectivity of the combined structure. As a rule of thumb [11], the relative resistances of the selective

layer and the microporous support layer must be in the range of at least 10 to 1. Low resistance supports tend to be more difficult to coat as they possess higher pore density, which is usually coupled with larger pore size. Penetration of the coating material into the pores results in an increase in the support gas transport resistance and may lead to loss of selectivity even the coating layer is not defective. A TFC having the polymer penetrated 1μm into the pores of a polycarbonate porous support of 2% surface porosity is approximately equal to a 50 μm thick dense membrane in terms of their performance [17].

Many factors can help in preventing the penetration of pores. Having a support with small pore size and narrow pore size distribution, the coating polymer molecules will remain on the surface of the support. Therefore, controlling the size of the coating polymer molecules in the coating solution is essential to prevent the intrusion of polymer into the support pores. This can be achieved by selecting high molecular weight polymers and using good solvents that result in larger swelling of the polymer coils in the coating solution. Using high concentration solution helps minimizing pore penetration as a result of polymer coils interlocking [16]. Choosing a solvent that does not wet the support would help in keeping the polymer solution out of the pores. Impregnation of the pores with a liquid while coating the support would help in keeping the polymer solution out of the pores [17].

Estimating the macromolecular coil dimensions in the solution is very helpful to assess the ability of the polymer to penetrate the pores. It was demonstrated that the radius of gyration, R_g, and the end-to-end distance, h, of a linear polymeric coil in solution could be estimated using the Einstein viscosity law for linear polymers [16,17].

$$[\eta]\, M = \Phi\, (6R_g^2)^{3/2} \qquad (6)$$

where $[\eta]$ is the intrinsic viscosity of the polymer solution in dL/g, M is the molecular weight of the polymer and Φ is a universal constant that equals to 2.8×10^{21}, it represents a frictional coefficient.

Fig.1.1: Schemtic of polymer coil showing the end-to-end, h, distance and radius of gyration, R_g.

It was demonstrated that defect free thin coatings of thickness as low as 0.16μm were obtainable when the radius of gyration of the polymer in the solution was larger than the pore size of the support. Koros and Rezac [16] used a ceramic support having a pore size of 200°A to prepare TFC membranes with selective layers from different polymers with different molecular weights. All TFC membranes prepared from polymers that had their estimated macromolecule coil diameter of 200°A or larger, regardless of the polymer chemical nature, were defect free. The intrinsic selectivity of a dense polymeric film was estimated to be 5.1 for O_2/N_2 system with O_2 permeability of 6.7 Barrer, while for a TFC having a coating layer of 0.16μm thickness of the same polymer, O_2/N_2 selectivity obtained was 4.6 and O_2 permeability was 38.2 GPU.

It was proven that a minimum polymer volume should be applied in order to get defect free coating. This minimum volume is not necessarily equivalent to a full surface coverage, as defects may arise from open channels due to incomplete coalescence of nodule aggregates, therefore, maybe more than one surface coverage is required to obtain

100% defect free coating [2, 11, 16].

Reactive formation of the selective layer of TFC membranes is achievable by polymerizing the monomers on the surface of the support membrane. In situ condensation of monomers on the surface of the support is initiated by irradiation of the monomers covering the surface of the porous support. The thickness of the polymer layer formed on the surface of the support is controlled by the time of irradiation [2, 11, 18]. Plasma polymerization is carried out in vacuum where partially ionized gas, a mix of electrons, ions, gas atoms, and gas molecules in the ground and excited state, is produced by the influence of electrical field. Although it seems attractive processes to form ultra-thin composite membranes, reactive plasma or interfacial polymer condensation are unlikely to widely spread as means for the production of TFC membranes mainly for economic reasons that limit its applicability to specialty usage as in sensors and drug delivery systems [11,18]. Thin films prepared by plasma polymerization are highly crosslinked that the high selectivity obtained from this type of membranes is coupled with unacceptable low gas permeability. As well, the mass production of such membranes is more complex and expensive as vacuum and slow reaction rates are encountered in the production process.

1.5 Research Focus and Objectives

1.5.1 Background and Objectives

This research is a part of previous and ongoing work being carried out in the Industrial Membrane Research Institute, Chemical Engineering Department - University of Ottawa. The goal of the research is to develop of gas and non-gas separation membranes based on high molecular weight PPO. PPO is known to possess high gas permeabilities and moderate selectivities. Introducing chemical modifications to the backbone structure proved to be effective in improving the selectivity of the resulting polymer over that of the parent PPO polymer. The chemical modifications of interest in this research were the introduction of sulfonic ($-SO_3H$) and bromine (-Br) groups on the phenyl ring of the polymer backbone. As reported in the literature and proved by different researchers at the Industrial Membrane Research Institute, introducing sulfonic groups to the backbone of the polymer enhances the selectivity of the polymer to the favor of CO_2 gas in CO_2/CH_4 systems and to the favor of O_2 gas in O_2/N_2 system. However, a major drawback associated with the sulfonation of PPO is the drop in gases permeabilities compared to that of the parent PPO polymer. On the other hand, bromination of PPO proved to enhance the permeability of the resulting polymer while maintaining the parent polymer selectivity. Replacement of the proton of the sulfonic group with a mono-, di- and trivalent metal cation is known in many instances to affect significantly the performance of the membranes.

Based on the background knowledge briefed above, the objectives of this research can be summarized:

(i) The effect of chemical modification on the membrane structure and gas separation performance is studied; a chemical structure-performance relation is sought.

(ii) The formation processes of dense homogeneous and composite PPO membranes are studied and correlated to the gas separation performance of each membrane.

(iii) The transport of gases in porous and composite membranes is mathematically simulated to predict the performance of thin composite membranes based on the intrinsic properties of the individual layers forming the composite membrane.

1.5.2 Scope of Research

To achieve the objectives of the research stated above, the following tasks are accomplished:

1. Chemical modification of PPO.
   - 1.1 Sulfonation of PPO and exchange of the proton of the sulfonic group with a mono-valent cations (H^+, Li^+, K^+, Cs^+), di-valent cations (Mg^{+2}, Ca^{+2}, Ba^{+2}), or tri-valent cation (Al^{+3}).
   - 1.2 Bromination of PPO.
   - 1.3 Sulfonation of the brominated PPO.
2. Preparation and characterization of dense homogeneous membranes.
   - 2.1 Preparation of dense homogeneous membranes from PPO and chemically modified PPO.
   - 2.2 Measurement of the density of the homogeneous dense membranes.

2.3 Measurement of gas permeability and solubility.

2.4 Study of interaction between penetrant gas and membrane by infrared (IR) technique and sorption measurements.

3. Preparation of composite membranes and comparison with dense homogeneous PPO.

3.1 Preparation of thin film composite membranes.

3.2 Investigation of surface images of the dense homogeneous membranes and the coated layer of composite membranes by atomic force microscopy (AFM).

3.3 Study on the effect of preparation for both dense homogeneous and thin composite membranes.

3.4 Comparison of gas separation performance of dense homogeneous membranes with that of composite membranes.

4. Performance prediction of thin film composite membranes

4.1 Characterization of porous substrate membranes by their gas transport properties.

4.2 Modeling of gas transport through thin film composite membranes.

4.3 Prediction of performance of thin composite membranes based on the gas transport properties of porous substrate membranes and coated layer of the composite membrane.

This thesis distinguishes itself from earlier works on the similar subjects in the following way.

Regarding the Kruczek's studies [15] on the performance of SPPO membranes in hydrogen and various metal cation forms, Kruczek used dense homogeneous membranes, whereas in this thesis composite membranes were used. A more through understanding on

the effect of metal cation substitution was obtained in this thesis by including gas sorption data.

In comparison to Chowdhury et al.'s study [19] on the effect of simultaneous sulfonation and bromination, the degrees of sulfonation and bromination were changed more systematically in this thesis covering a much broader range of substitution. Moreover, infrared spectroscopy enabled more thorough understanding of macromolecular conformation.

1.6 Contributions

The contributions of this research to the field of membrane science and technology are summarized as follows:

1. Additional data base for the transport of CO_2, O_2, N_2 and CH_4 gases, through membranes made from PPO and its derivatives; i.e. brominated PPO, sulfonated PPO in hydrogen and metal forms, and sulfonated brominated PPO, is provided.
2. A firm structure-performance relationship within the group of polymers mentioned above is provided.
3. A plausible model for the kinetics involved in the permeant gas-membrane interaction is provided.
4. A prediction model for the performance of thin film composite membranes is provided based on the intrinsic transport properties of individual layers.

1.7 SI and Conventional Units

The membrane science is based on many other disciplines of science to mention some: polymer solutions rheology, polymer chemistry and synthesis, fluid mechanics, adsorption, transport phenomena, and thermodynamics. This made the membrane science

open to the methods and techniques as well as the terms and units conventionally used in various disciplines. In this thesis, many of these conventional terminology and units will be frequently used. Therefore, for the readers' convenience, Table 1.3 is attached to provide the conversion factors from the conventional units to the corresponding accepted SI units.

Table 1.3: Conversion factors from some conventional units to SI accepted units.

Quantity	Conventional unit	SI unit	Conversion factor (multiply by)
Kinetic diameter of gas molecules	°A	m	10^{-10}
Intrinsic viscosity [η], or reduced viscosity η of polymer solution	dL/g	m^3/kg	10^{-1}
Polymer solution concentration, C	g/dL	kg/m^3	10
Gas permeability of membrane	Barrer	$\frac{m^3(STP)\ m}{m^2\ s\ Pa}$	7.50×10^{-18}
Gas permeance of membrane, p	GPU	$\frac{m^3(STP)}{m^2\ s\ Pa}$	7.50×10^{-10}
Friction coefficient, Φ	dL/(mol cm^3)	m^3/ (mol m^3)	10^2
Kinematic viscosity, v	cSt	m^2/s	10^{-6}
Pressure	psi	Pa	6891.156
	cmHg	Pa	1332.89
	Torr or mmHg	Pa	133.289

1.8 References

[1] W. Koros and G. Fleming: "*Membrane-Based Gas Separation*", J. Membr. Sci., 83, (1993) 1.

[2] R. Kesting and A. Fritzche:, "*Polymeric Gas Separation Membranes*", Wiley Interscience, NY (1993).

[3] W. Koros and M. Hellums: " *Transport Properties*, in *Encyclopedia of Polymer Science*", 2nd edn., Wiley Interscience, NY, Supplement Volume 724 (1989).

[4] W. Koros, M. Coleman, and D. Walker: "*Controlled Permeability Polymer Membranes*", in: Annual Review of Material Science, 22 (1991).

[5] H. Hoehn: "*Heat Treatment of Membranes of Selected Polyimides, Polyester and Polyamides*", U.S. Patent *3,822,202 (1977).*

[6] D. Aycock: "*Poly (Phenylene Ether),* in *Encyclopedia of Polymer Science and Technology*", V 13, Interscience Publishers, NY (1974).

[7] S. Percec and G. Li: "*Chemical Modification of Poly(2,6-Dimethyl-1,4-Phenylene Oxide) and Properties of the Resulting Polymers*", ACS Symposium Ser., 364, American Chemical Society, Washington DC (1988).

[8] R. Chern, L. Jia, S. Shimoda, and H. Hopfenberg: "*A Note on the Effects of Mono- and Di-Bromination on the Transport Properties of Poly(2,6-Dimethylphenylene Oxide*", J. Membr. Sci., 48, (1990) 333-341.

[9] B. Story and W. Koros: "*Sorption and Transport of CO_2 and CH_4 in Chemically Modified Poly (Phenylene Oxide)*", J. Membr. Sci., 67, (1992) 191-210.

[10] B. Story and W. Koros: "*Sorption of CO_2/CH_4 Mixtures in Poly(Phenylene Oxide) and a Carboxylated Derivative*", J. Appl. Polym. Sci., 42, (1991) 2613-2626.

[11] D. Paul and Y. Yampol'skii: "*Polymeric Gas Separation Membranes*", CRC Press, Boca Raton (1994).

[12] H. Fu, L. Jia, and J. Xu: " *Studies on the Sulfonation of Poly Phenylene Oxide and Permeation Behaviour of Gases and Water Vapor Through Sulfonated PPO*

Membranes. I. Sulfonation of PPO and Characterization of the Products. II. Permeation Behaviour of Gases and Water Vapor Through Sulfonated Membranes", J. Appl. Polym. Sci., 51, (1994) 1399-1409.

[13] G. Olaf, S. Kobayashi, and J. Nishimura, J.A.C.S., 95, (1973) 564.

[14] R. Chern, F. Sheu, L. Jia, V. Stannet, and H. Hopfenberg: "*Transport of Gases in Unmodified and Aryl-Brominated 2,6-Dimethyl-1,4-Poly (Phenylene Oxide)*", J. Membr. Sci., 35, (1987) 103-115.

[15] B. Kruczek: "*Development and Characterization of Dense Membranes for Gas Separation Made from High Molecular Weight Sulfonated Poly (Phenylene Oxide)*", Ph.D. Thesis, Chemical Engineering Department, U. of Ottawa, 1998.

[16] A. Rezac and W. Koros: "*Preparation of Polymer-Ceramic Composite Membranes with Thin Defect-Free Separating Layers*", J. Appl. Polym. Sci., 46, (1992) 1927-1938.

[17] K. Ebert, A. Bezjak, K. Nijmeijer, M. Mulder, and H. Strathmann: "*The Preparation of Composite Membranes with a Glassy Top Layer*", J. Appl. Polym. Sci., 46, 1927-1938 (1992).

[18] C. Liu and C. Martin: "*Composite Membranes from Photochemical Synthesis of Ultrathin Polymer Films*", Nature, 352, July 1991.

[19] G. Chowdhury, R. Vujosevic, T. Matsuura, and B. Laverty: *"Effects of polymer molecular weight and chemical modification on the gas transport properties of poly (2,6-dimethyl-1,4-phenylene oxide"*, J. Polym. Sci., 77, (2000) 1137-1143.

1.9 Nomenclature

D_A Diffusivity of gas A in the membrane, m^2/s.

F_{AB} Separation factor of the membrane toward a gas mixture of A and B.

h Root mean-square end-to-end distance of the polymer coil, cm.

M Molecular weight of polymer, g/mol.

P_A, P_B Partial pressure of gas A and gas B, respectively, Pa.

p_A, p_B Permeability of the membrane for gas A and gas B, respectively, m^3 m/ (m^2 Pa s).

Q_A Flux of gas A through the membrane, m^3/ (m^2 s).

R_g Polymer coil radius of gyration, cm.

S_A Solubility of gas A in the membrane, m^3 /(m^3 Pa).

X_A,X_B Mole fraction of gas A and gas B.

ΔP_A, ΔP_B Transmembrane partial pressure difference for gas A and B, respectively.

α_{AB} Membrane ideal gas selectivity, or permeability ratio, for gas A and B.

δ Thickness of the membrane, m.

Φ Frictional coefficient, 2.8×10^{21}dL/(mol cm^3).

$[\eta]$ Intrinsic viscosity of polymer solution, dL/g.

Chapter 2

General Experimental Procedures and Methods

2.1 Bromination of PPO

Aryl bromination via electrophilic substitution occurs when the reaction is carried out under mild conditions in chloroform solution in the absence of catalysts [1]. Many researchers used this method to brominate PPO at the aryl carbon to different bromination degrees [2-5].

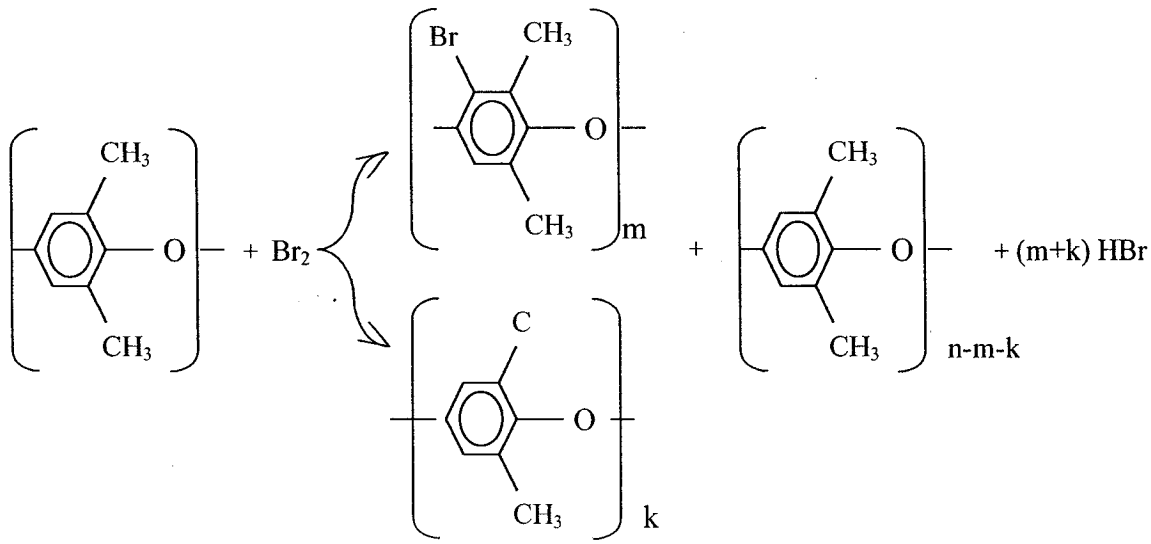

Depending on the reaction conditions, the bromine group may be selectively attached to the aryl carbon atom or to the methyl carbon atom. Mahajan [4] brominated PPO at the alkyl (methyl) chain via radical mechanism at high reaction temperatures. Chern et al. [5] brominated PPO at 0°C where mono- and di- bromination of the polymer was obtained.

Reaction vessel and glassware used in this study were dried in vacuum for 24 hours prior to bromination. PPO samples were dried in vacuum at room temperature for 24 hours prior to bromination procedure.

PPO sample was weighed and dissolved (completely) in 300 to 400 mL of chloroform in the reaction vessel. The reaction medium was kept stirred using a motor that drove a mixer shaft. Bromine (Br_2) liquid was dissolved in 50 mL chloroform in the reactant

pipet. Prior to adding the bromine solution to the reaction vessel, N_2 was let to bubble through the reaction media, and the reaction set up was covered with aluminum foil to prevent any radical formation. The bromine-chloroform solution in the pipet then was dispensed into the reaction vessel over a period of 2 minutes. The reaction media was stirred and N_2 bubbled for another 90 minutes. N_2 flow is needed to purge out HBr forming during the bromination reaction. Figure 2.1 represents a schematic of the reaction set up.

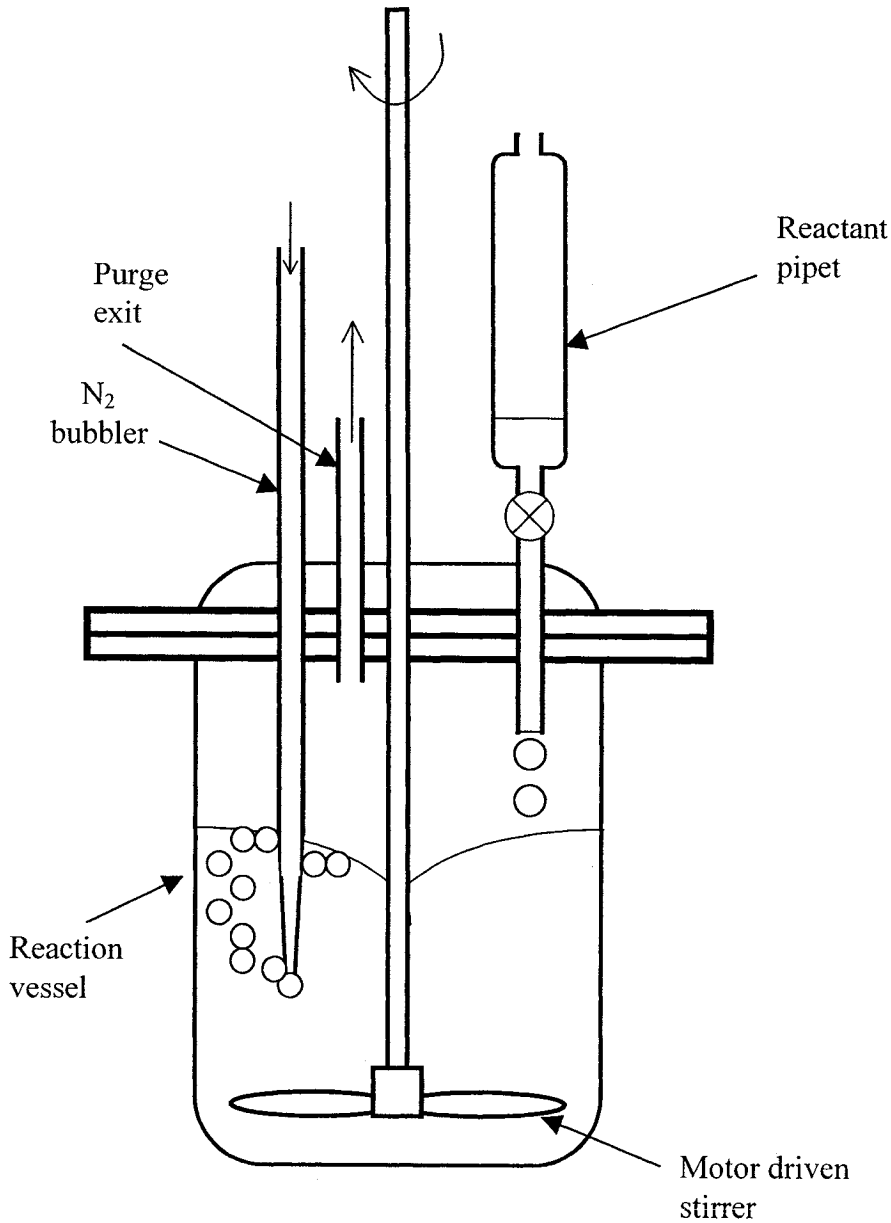

Fig. 2.1: Schematic of the reaction apparatus.

After the reaction was completed, 100 mL of methanol was added into the reaction vessel slowly in order to terminate the reaction and to precipitate the brominated polymer.

The amount of bromine liquid, V_B (mL), needed to achieve a certain degree of bromination (*DBr*) is calculated according to the following equation:

$$V_B = 0.005\, Q\, DBr \qquad (1)$$

where Q is the mass of PPO (g) to be brominated. For example, 1 mL of bromine liquid is needed to brominate 10.0g of PPO to 20% DBr.

The degree of bromination that was achieved was determined based on proton nuclear magnetic resonance (^{1}H-NMR) spectrum for the brominated PPO [6]. Hydrogen atoms attached to the aryl carbon of a PPO repeat units give a signal at 6.45 ppm. Because of bromination, a ^{1}H-NMR signal, for protons attached to aryl carbons in brominated PPO units, appears shifted to a lower field values. For example, a brominated PPO (target bromination degree was 40.0%) was analyzed using the facilities available at the Chemistry Department/ University of Ottawa. The obtained ^{1}H-NMR signal intensity at 6.42 ppm (I_1) was 0.986; and the intensity of the shifted signal at 6.1 ppm (I_2) was 0.294. The degree of aryl bromination then can be calculated using the following equation:

$$\text{Degree of bromination} = \frac{I_2}{\frac{I_1}{2} + I_2} \times 100 \qquad (2)$$

$$= \frac{0.294}{\frac{0.986}{2} + 0.294} \times 100 \approx 37.4\%$$

2.2 Sulfonation of PPO

Aryl sulfonation of PPO is described in the literature [7-10]. Sulfonation of PPO with sulfuric acid is a slow reaction and results in relatively low conversion (degree of

sulfonation) [10]. The procedure of Plummer et al. [7] was followed in this work, where chlorosulfonic acid was used. The reaction equation is:

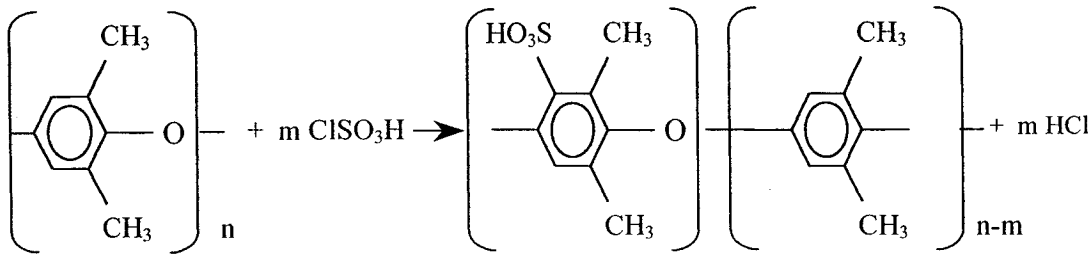

Reaction vessel and glassware used in the reaction process were dried in vacuum for 24 hours prior to sulfonation. PPO samples were dried in vacuum at room temperature for 24 hours prior to sulfonation procedure. PPO sample was weighed and dissolved (completely) in 300 to 400 mL of chloroform in the reaction vessel. Stoichiometric amount of chlorosulfonic acid, W_S (g), was added to 50 mL chloroform in the reactant pipet. Prior to adding chlorosulfonic acid to the reaction vessel, N_2 was let to bubble through the reaction media. The chlorosulfonic acid-chloroform solution in the pipet was dispensed into the reaction vessel over a period of 5 minutes. The reaction media was stirred and N_2 bubbled for another 45 minutes. N_2 is needed to purge out HCl forming during the sulfonation reaction. The reaction apparatus for sulfonation is similar to that used for bromination (Fig. 2.1), however, there is no need to cover it with aluminum foil. The reaction was terminated by the addition of methanol. The amount of methanol that was added depended on the ion exchange capacity (IEC) achieved; when the IEC value achieved was not high enough to precipitate the sulfonated polymer, methanol was added until the reddish color of the reaction media turned into yellowish. On the other hand, when the IEC value achieved was high enough to precipitate the sulfonated polymer from the reaction medium solution, the sulfonated PPO precipitate was filtered, and then dissolved in methanol. The sulfonated PPO solution was then transferred into a glass tray

to evaporate methanol and dry the polymer. The sulfonated PPO then was washed from the traces of organic solvents and acids by soaking it in demineralized water for 10 days replacing daily the water. The amount of chlorosulfonic acid, W_s (g), needed to achieve a target IEC value can be determined based on the following equation:

$$W_S = 116.5\, Q \frac{IEC}{(1000 - 80\, IEC)} \tag{3}$$

where Q is the mass of PPO (g) to be sulfonated. The degree of sulfonation, DSul, of PPO can be determined upon determining the achieved IEC using the following equation:

$$IEC = \frac{1000\, DSul}{200\, DSul + 120\, (1 - DSul)} \tag{4}$$

where the coefficients 116.5, 80, 200 and 120 in equations (3 and 4) represent the molecular weight of chlorosulfonic acid, sulfonate group, sulfonated PPO repeat unit, and PPO repeat unit, respectively.

^{1}H-NMR and ^{13}C-NMR study on sulfonation of PPO [11] following the procedure given above, confirmed that sulfonation occurred at the aryl carbon rather than the methyl carbon of PPO repeat unit. A back titration approach was also used to determine the IEC value achieved; a known amount of the dry sulfonated PPO, W_P (g), was soaked in a known volume, V_{BN} (mL), of 0.1N NaOH solution for a week. Then a known volume, V_{SB} (mL), of the NaOH solution in which the sulfonated PPO sample was soaked, was titrated against 0.1N HCl acid solution. Then, the IEC of the sulfonated PPO can be calculated using the following equation:

$$IEC = 0.1 \frac{V_{BN}}{W_P} \left(1 - \frac{V_{HCl}}{V_{SB}} \right) \tag{5}$$

where V_{HCl} (mL) is the volume of HCl acid used to titrate the solution sample, V_{SB}.

2.3 Sulfonation of Brominated PPO

The same experimental procedure in regard to carrying out the sulfonation reaction was followed.

Let the targeted degree of sulfonation and the *IEC* value based on the sulfonated brominated PPO be $DSul_b$ and IEC_b, respectively. In order to use equation (3) to calculate the required chlorosulfonic acid, Q and IEC (which are based on the un-brominated part of the polymer) need to be calculated.

Q can be calculated using the following equation:

$$Q = \frac{120\ (1 - DBr)}{199\ DBr\ +\ 120\ (1 - DBr)} Q_b \qquad (6)$$

where Q_b is the mass of the brominated PPO sample (g) to be sulfonated. $DSul_b$ can be calculated based on the IEC_b value, using the following equation:

$$DSul_b = \frac{IEC_b\ (79\ DBr\ +\ 120)}{1000\ -\ 80\ IEC_b} \qquad (7)$$

Then, the degree of sulfonation based on the un-brominated PPO, *DSul*, can be calculated using the following equation:

$$DSul = \frac{DSul_b}{(1 - DBr)} \qquad (8)$$

Then, the *IEC* value based on the un-brominated PPO repeat units can be calculated using equation (4).

2.4 Intrinsic Viscosity Measurements

The details of the measurement of intrinsic viscosities are given in [12]. The reduced viscosity is given by:

$$\eta_{red} = \frac{v - v_o}{c\, v_o} = \frac{K\, t - K\, t_o}{c\, K\, t_o} = \frac{t - t_o}{c\, t_o} \qquad (9)$$

where v and v_o are the kinematic viscosity (cSt) of the polymer solution and the solvent, respectively. c is the concentration of polymer in solution (g/dL). Kinematic viscosities are related to the efflux time of the solution, t, and the solvent, t_o, by the viscometer capillary constant K (cSt/s). Intrinsic viscosity is the reduced viscosity of solution at infinite dilution. Hence, it is determined by linear extrapolation of the reduced viscosity of dilute solutions.

Figure 2.2 shows the plot of the reduced viscosity for dilute solutions of PPO (1.57 dL/g intrinsic viscosity in chloroform) in trichloroethylene (TCE). Efflux times were measured on capillary viscometer (Cannon-Fenske #100). PPO-TCE solutions of different

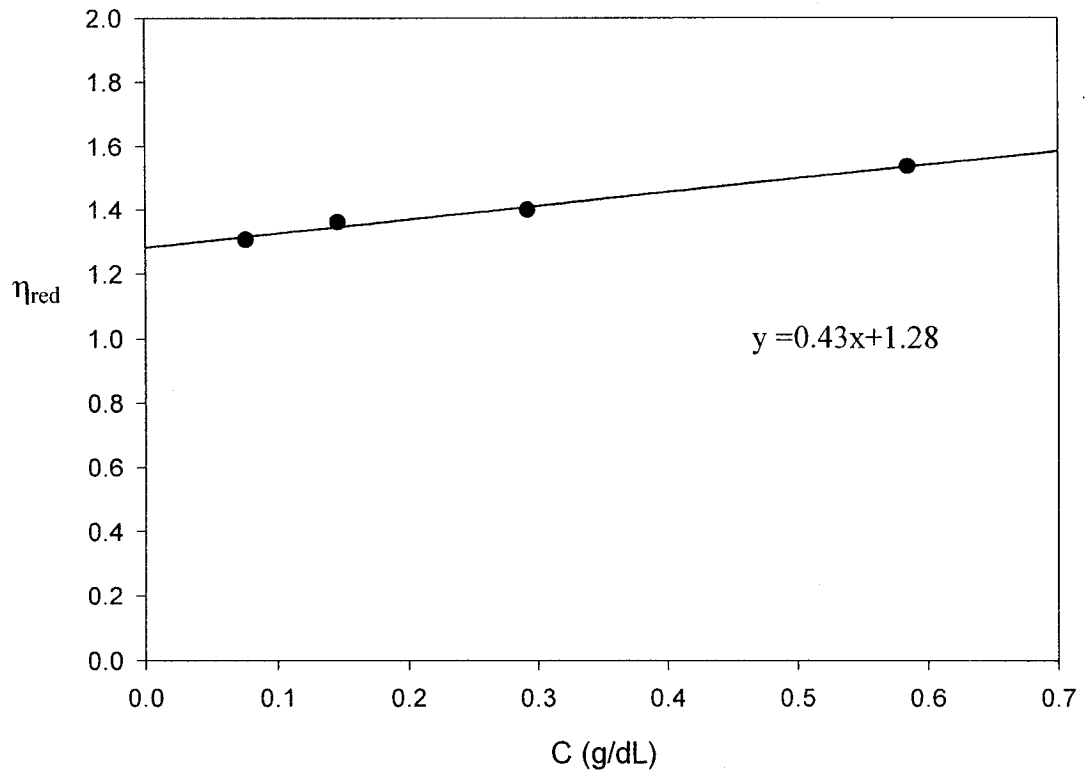

Fig. 2.2: Reduced viscosity of PPO-TCE solution measured at room temperature (22°C), as a function of PPO concentration in the solution.

concentrations were prepared by diluting from 1% (w/w) PPO-TCE solution that was filtered through 3 μm Teflon filters.

2.5 Infrared Spectroscopy

The experimental setup consists of a double-beam IR equipment (Perkin-Elmer 267) and two Pyrex gas cells with NaCl crystal windows. The gas cells were fabricated specifically to handle a membrane suspended vertically in a gas stream. The two cells are leak-proof when operating at low pressure (atmospheric pressure). The membrane was fixed on a perforated holder that permits gas to flow in the sample cell and over the membrane. The gas pressure during gas flow was always atmospheric. The two gas cells (the sample cell and the reference cell) are connected to each other from both ends of the cells to assure equal pressure in both cells. The flow was stopped by closing the inlet and outlet valves prior to IR scan.

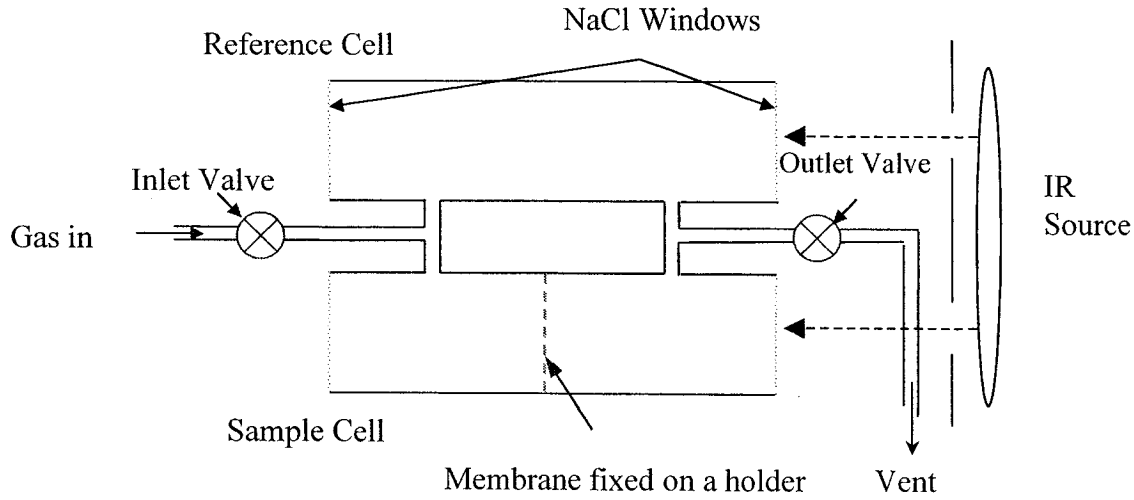

Fig. 2.3: Schematic of the experimental IR setup.

2.6 Determination of Membranes Density

Determining the density of a membrane, ρ (g/cm^3), requires measuring the mass, W_m (g) and the volume, V_m (cm^3) of the membrane, where:

$$\rho = \frac{W_m}{V_m} \tag{10}$$

The mass of the membrane was measured using a 4-digit electronic balance. The volume of the membrane was determined using the constant volume (CV) system technique. Figure 2.4 shows a schematic of the constant volume system. The method is based on expanding a gas from the gas manifold, the volume of which is V_{gc} (cm^3), into the sample column containing the membrane sample. Let V_{sce} be the volume (cm^3) of the empty sample column, and V_{scm} be the volume (cm^3) of the sample column with the membrane inside. Then, the volume of the membrane can be calculated from:

$$V_m = V_{sce} - V_{scm} \tag{11}$$

The volume of the empty sample column (V_{sce}) is known; however, the volume of the sample column while containing the membrane (V_{scm}) needs to be determined. The following is the procedure that was used in order to determine V_{scm}:

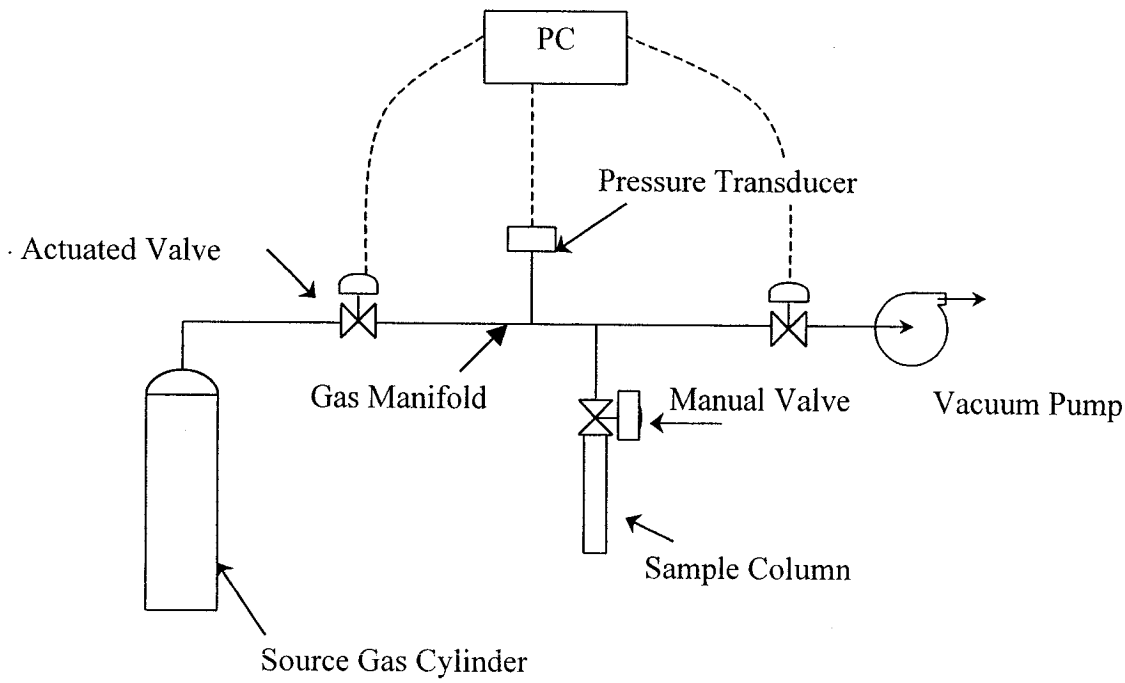

Fig. 2.4: Schematic of the constant volume system used in solubility and density measurements.

1. Initially, the gas manifold and the sample column (containing the membrane) are open to each other and maintained at low-pressure value, P_1 (Pa).
2. The sample column is isolated by closing the manual valve.
3. Helium gas (*He*) is introduced into the gas manifold. The pressure reading in the gas manifold (P_2) is recorded once it stabilizes.
4. The manual valve (connecting the gas manifold and the sample column) is opened and the helium gas is let to expand from the gas manifold into the sample column. The pressure in the gas manifold and the sample column, P_f, is recorded once it stabilizes.

Assuming that *He* gas is not adsorbed in the membrane, then V_{scm} can be calculated by:

$$V_{scm} = V_{gc} \frac{\left(P_2 - P_f\right)}{\left(P_f - P_1\right)} \tag{12}$$

Pretreatment of the membrane is needed before starting the above procedure in order to dry and degas the membrane. This was achieved by keeping the membrane in vacuum for 24 hours.

2.7 Gas Sorption

Gas sorption measurement runs proceed after determining the volume of the sample column containing the membrane, V_{scm}, according to the previous section. The following is the procedure that was used to determine the amount of gas sorption in a membrane:

1. The gas manifold and the sample column are opened to each other and let to evacuate at very high vacuum (less than 6.6 Pa absolute) for 24 hours prior to gas adsorption run.
2. The pressure in the sample column and the gas manifold is measured (P_1).

3. The sample column is isolated by closing the manual valve.

4. The gas to be tested is introduced into the gas manifold and the pressure is recorded once it has stabilized (P_2).

5. The manual valve is opened and the gas is let to expand into the sample column. The pressure is recorded once it equilibrates (P_e).

In order to determine the amount of gas adsorbed in the membrane, it is required to know the total pressure (P_f), in the gas manifold and the sample column, the gas would acquire if it would expand from the gas manifold into the sample column without being adsorbed by the membrane. It can be calculated using the following equation:

$$P_f = \frac{T_e}{T_1}\frac{\left(P_2 V_{gc} + P_1 V_{scm}\right)}{\left(V_{gc} + V_{scm}\right)} \tag{13}$$

where T_1 and T_e are the system temperatures just before the gas expansion and at equilibrium. The amount of gas adsorbed can be determined according to the following equation (assuming ideal gas behaviour):

$$N_a = \frac{(V_{gc} + V_{scm})}{R\ T_e}\left(P_f - P_e\right)$$
$$\mathrm{V}_a = \frac{T_s}{P_s}\frac{(V_{gc} + V_{scm})}{T_e}\left(P_f - P_e\right) \tag{14}$$

where R (J mol K^{-1}) is the universal gas constant. N_a is the number of moles of the tested gas that is adsorbed by the membrane, and V_a (cm^3) is the volume of the gas adsorbed in the membrane at standard temperature and pressure (STP), T_s and P_s are the standard temperature (0°C) and pressure (1.0 atmosphere), respectively. The concentration of the adsorbed gas, C (cm^3 (STP)/g) or C^* (mol/m^3) in the membrane then can be calculated:

$$C = \frac{V_a}{W_m}$$
$$C^* = \frac{N_a}{V_m} \qquad (15)$$

To determine the solubility of the gas in the membrane, S (cm^3 (STP)/(cm^3 cmHg)) or S^* (mol/(m^3 Pa)), the following equation is used:

$$S = \frac{C\rho}{P_e}$$
$$S^* = \frac{C^*\rho}{P_e} \qquad (16)$$

where ρ is the membrane density, and P_e is the equilibrium pressure of the gas corresponding to C.

2.8 Gas Permeation Testing

The system which was used to test gas permeation through the membranes is based on collecting the permeate in a chamber of known volume; hence it is called the constant volume system. Figure 2.5 shows a schematic of the constant volume system. The permeation rate can be determined by monitoring the rate of change in the permeate pressure detected by the pressure transducer on the permeate side. Assuming an ideal gas behaviour, which is a very safe assumption since the permeate side was always maintained at sub-atmospheric pressure, the permeation rate is given by,

$$\dot{Q} = \frac{V}{RT}\frac{dP}{dt} \qquad (17)$$

where $\dot{Q}$ is the permeation rate (mol/s), V is the permeate side volume (m^3), R is the universal gas constant, T is the absolute temperature (K), $\frac{dP}{dt}$ is the rate of increase in the

permeate side pressure (Pa/s). The gas permeability of the membrane, p (mol/(m^2 s Pa)), can be calculated:

$$p = \frac{\dot{Q}}{(A/\delta)\,\Delta P} \tag{18}$$

where A is the membrane area (m^2), δ is the membrane thickness (m), and ΔP is the transmembrane pressure difference (Pa).

Gas permeation experiments were carried out at room temperature (21±1°C). The feed pressure was maintained at 700 kPa (absolute) by controlling the flow of the gas into the system. Purging stream was always maintained at 10.0 (cm^3/min). The permeate pressure was allowed to cycle between 0.133 and 100 kPa (absolute). All measurement devices

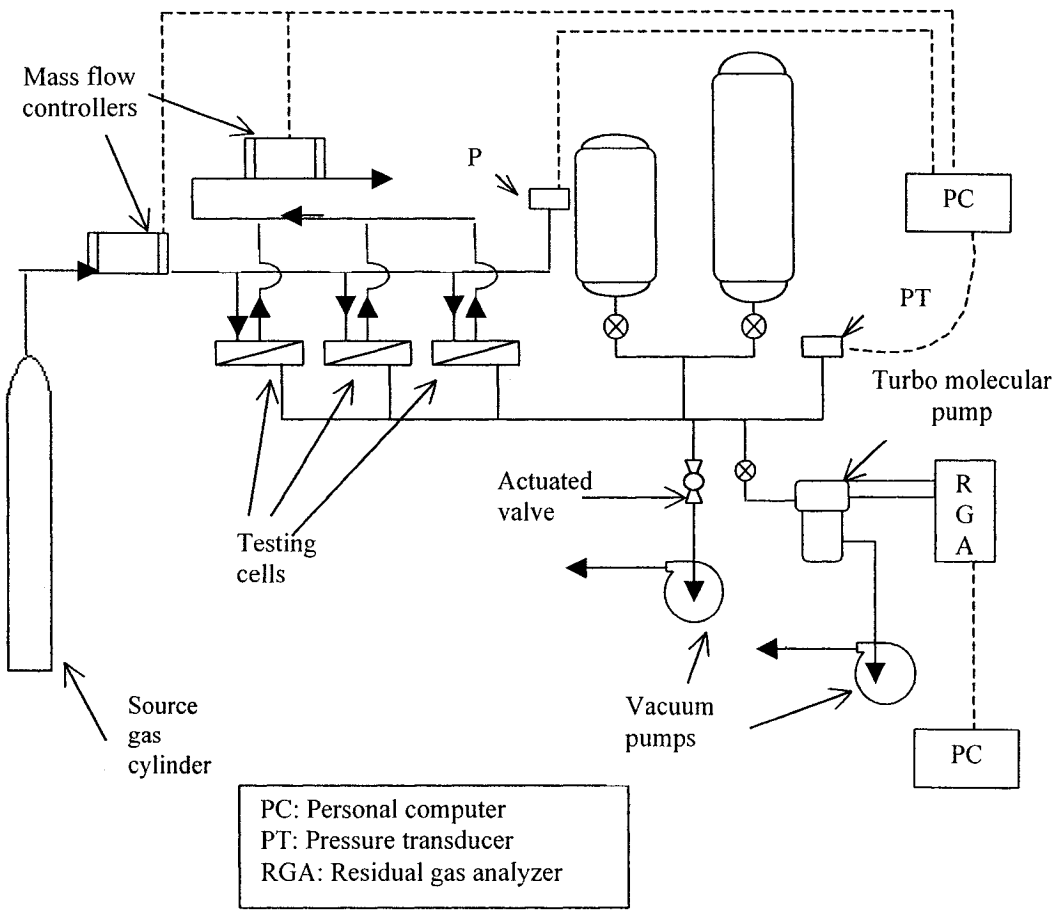

Fig. 2.5: Schematic of the constant volume system used for membrane gas permeation testing.

(pressure transducers, thermocouples), automatic valves, and mass flow controllers, are interfaced with and manipulated through the computer using LabView software.

The testing of gases was carried out in two cycles. In a testing cycle, the gas testing took the order O_2, N_2, CH_4, and CO_2. Each gas was allowed to permeate through the membrane for at least two days before permeation data were collected. The collection of permeation data took another 24 to 48 hours.

Knowing the gas permeability and solubility of the membrane, the gas diffusivity, D (m^2/s), of the membrane can be calculated as follows:

$$D = \frac{p}{S} \tag{19}$$

For gas permeation experiments that involved gas mixtures, the permeate side was analyzed using the residual gas analyzer. The gas permeability, based on gas mixture permeation experiments, can be calculated according to the following equation:

$$p = \frac{X_P \dot{Q}}{(A/\delta)\ (X_F P_F - X_P P_P)} \tag{20}$$

where X_F and X_P are the mole fraction of the gas in the feed and in the permeate sides, respectively, and, P_F and P_P are the feed and the permeate sides pressures, respectively.

Testing cells were fabricated to handle very high vacuum levels, as well as to handle composite or homogeneous membranes. Figure 2.6 presents a detailed schematic of the testing cells.

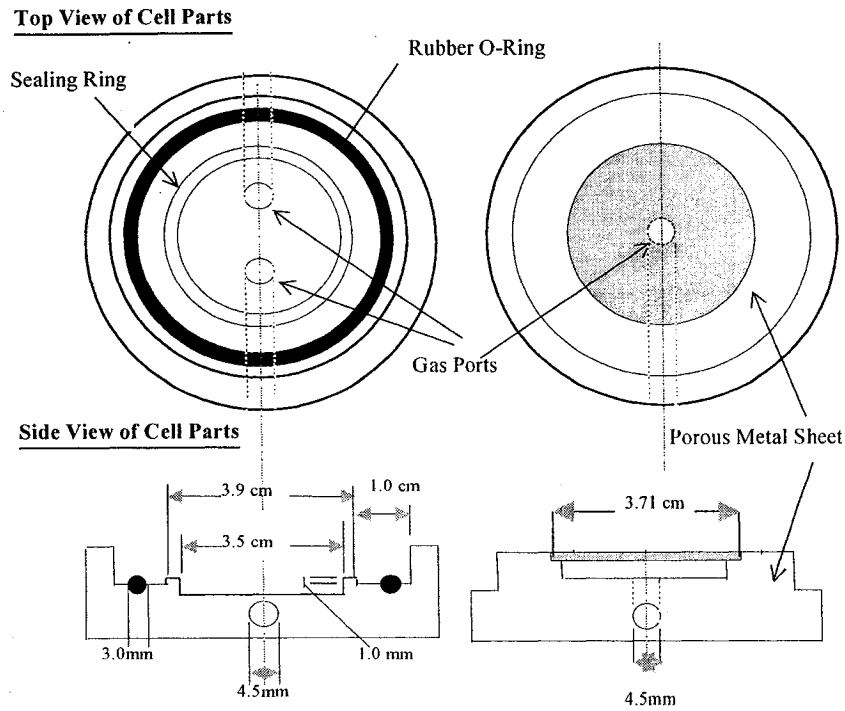

Fig. 2.6: Schematic of the testing cell parts in which membranes were held for gas permeation testing.

2.9 References

[1] D. M. White: "*Brominated Poly(2,6-dimethyl-1,4-phenylene oxide)*", ACS Polym. Preprints, 15 (1), (1974) 210-215.

[2] B. Story and W. J. Koros: "*Sorption and Transport of CO_2 and CH_4 in Chemically Modified Poly (phenylene oxide)*", J. Membr. Sci., 67, (1992) 191-210.

[3] G. Chowdhury, R. Vujosevic, T. Matsuura, and B. Laverty: " *Effect of Polymer Molecular Weight and Chemical Modification on the Gas Transport Properties of Poly (2,6-Dimethyl-1,4-Phenylene Oxide)*", J. Appl. Polym. Sci., 77, (2000) 1137-1143.

[4] S. Mahajan: "*Structural Modification of Poly (2,6-dimethyl-1,4-phenylene oxide)*",

Polym.-Plast. Tech. Eng., 30, (1991) 1.

[5] R. T. Chern, F. R. Sheu, L. Jia, V. T. Stannett, and H. B. Hopfenberg: *"Transport of Gases in Unmodified and Aryl-Brominated 2,6-Dimethyl-1,4-Poly (Phenylene Oxide),* J. Membr. Sci., 35, (1987) 103-115.

[6] C. Bonfanti, L. Lanzini, A. Roggero, and R. Sisto: "*Chemical Modification of Poly (2,6-Dimethyl-1,4-Phenylene Oxide) by Bromination-Alkynylation*", J. Polym. Sci.: Part A: Polym. Chemistry, 32, (1994) 1361-1369.

[7] W. Plummer, G. Kimura, and A. B. LaConti: "*Development of SPPO Membranes for Reverse Osmosis"*, office of Saline water Research and Development Progress Report No. 551, General Electrics, Lynn Mass., 1970.

[8] B. Bikson and K. Nelson: "*Production and Use of Improved Composite Fluid Separation Membranes*", U.S. Patent 5,356,459 (1994).

[9] G. Polotskaya, S. Agranova, T. Antonov, and G. Elyashevich: "*Gas Transport and Structural Features of Sulfonated Poly (Phenylene Oxide)",* J. Appl. Polym. Sci., 66, (1997) 1439-1443.

[10] H. Fu, L. Jia, and J. Xu: "*Studies on the Sulfonation of Polyphenylene oxide and Permeation Behaviour of Gases and Water Vapor through Sulfonated PPO Membranes. I. Sulfonation of PPO and Characterization of the Products. II. Permeation Behaviour of Gases and Water Vapor through Sulfonated Membranes*", J. Appl. Polym. Sci., 51, (1994) 1399-1409.

[11] C. Wang, Y. Huang, and G. Cong: "Preparation and Characterization of Sulfonated Poly (Phenylene Oxide)", Polym. J., 27 (2), (1995) 173-178.

[12] P. Flory, "*Principles of Polymer Chemistry*", George Banta Company, Mensha, Wisconsin (1953).

2.10 Nomenclature

A Total membrane surface area, cm^2.

c Concentration of polymer solution, g/dL.

D Gas diffusivity of the membrane, m^2/s.

DBr Degree of bromination, %.

$DSul$ Degree of sulfonation based on PPO, %.

$DSul_b$ Degree of sulfonation based on brominated PPO, %.

IEC Ion exchange capacity based on PPO, meq/g.

IEC_b Ion exchange capacity based on brominated PPO, meq/g.

K Capillary viscometer constant, cSt/s.

N_a Total number of moles of gas adsorbed, mol.

p Gas permeability of membrane, (mol/(m^2 s Pa)) or (cm^3(STP) /(cm^2 s cmHg)).

P_1 Gas pressure in the manifold and sample column before introducing the gas into the CV system, Pa.

P_2 Gas pressure in the manifold after introducing the gas into the CV system, Pa.

P_e Gas pressure at equilibrium, Pa.

P_f Final pressure of gas in CV system after expansion when there is no gas adsorption occurring, Pa.

P_F Gas pressure in the feed side, Pa.

P_P Gas pressure in the permeate side, Pa.

P_s Gas pressure at standard conditions, Pa.

Q Mass of PPO, g.

Q_b Mass of brominated PPO, g.

$\dot{Q}$ Total gas flow permeating through the membrane, mol/s.

R Universal gas constant, 8.314 J/(mol K).

S Gas solubility of the membrane, cm^3(STP)/(cm^3 cmHg).

S^* Gas solubility of the membrane, mol/(m^3 Pa).

T_e Temperature of CV system at equilibrium, K.

T_s Temperature at standard conditions, K.

T_1 Temperature of CV system before gas expansion, K.

t_o, t Time elapsed for solvent and solution, respectively, to flow in capillary viscometer, s.

V_a Volume of adsorbed gas at standard pressure and temperature, cm^3.

V_B Volume of liquid bromine needed for bromination reaction, cm^3.

V_{BN} Volume of NaOH solution used to soak the sulfonated PPO sample, cm^3.

V_{gc} Volume of manifold of CV system, cm^3.

V_{HCl} Volume of HCl solution consumed in titrating V_{SB} of NaOH solution, cm^3.

V_m Volume of membranes sample, cm^3.

V_{SB} Volume of NaOH solution sample used for back titration, cm^3.

V_{sce} Volume of empty sample column, cm^3.

V_{scm} Volume of the sample column with the membrane inside, cm^3.

W_m Membranes sample mass, g.

W_p Mass of sulfonated PPO sample, g.

W_s Mass of chlorosulfonic acid needed for sulfonation reaction, g.

X_F Mole fraction of gas in the feed side.

X_P Mole fraction of gas in the permeate side.

ΔP Transmembrane pressure difference, Pa.

δ Thickness of membrane, m.

η_{red} Reduced viscosity of polymer solution, dL/g.

$[\eta]$ Intrinsic solution viscosity, dL/g.

v_o, v Kinematic viscosity of solvent and polymer solution, cSt.

ρ Membrane density, g/cm^3.

Chapter 3

Characterization of Gaseous Hydrocarbons-PPO Membrane Interaction: Sorption and Infrared Spectroscopic Methods

- Journal of Membrane Science, 204 (1) (2002) pp. 27-36.
- Journal of Membrane Science, 186 (2) (2001) pp. 281-284.

Abstract

In the presence of gaseous hydrocarbons (methane, acetylene, ethane and ethylene), the infrared (IR) spectrum of poly (phenylene oxide) (PPO) membrane changed at particular bands. When air or helium gas was passed over the PPO membrane sample after its exposure to gaseous hydrocarbons, the IR spectra regained its original shape and intensity. Thus, this phenomenon is reversible and suggests the formation of an unstable complex by the physical interaction between PPO molecules and physically adsorbed gaseous hydrocarbons. Methane and acetylene reacted or affected the PPO IR spectra in the same position, while ethylene in a different position. The effect of ethane gas on the IR spectra of PPO was similar to that observed for ethylene. It was further observed that the physical interaction between the gaseous hydrocarbons and PPO molecules possesses kinetic characteristics; i.e. depends on time and gas partial pressure. The molecular weight of PPO and the solvent (used in preparing PPO solution) boiling point affected the extent of interaction of these gases with the polymeric membranes. A plausible kinetic model is presented.

3.1 Introduction

Infrared spectroscopy (IR) is of greatest value in structural determination of molecules. Its application to the study of surface chemistry has provided one of the most direct means of observing the interactions and perturbations that occur at the surface during adsorption and of determining the structure of adsorbed species. It has been found that certain structural groups of atoms give rise to vibrational bands in the same region of the infrared spectrum, irrespective of the complexity of the molecule in which the group is situated. In such cases it can be assumed that a particular vibration is localized in the structural group.

Electron Spin Resonance (ESR) technique proved that PPO contains free radicals [1]. The number of free radicals was proved to be dependent on whether PPO is in powder form or it is in membrane form. Furthermore, it depends on how the membrane is prepared. The number of spins/g in PPO powder or membrane was found to be higher in the presence of CH_4 gas than CO_2 gas. The spins/g decreased as the preparation temperature of the PPO decreased or the boiling point of the solvent increased. It was concluded that PPO contains electron-donating sites [2].

Puleo and Paul [3] employed IR to study the effect of CO_2 on cellulose acetate membranes. They observed a shift of 4 cm^{-1} in the carbonyl band position (1700-1800 cm^{-1}) upon scanning a "2.45-DS" cellulose acetate film (DS is degree of substitution in a repeat unit) after exposure to CO_2. They also observed a decrease in the intensity of hydroxyl bands of a "2.48-DS" cellulose acetate film in the presence of CO_2. They suggested that it was due to the dipole-dipole interaction between CO_2 and the carbonyl (1700-1800 cm^{-1}) and hydroxyl groups (3000-3600 cm^{-1}). Koros and Story [4] observed

the presence of a peak shoulder at (1740 cm^{-1}) in the spectra of CPPO (carboxylated PPO) membranes after exposure to CO_2 indicating a shift in the carbonyl bands towards their non-hydrogen-bonded position.

In the present chapter, the results of a preliminary study conducted to characterize the interaction of some hydrocarbon gases with PPO membranes, are presented. This study includes:

1. Permeability and sorption measurement of CH_4, C_2H_6, C_2H_4, and C_2H_2 gases in PPO membranes.
2. Characterization of the adsorption of the gaseous hydrocarbons in PPO using IR technique.

3.2 Experimental

3.2.1 Materials

High molecular weight PPO (HMW PPO), having an intrinsic viscosity in chloroform equal to 1.58 dL/g, was kindly supplied by General Electric Company, Selkirk, NY. Low molecular weight PPO (LMW PPO), having an intrinsic viscosity in chloroform equal to 0.76 dL/g, was purchased from Aldrich company. Trichloroethylene (TCE) and bromobenzene, which were used as solvents for PPO, were of reagent grade.

3.2.2 Preparation of Dense Homogeneous Membranes

Dense homogeneous membranes were prepared by pouring 2% (w/w) PPO solutions into stainless steel rings. Table 3.1 lists the different PPO solutions used to prepare the membranes. The stainless steel rings, about 5.5 cm in diameter, were clamped onto the surface of a clean Pyrex glass plate. TCE solvent was removed by drying at room temperature for 24 hours, while bromobenzene was removed by drying in a convective oven at 60°C for 24 hours. Membranes were tested after storing in vacuum at room temperature for at least 48 hours.

Table 3.1: Casting solutions used in the preparation of dense PPO membranes.

Casting solution	Intrinsic viscosity of PPO (dL/g)	Solvent boiling point (°C)
HMW PPO – TCE	1.58	81
LMW PPO – TCE	0.76	81
HMW PPO – Bromobenzene	1.58	153

3.2.3 Permeability Measurements

Three membranes were installed and run simultaneously on the constant volume system. The feed pressure (absolute) was maintained at around 5250±50 mmHg (700 kPa) and

the permeate pressure (absolute) cycle was maintained between 1 mmHg to 750 mmHg (0.133 and 100 kPa absolute). Description of the constant volume system is found in the **General Experimental Methods** chapter.

3.2.4 Density and Sorption Measurements

Experimental procedure and calculations used in determining the density of the membranes, and the sorption of gases in the membranes are detailed in the **General Experimental Methods** chapter.

3.2.5 Infrared Measurements

The infrared setup and operation is explained and discussed in the **General Experimental Methods** chapter.

3.3 Results and Discussion

3.3.1 Sorption and Permeability of Gaseous Hydrocarbons in Denese PPO Membranes

Figure 3.1 presents the sorption of CH_4, C_2H_6, C_2H_4, and C_2H_2 gases, measured in dense PPO membranes prepared from HMW PPO-TCE solution. Table 3.2 reports the sorption and permeability of these hydrocarbon gases in the prepared PPO dense membranes. As noticed in Table 3.2, the sorption of gases increases with the increase of critical temperature [5].

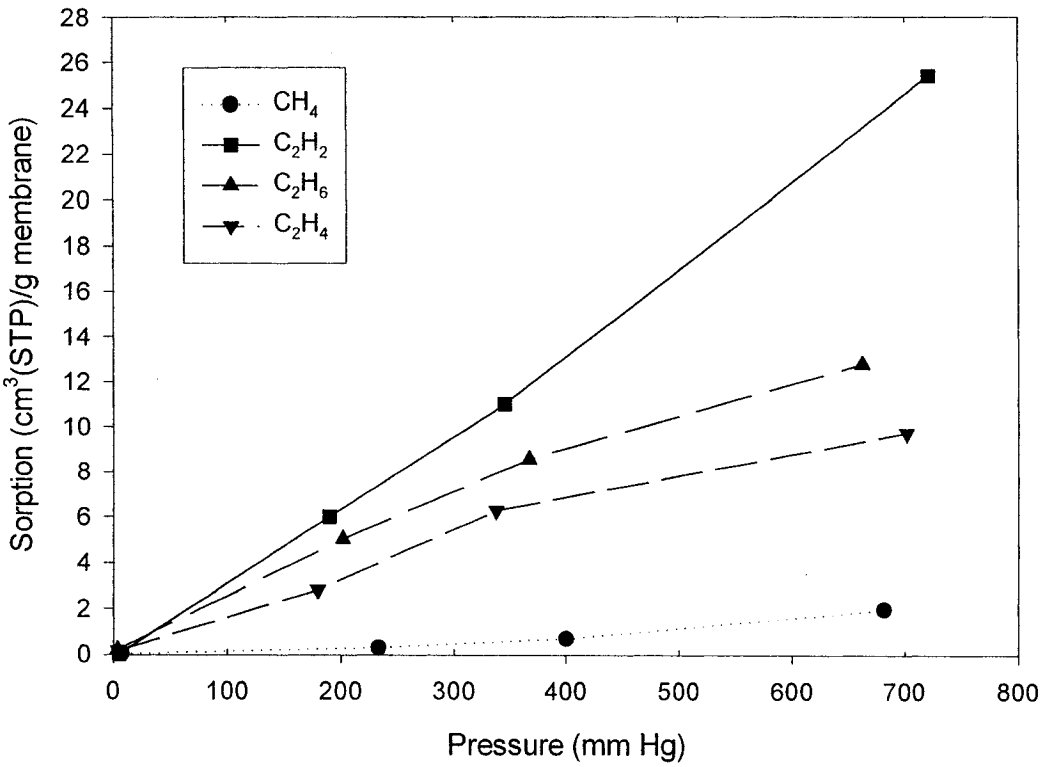

Fig. 3.1: Sorption of CH_4, C_2H_6, C_2H_4, and C_2H_2 gases, in dense PPO membranes prepared from 2% (w/w) HMW PPO-TCE solution.

Table 3.2: Permeability and sorption of gaseous hydrocarbons in dense PPO membranes prepared from HMW PPO-TCE solution.

Gaseous hydrocarbon	Molecular weight	Critical temperature (°C)	Permeability[1] (Barrer)	Sorption[2] (cm^3 (STP)/g membrane)
Acetylene	26	36	17.8	26.0
Ethane	30	32.1	3.6	13.5
Ethylene	28	9.7	9.6	10.5
Methane	16	-82.5	5.0	2.3

[1]Measured at permeate pressure ≈ 750 mmHg.
[2]Obtained by linear extrapolation to 750 mmHg pressure based on data presented in Fig. 3.1.

3.3.2 IR Spectra of PPO Membranes in the Presence of Gaseous Hydrocarbons

Figures 3.2 and 3.3 compare the IR spectra of PPO dense membranes prepared from 2% HMW PPO-TCE solution. IR spectra were taken upon exposing dense membranes to helium gas and to mixtures of helium and gaseous hydrocarbons. The thickness of dense PPO membrane samples used for the IR study was 6.0μm (variability less than 1.0μm). Upon exposing HMW PPO membranes to these gaseous hydrocarbons, the IR spectra of PPO were affected at different bands.

Figure 3.2 shows that C_2H_2 affected the same bands as CH_4 gas did, i.e. bands 3100 to 2600 cm^{-1} and 1300 cm^{-1}, while Fig. 3.3 shows that C_2H_6 and C_2H_4 gases affected bands at 1450 cm^{-1} and 3100 to 2600 cm^{-1}. All these changes were reversible upon purging the membrane with He gas or air.

Table 3.3 lists the possible IR frequency assignment for the different PPO bands [6,7,8]. Figure 3.4-a shows the IR spectrum of acetylene. Bands at 3200~3400 cm^{-1} are due to acetylenic (alkynes) C-H stretching, and band at 700~750 cm^{-1} is due to alkyne C-H bending with its overtone at 1300~1200cm^{-1}. Figure 3.4-b shows the IR spectrum of methane gas. Methyl C-H bending has bands at 1250-1350 cm^{-1}, and bands at 2900~3000

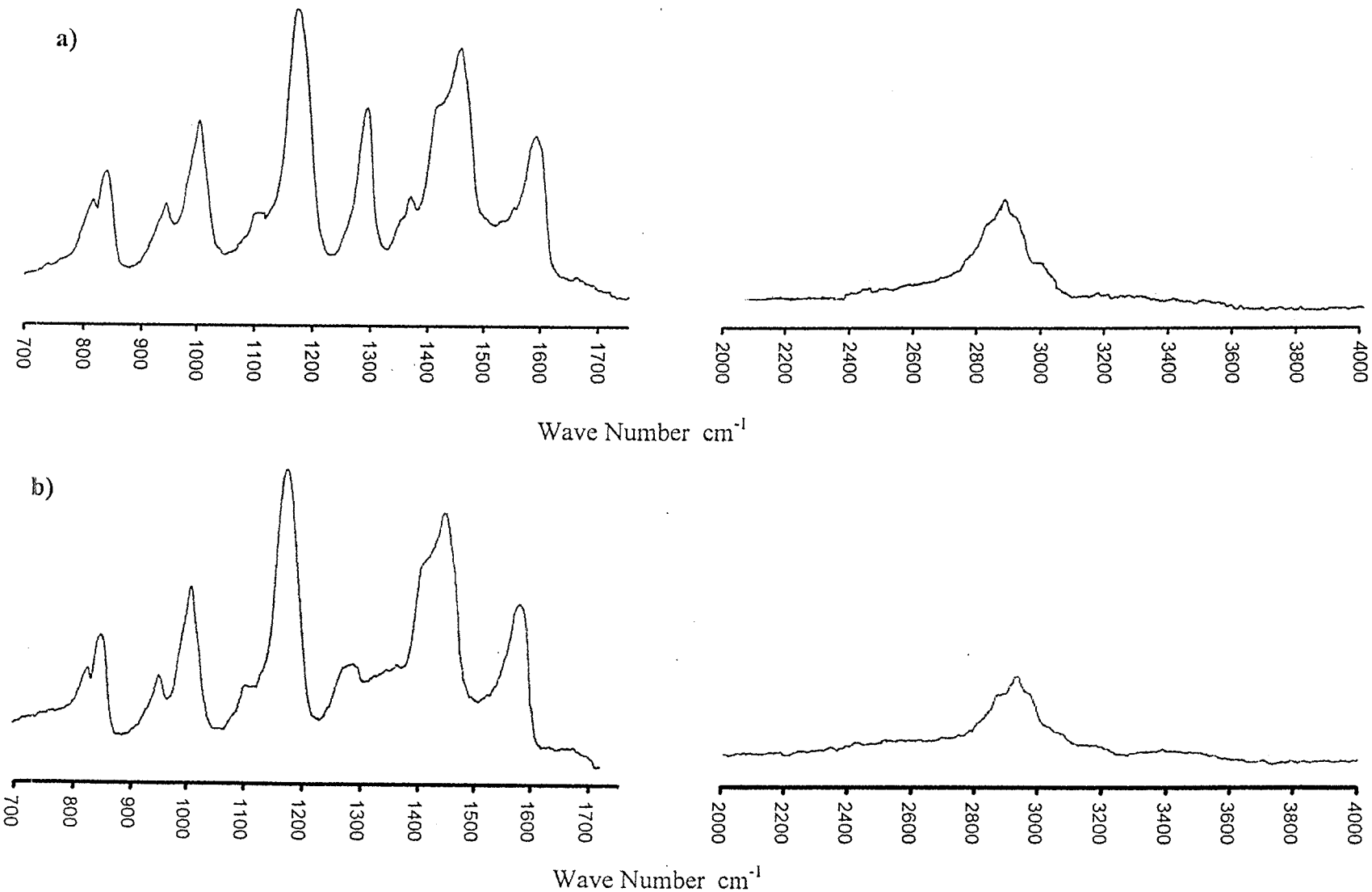

Fig. 3.2: IR spectrum of PPO in the presence of: **a)** He; **b)** 45% C_2H_2 in He; and **c)** 43% CH_4 in He.

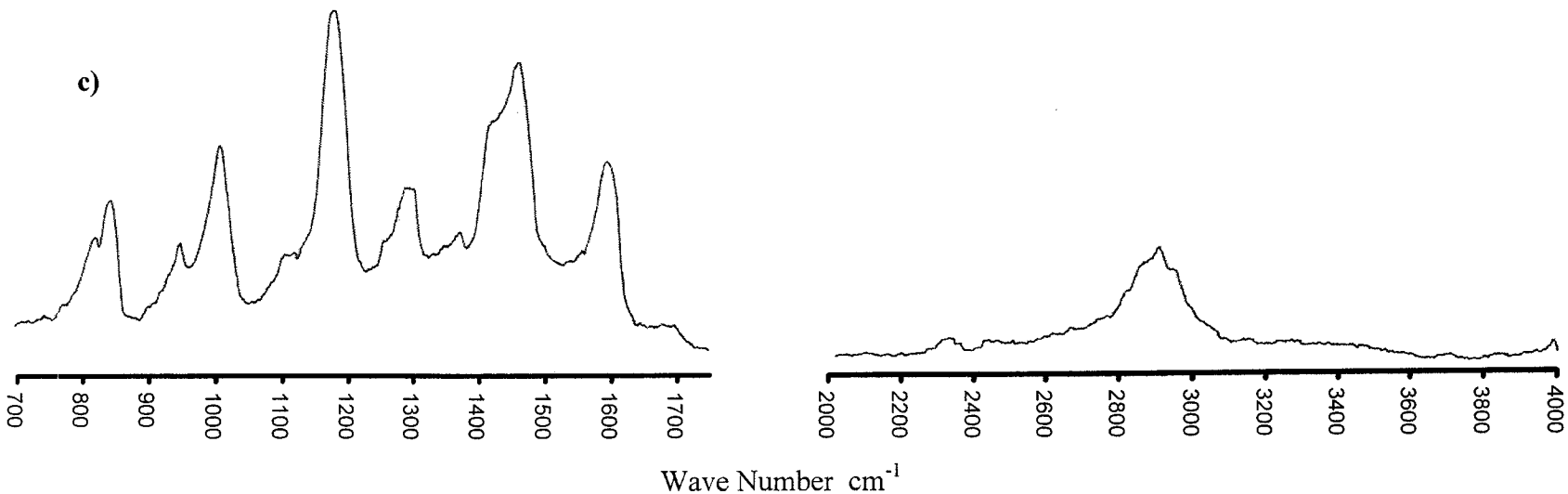

Fig. 3.2 – continued.

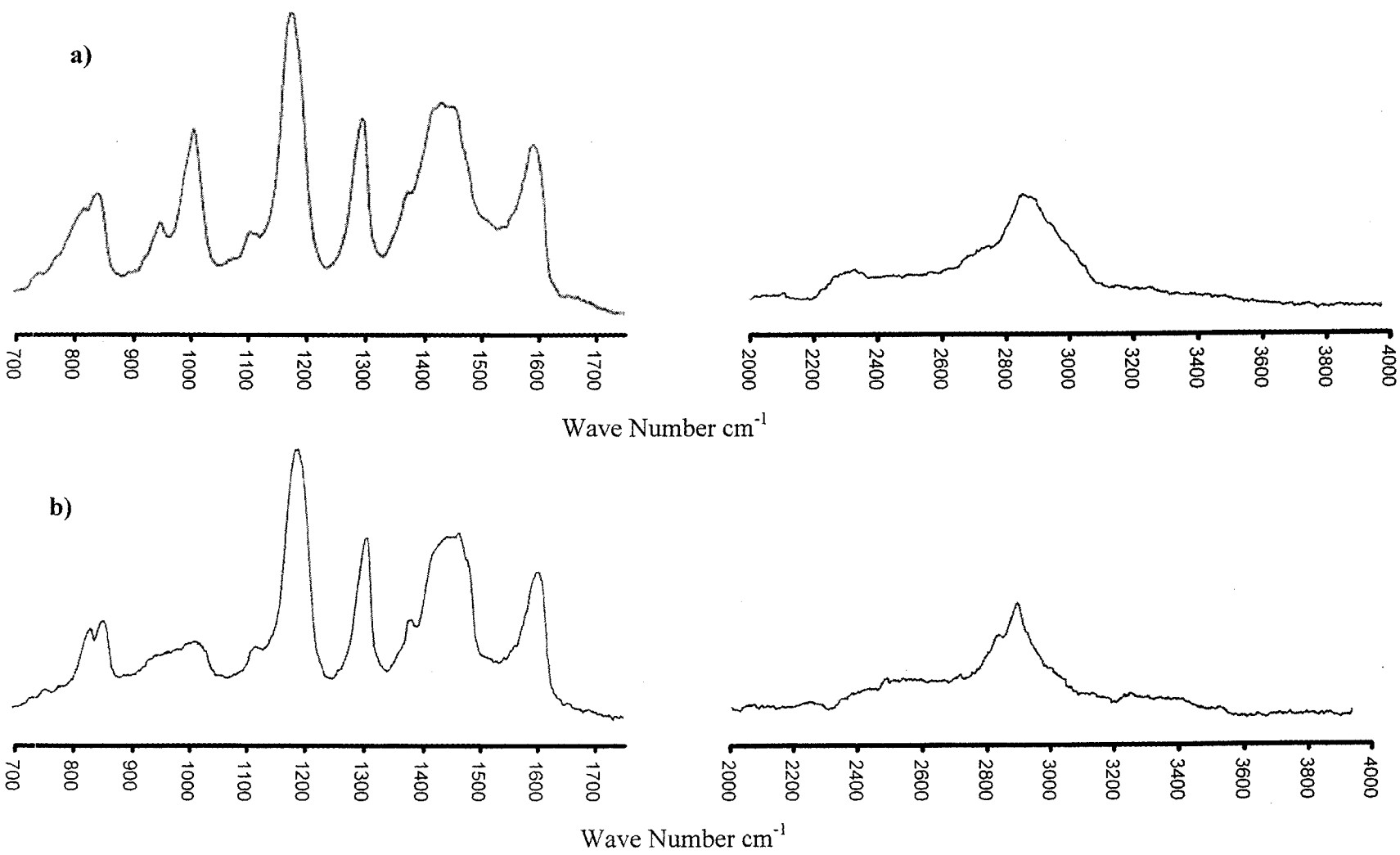

Fig. 3.3: IR spectrum of PPO in the presence of: **a)** 14% C_2H_6 in He; and **b)** 20% C_2H_4 in He.

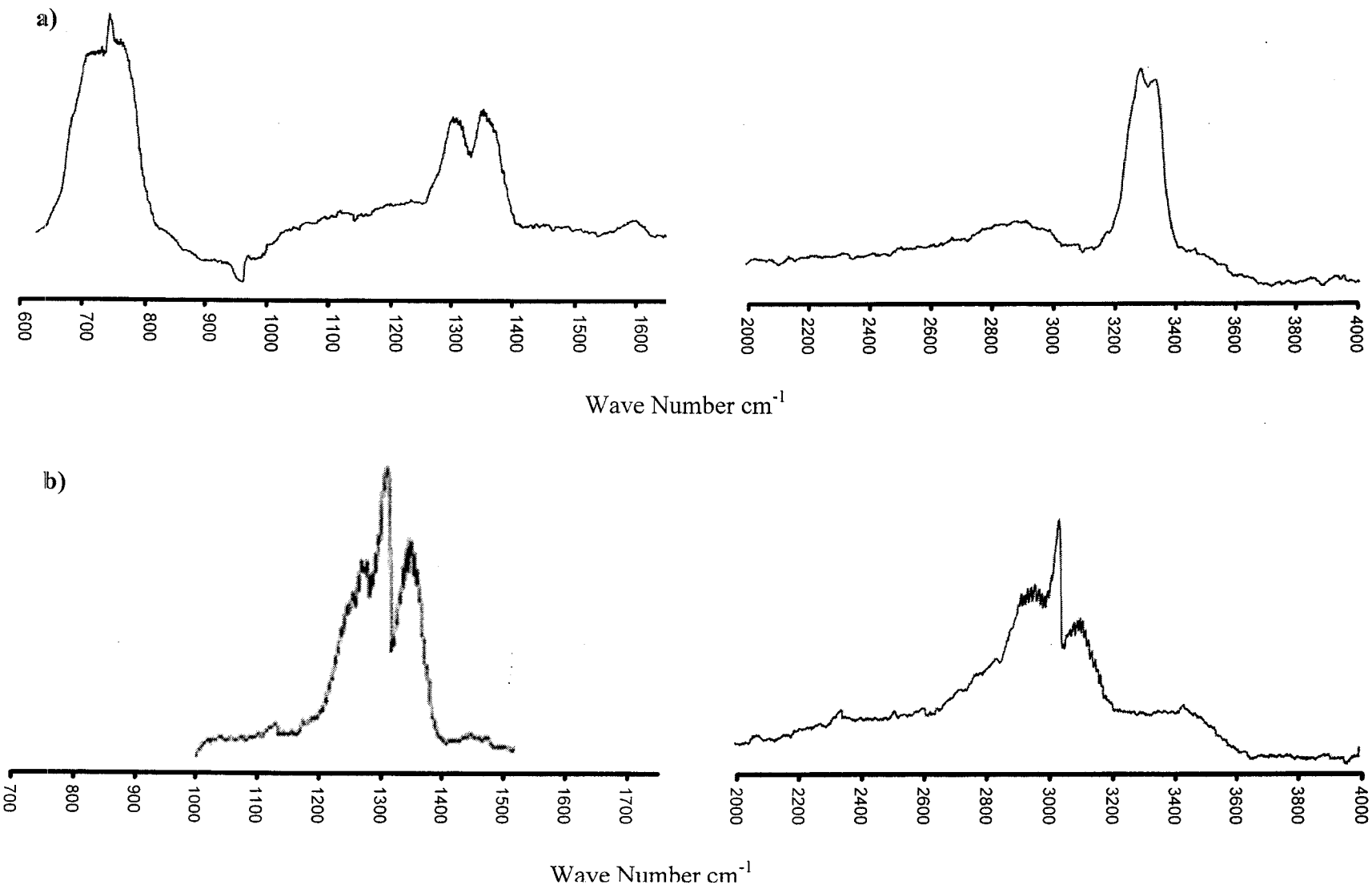

Fig. 3.4: IR spectrum of gaseous hydrocarbon-He mixture: **a)** 10% C_2H_2, **b)** 10% CH_4, **c)** 17% C_2H_6, and **d)** 15% C_2H_4.

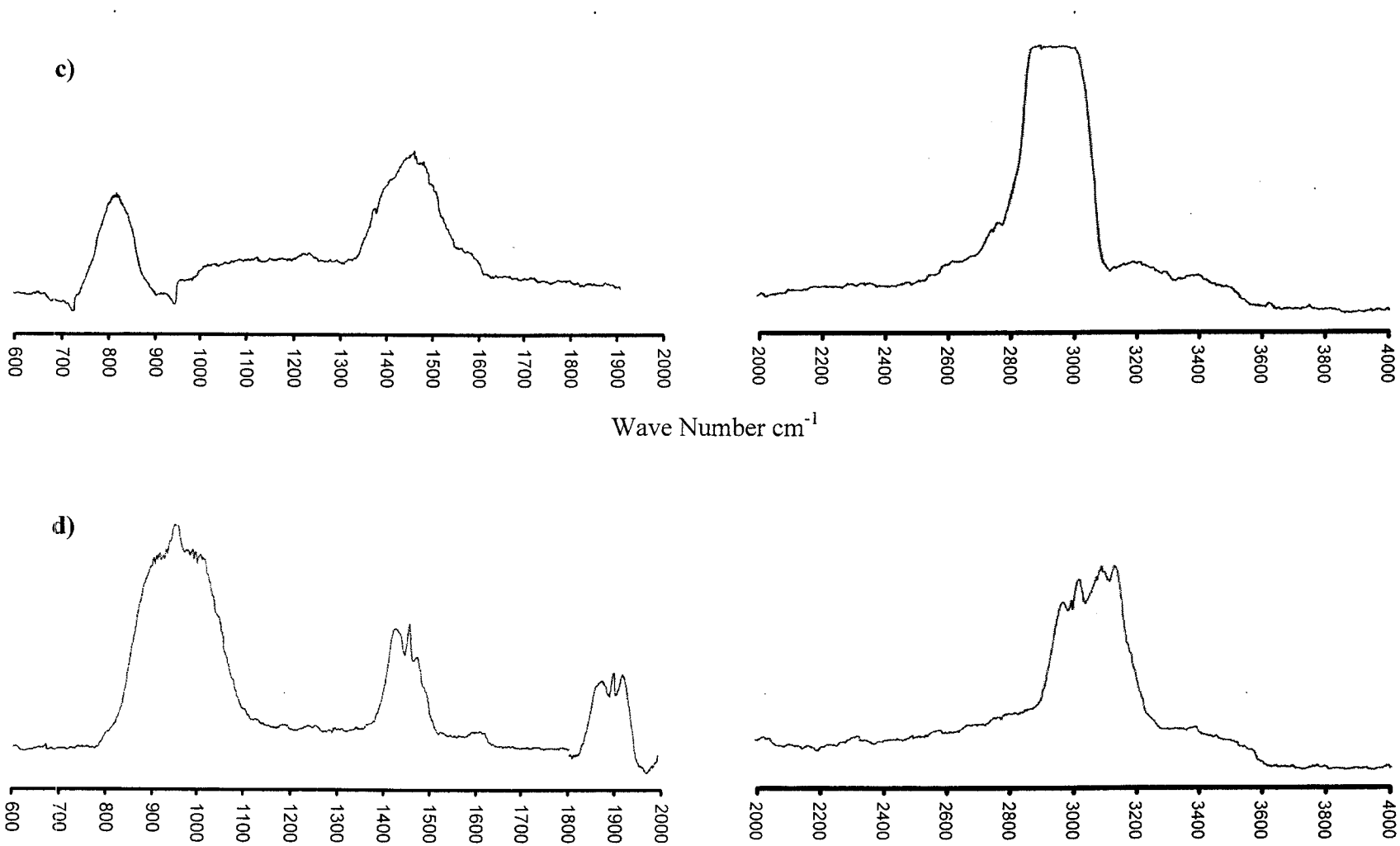

Figure 3.4 – continued.

Table 3.3: IR frequency assigned to PPO bands.

Frequency cm^{-1}	Intensity	Vibration
3080-2800	Broad	Stretching alkane and aromatic C-H
1600	Sharp	C-C aromatic ring
1470	Sharp	Bending CH_2, anti-bending CH_3
1420-1450	Weak	Stretching CC aromatic
1380	Weak	Symmetric bending CH_3
1300	Sharp	C-O-C, C-C bridge bond
1180	Sharp	Plane CH bend
1120	Shoulder	Anti-stretching C-O-C
1010	Sharp	Trigonal ring breathing
950	Weak	Bending C-O-C
850	Sharp	Aromatic C-H out of plane bending
820	Sharp	Unknown

cm^{-1} are assigned to alkane C-H stretching. The IR spectrum of ethane (alkanes) is shown in Fig. 3.4-c. Alkane C-H stretching band appears at 2800~3000 cm^{-1}. Methyl C-H bending appears at 1450 cm^{-1}. Figure 3.4-d shows the IR spectrum of ethylene. Olefinic (alkenes) C-H stretching appears at 3000~3200 cm^{-1}. In plane and out of plane alkene C-H bending shows at 1450 and 950 cm^{-1}, respectively [9,10].

It is known that physical adsorption of molecules involves the formation of weak bonds due to hydrogen bonding and other weaker forces. These weak forces allow the adsorbed molecules to be removed by purging or evacuating the gas. Physical adsorption of molecules gives rise to a similar IR spectrum to that of the liquid phase on condensation [11]. However, because of the asymmetric nature of the force field at the surface, in comparison to the symmetric environment surrounding a molecule in the liquid phase, adsorbed molecules can give rise to additional effects on the IR spectrum. As observed in Figs. 3.2 and 3.3, affected PPO bands had broadened and their intensities decreased in the presence of the different gaseous hydrocarbons. Ethane and ethylene had affected mainly the bands at 1450 cm^{-1} and 3100 to 2600 cm^{-1}, while methane and acetylene had affected

mainly the 1300 cm^{-1} and 3100 to 2600 cm^{-1}. The adsorbed hydrocarbon molecules are interacting with PPO molecules by forming unstable complexes resulting in the distortion of the bands common to PPO and gaseous hydrocarbons. Therefore, the intensities of these bands are reduced, however, the broadening of the bands is due to the increase in the population of molecules in the IR active area.

3.3.3 CH_4-PPO Membranes Interaction

It is observed that the interaction between methane gas and the PPO membrane, as monitored by the change in the 1300 cm^{-1} IR band, is dependent on the molecular weight of PPO (intrinsic viscosity in chloroform as a measure of weight average molecular weight) used to prepare the membrane. As well, it is dependent on the volatility or the boiling point of the solvent used in preparing the PPO solution. This is clearly noticed in Table 3.4. As the molecular weight of PPO decreases or the boiling point of the solvent used in preparing the PPO solution increases, the interaction becomes less.

Table 3.4: Effect of the molecular weight of PPO and solvent used in preparing PPO solutions on the reduction in 1300 cm^{-1} IR band of PPO.

PPO (intrinsic viscosity)	Solvent (boiling point)	Reduction in 1300 cm^{-1} band area (%)
HMW (1.58 dL/g)	TCE (81°C)	48.0
LMW (0.76 dL/g)	TCE (81°C)	28.1
HMW (1.58 dL/g)	Bromobenzene (153 °C)	19.8

It is expected that the crystalline domain in the polymer decreases and the polymer also becomes more relaxed as the molecular weight decreases and as the polymer solution is prepared from less volatile solvent. Therefore, it is expected that the irregularities in the PPO backbone to decrease as the molecular weight of PPO decreases, or as the volatility

of the solvent decreases.

It is interesting to note that the change in the 1300 cm^{-1} IR band of PPO in the presence of CH_4 shows that this interaction possesses kinetic characteristics; i.e. the change in the 1300 cm^{-1} IR band is dependent on both time and concentration of CH_4 gas. In Figs. 3.5 and 3.6, the ratio of the 1300 cm^{-1} band area in the presence of CH_4 to the band area in the absence of CH_4 gas is denoted as A, and (1-A) is plotted as a function of CH_4 gas concentration (mol/mol %) in CH_4/He mixtures. The higher the gas concentration is, the more reduction in the 1300 cm^{-1} band is observed. This reduction in the 1300 cm^{-1} band follows a trend similar to a first order dynamic system, as seen in Fig. 3.6.

A kinetic model is presented in the following to describe quantitatively the change in the

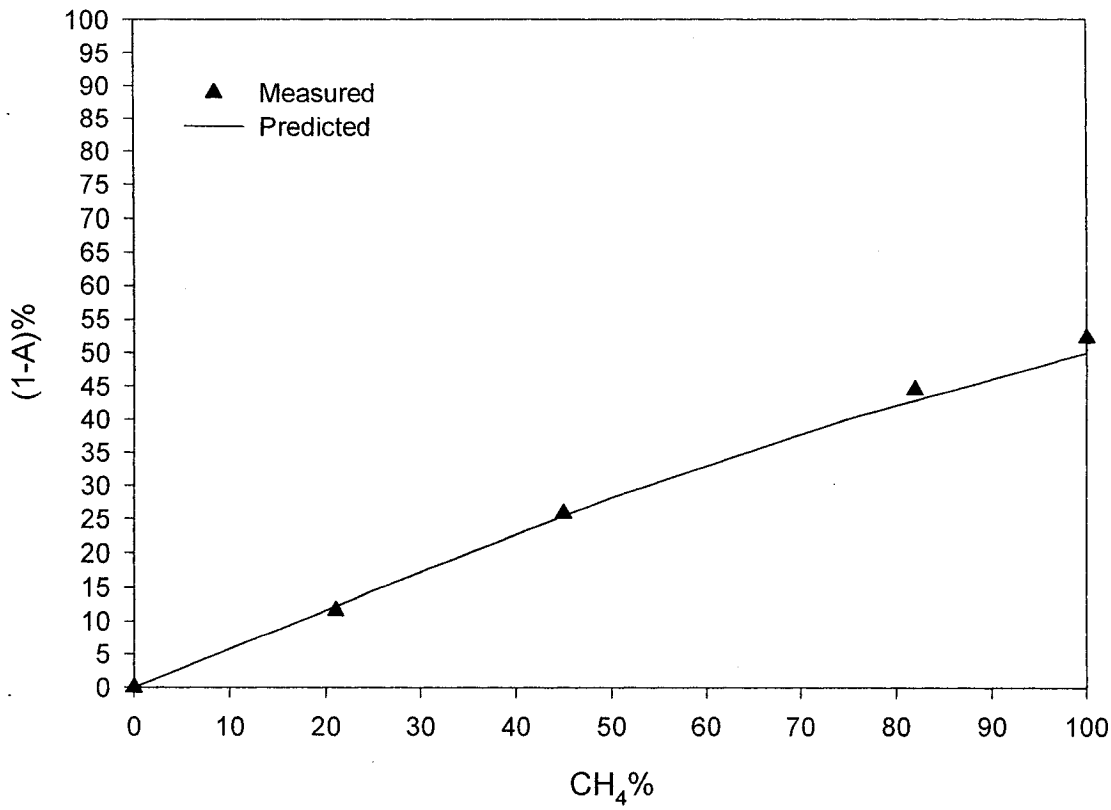

Fig. 3.5: Reduction in band 1300 cm^{-1} area at plateau as a function of CH_4 concentration (mol/mol%) in He mixture.

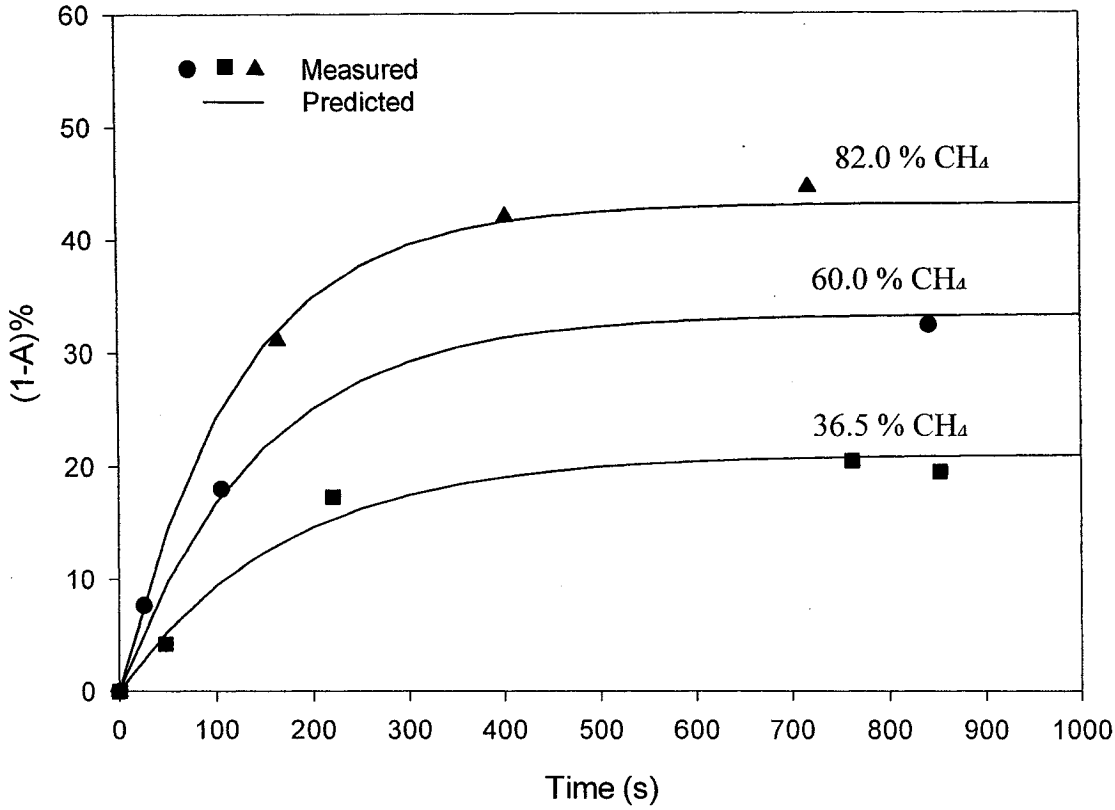

Fig. 3.6: Reduction in band 1300 cm^{-1} area as a function of time.

area of band 1300 cm^{-1} observed above. The model assumes that the interaction between methane gas and the PPO membrane occurs in two steps; a swift adsorption of methane gas (CH_{4g}) into the PPO membrane, followed by a slow interaction (reaction) of the adsorbed methane molecule ($CH_{4\,ads}$) with an active site.

$$CH_{4_g} \underset{k'_2}{\overset{k'_1}{\rightleftharpoons}} CH_{4_{ads}} \quad (1)$$

$$CH_{4_{ads}} + S_e \underset{k_2}{\overset{k_1}{\rightleftharpoons}} S_o \quad (2)$$

where k_1' and k_2' are adsorption and desorption rate constants, respectively. k_1 and k_2 are forward and backward reaction rate constants, respectively. S_e represents empty active sites in the membrane and S_o represents the occupied active sites in the membrane. The sum of the concentration of S_e, $[S_e]$, and the concentration of S_o, $[S_o]$, is constant.

$$[S_e] + [S_o] = [S_T] \quad (3)$$

Assuming that step (1) above is very fast in comparison to step (2), then step (2) is controlling the interaction rate and it can further be assumed that the adsorption step (1) is always at equilibrium. Therefore, the concentration of CH_4 adsorbed, $[CH_4]_{ads}$, can be related to its concentration in the gaseous phase, $[CH_4]_g$ by

$$[CH_4]_{ads} = \frac{k_1'}{k_2'} \cdot [CH_4]_g = K_{eq} \cdot [CH_4]_g \qquad (4)$$

where K_{eq} is the adsorption equilibrium constant. The rate of interaction is then determined by step (2):

$$\frac{d[S_e]}{dt} = k_2 \cdot [S_o] - k_1 \cdot [CH_4]_{ads} \cdot [S_e]$$

$$\frac{d[S_e]}{dt} = k_2 \cdot ([S_T] - [S_e]) - k_1 \cdot [CH_4]_{ads} \cdot [S_e] \qquad (5)$$

Assuming that the area of band 1300 cm^{-1} is proportional to the concentration of the empty active sites, then:

$$A = [S_e] / [S_T]$$

Therefore, A =1 when the membrane is in helium environment since all active sites are empty.

Then, dividing equation (5) by $[S_T]$ and rearranging:

$$\frac{dA}{dt} = k_2 \cdot (1 - A) - k_1 \cdot [CH_4]_{ads} \cdot A \qquad (6)$$

Further rearranging of equation (6) and integrating:

$$\int_1^A \frac{dA}{(k_1 \cdot [CH_4]_{ads} + k_2) \cdot A - k_2} = -\int_0^t dt$$

$$(1 - A) = \left[\frac{k_1 \cdot [CH_4]_{ads}}{k_1 \cdot [CH_4]_{ads} + k_2}\right] \cdot \left[1 - Exp\left(-(k_1 \cdot [CH_4]_{ads} + k_2) \cdot t\right)\right] \qquad (7)$$

The value of $[CH_4]_{ads}$ was estimated via sorption measurements for CH_4 gas in PPO (see Fig. 3.1) using the constant volume method detailed in the **General Experimental Methods** chapter. The values of k_1 and k_2 were estimated by applying equation (6) to the measured area ratio of the 1300 cm^{-1} band obtained at different times. Appendix A details the process of obtaining k_1 and k_2. Values of k_1 and k_2 were obtained from runs 36.5 and 60.0% CH_4/He mixtures. The average values for k_1 and k_2 were estimated to be 67.3 [cm^3 (membrane)/ (s. mole adsorbed gas)] and 0.0047 [s^{-1}], respectively. Figures 3.5 and 3.6 show that the prediction of the derived model, equation (7), is in very good agreement with the experimental observations.

It should be noted that the model assumes that helium gas does not adsorb into the membrane. When this model is used to predict the change in the 1300 cm^{-1} band using CH_4/N_2 gas mixture instead, the prediction deviates significantly from the experimental observations, as can be seen in Fig. 3.7. The plateau area ratio of band 1300 cm^{-1} (A) when CH_4/N_2 gas mixture was used is less than that when CH_4/He gas mixture was used. This could be explained by considering that N_2 is yet a more soluble gas when compared to He. N_2 molecules are competing with CH_4 molecules to adsorb into PPO membrane and therefore displacing some of CH_4 molecules from the active site.

It is necessary to mention that the model may not be applicable in the case of desorption of CH_4 from PPO membrane. Other intermediate steps could become significant.

3.5 Conclusions

1. Gaseous hydrocarbons interact physically with PPO membranes to form unstable complexes that can be easily removed by purging the membranes with an inert gas such as helium.
2. The physical interaction between the gaseous hydrocarbons and the PPO membrane

possesses kinetic characteristics; i.e. it depends on time and the gas partial pressure.

3. Physical factors that contribute to the presence of irregularities in the polymer backbone in the membrane; such as the polymer molecular weight and the solvent boiling point used in the casting solution, affect the extent of interaction of these gases with polymeric membranes.

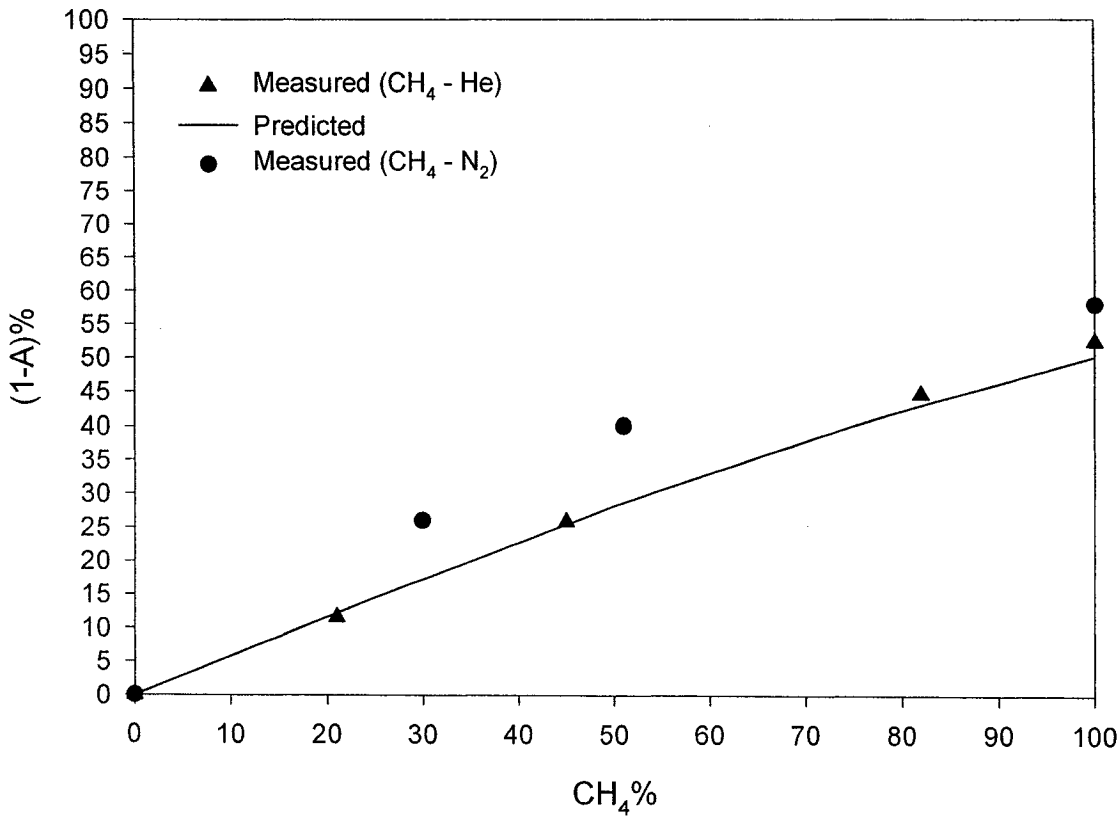

Fig. 3.7: Reduction in band 1300 cm^{-1} area at plateau as a function of CH_4% in He and N_2 mixtures.

3.6 References

[1] K.C. Khulbe and T. Matsuura: "*Characterization of Synthetic Membrane by Raman Spectroscopy, Electron Spin Resonance, and Atomic Force Microscopy; A Review*", Polymer, 41, (2000) 1917-1935.

[2] K.C. Khulbe, G. Chowdhury, B. Kruczek, R. Vujosevic, T. Matsuura, and G.

Lamarche: "*Characterization of the PPO Dense Membranes Prepared at Different Temperatures by ESR, Atomic Force Microscope, and Gas Permeation*", J. Membr. Sci., 126, (1997) 115-122.

[3] D. P. Puleo: "*Effect of Degree of Acetylation on Gas and Transport Behaviour in Cellulose Acetate* ", J. Membr. Sci., 47 (3), (1989) 301-332.

[4] W.J. Koros and B.J. Story: "*Sorption and Transport of CO_2 and CH_4 in Chemically Modified Poly (Phenylene Oxide)*", J. Membr. Sci., 67, (1992) 191-210.

[5] R. Kesting and A. Fritzche: "*Polymeric Gas Separation Membranes*", Wiley Interscience, New York, 1993.

[6] D. Lin-Veien, N.B. Colthup, W.G. Fateley, and J.G. Grasselli: "*The Handbook of IR and Raman Characteristic Frequencies of Organic Molecules*", Academic Press, New York, 1991.

[7] I. W. Shepherd: "*Advances in Infrared and Raman Spectroscopy*", Vol. 3, R.J.H. Clark and R. Hester (Eds.), Heydon, London, 1977.

[8] G. Varsanyi: "*Assignments of Vibrational Spectra of 700 Benzene Derivatives*", Wiley and Sons, New York, 1975.

[9] G. Socrates: "*Infrared Characteristic Group Frequencies: Tables and Charts*", 2nd edn., John Wiley and Sons, New York, 1994.

[10] N.B. Colthup, L.H. Daly, and S.E. Wiberly: "*Introduction to Infrared and Raman Spectroscopy*", 3rd edn., Academic Press, New York, 1991.

[11] L.H. Little: "*Infrared Spectra of Adsorbed Species*", Academic Press, New York, 1966, chapter 11, pp 296.

3.7 Nomenclature

A Ratio of empty active sites concentration to total active sites concentrations.

$[CH_4]$ Concentration of methane in the gaseous phase, mol/cm^3.

$[CH_4]_{ads}$ Concentration of methane adsorbed in the membrane, $mol/(cm^3_{membrane})$.

K_{eq} Adsorption equilibrium constant of methane-PPO system, $(cm^3_{gas})/(cm^3_{membrane})$.

k_1 Forward reaction rate constant, $(cm^3_{membrane})/(s\ mol)$.

k_2 Backward reaction rate constant, 1/s.

k_1' Adsorption rate constant, $(cm^3_{gas})/s$.

k_2' Desorption rate constant, $(cm^3_{membrane})/s$.

$[S_e]$ Concentration of empty active sites, $mol/(cm^3_{membrane})$.

$[S_o]$ Concentration of occupied active sites, $mol/(cm^3_{membrane})$.

$[S_T]$ Total concentration of active sites, $mol/(cm^3_{membrane})$.

Appendix

3.A Evaluation of k_1 and k_2

Equation (6) can be rearranged to give the following equation:

$$-\frac{dA}{dt} = \left(k_1 \cdot [CH_4]_{ads} + k_2\right) \cdot A - k_2 \qquad (6\text{-a})$$

Equation (6-a) represents the rate of interaction, or the rate of change in the area of the 1300 cm^{-1} band.

Table 3.A.1 provides some experimental data and calculated area ratio obtained for the run with a feed mixture containing 36.5% of CH_4 in He (mol/mol). The experimental data include the time of exposure and the corresponding 1300 cm^{-1} band area. It is important to note that the area of band 1300 cm^{-1} at the beginning of the run (time = 0 s.) corresponds to that particular band area in the presence of He gas (i.e. before CH_4 is introduced).

Table 3.A.1: Experimental and calculated data concerning the 1300 cm^{-1} band area for the run with a feed mixture containing 36.5% CH_4 in He gas.

Time (s)	1300 cm^{-1} band area (cm^2)	A	(1-A) %	$-\frac{dA}{dt}$ (s^{-1})
0	5.03	1	0	8.82×10^{-4}
47	4.82	0.958	4.2	8.19×10^{-4}
221	4.16	0.827	17.3	4.07×10^{-4}
762	4.00	0.795	20.5	-2.52×10^{-5}
853	4.05	0.805	19.5	3.46×10^{-5}

The rate of interaction is calculated using the finite difference concept; forward finite difference was used to calculate rate at time = 0 s, while backward finite difference was used for last point (time = 853 s), and central finite difference was used for middle points.

The plot of the rate of interaction (-dA/dt) vs. the area ratio of band 1300 cm^{-1} (A) was made for CH_4/He gas mixtures with 36.5 and 60.0% CH_4 and a set of k_1 and k_2 was obtained. Figure A.1 presents the plot of (-dA/dt) vs. (A) for 36.5% CH_4/He mixture. The linear correlation between (-dA/dt) was obtained using the linear regression utility of SIGMA PLOT software used to construct Fig. 3.A.1.

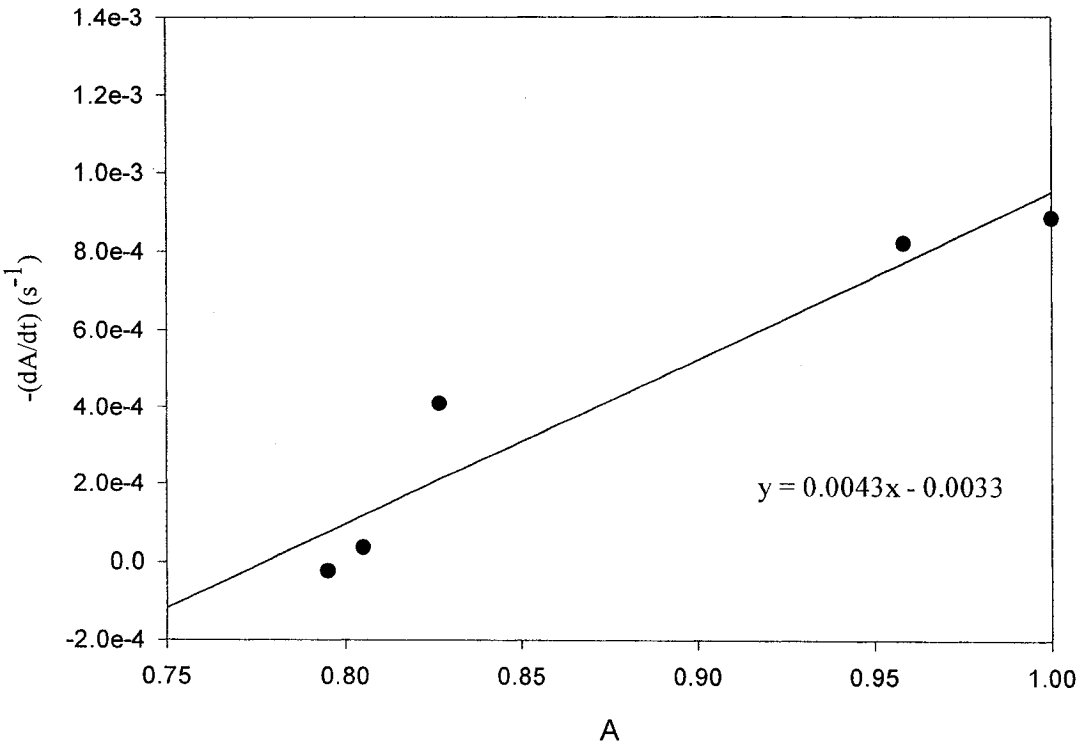

Fig. 3.A.1: Plot of interaction rate vs. A for run 36.5% CH_4 in He gas.

From the linear regression correlation shown in Fig. A.1, k_1 and k_2 can be deduced as follows:

$$-\frac{dA}{dt} = \left(k_1 \cdot [CH_4]_{ads} + k_2\right) \cdot A - k_2$$

$$k_2 = 0.0033\ (s^{-1})$$

$$k_1 \cdot [CH_4]_{ads} + k_2 = 0.0043\ (s^{-1})$$

$$k_1 = \frac{0.0043 - 0.0033}{[CH_4]_{ads}} = \frac{0.0010}{1.55 \times 10^{-5}} = 64.5\ (\frac{cm^3}{s \cdot mol})$$

Table 3.A.2 summarizes the values of k_1 and k_2 obtained based on 36.5 and 60.0% CH_4/He gas mixtures. $[CH_4]_{ads}$ can be obtained from Fig. 3.1. It is important to note that in the previous derivations and calculations, helium gas did not adsorb in the membrane at all, while only CH_4 gas did.

Table 3.A.2: k_1 and k_2 values calculated from linear regression analysis of the correlation between the interaction rate (-dA/dt) vs. 1300 cm^{-1} area ratio (A) for runs with 36.5 and 60.0% CH_4/He feed gas mixture.

	36.5% CH_4/He	60.0% CH_4/He	Average
k_1 (cm^3/s/mol)	64.5	66.7	65.6
k_2 (s^{-1})	0.0033	0.0061	0.0047

The values of k_1 and k_2 shown in Table 3.A.2 were deduced from the linear regression analysis of the differential form of the rate equation (6). Equation (7) could be used as well to obtain the k_1 and k_2 using a nonlinear regression technique. The values of k_1 and k_2 shown in Table 3.A.3 were solved for using equation (7) to minimize the sum of square errors between the experimental and predicted values.

Table 3.A.3: k_1 and k_2 values calculated based on equation (7) using a nonlinear regression technique.

	36.5% CH_4/He	60.0% CH_4/He
k_1 (cm^3/s/mol)	93.4	76.5
k_2 (s^{-1})	0.0057	0.0056
Sum of Square Errors	4.7×10^{-4}	3.0×10^{-4}

It should be noted that k_1/k_2 obtained by both methods are very similar, while there are considerable differences for individual k_1 and k_2.

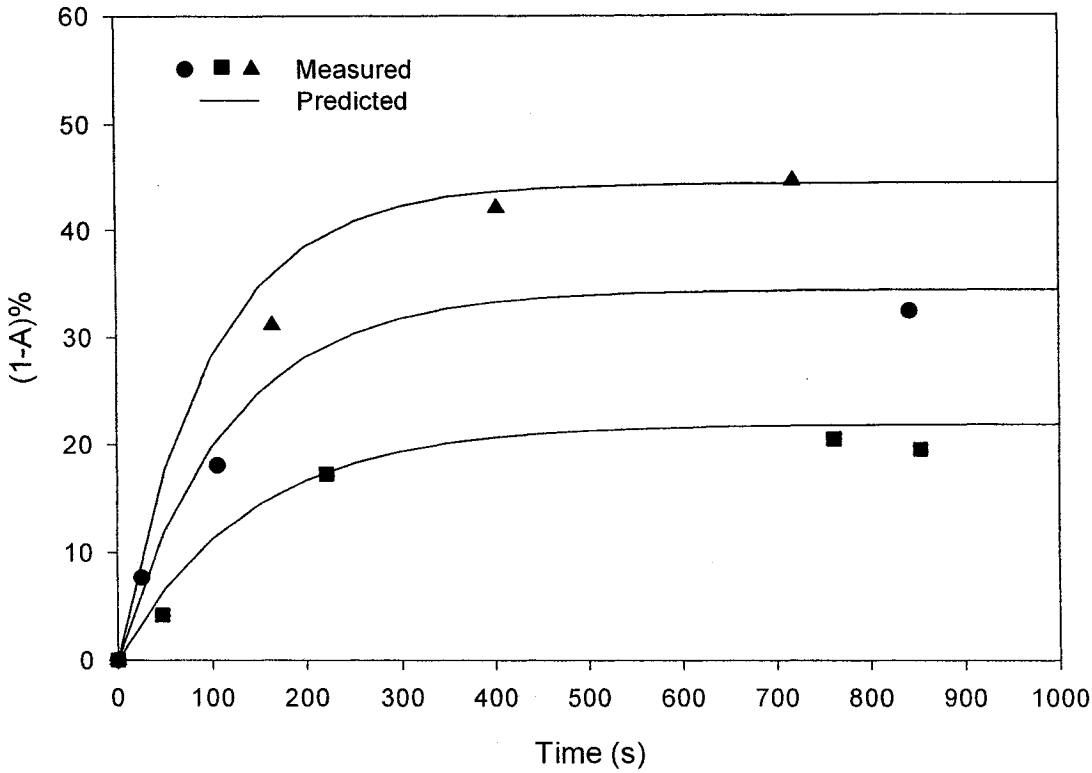

Fig. 3.A.2: Reduction in band 1300 cm^{-1} area as a function of time. Predicted trends are based on k_1 and k_2 values shown in Table 3.A.3.

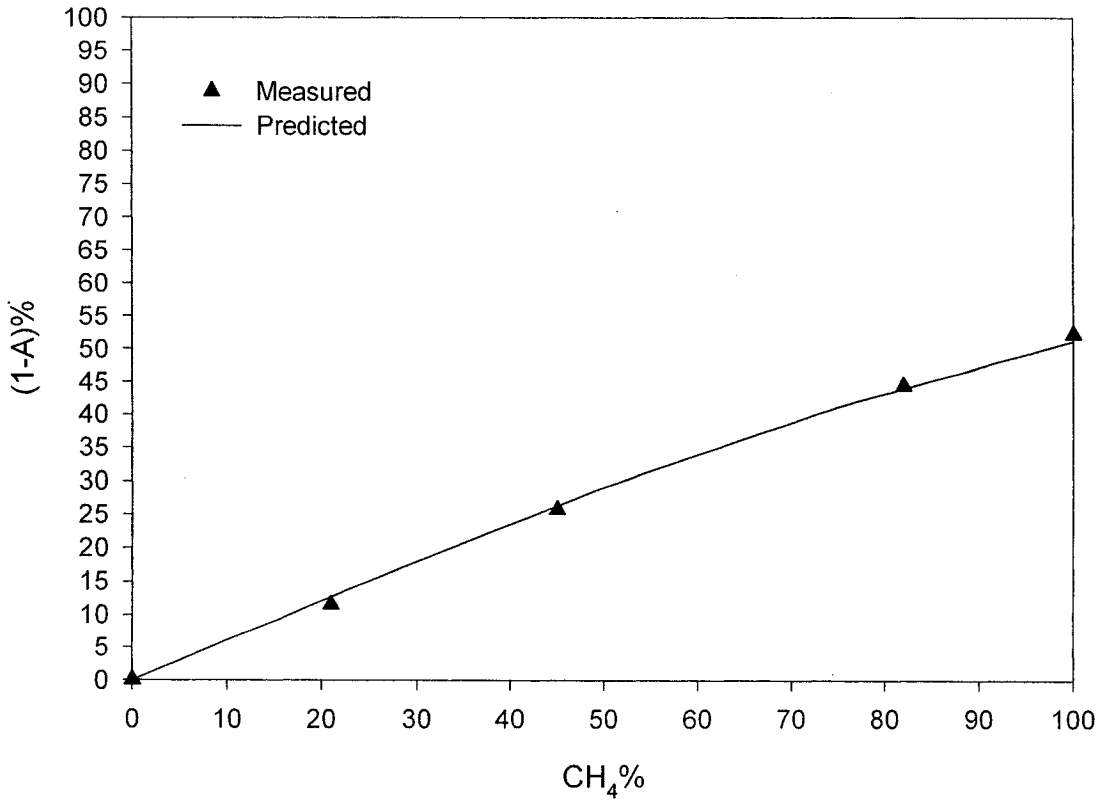

Fig. 3.A.3: Reduction in band 1300 cm^{-1} area at plateau as a function of CH_4. Predicted trend is based on k_1 and k_2 values shown in Table 3.A.3.

Chapter 4

Gas Separation Performance of Membranes Made from Sulfonated Poly (Phenylene Oxide): Effect of Counter-Cations on the Gas Transport Properties

- Proceedings of the International Congress on Membranes and Membrane Processes (ICOM 2002), Desalination 145 (2002) 365–370.
- Journal of Membrane Science, 191 (1-2) (2001) pp. 71-83.

Abstract

Composite membranes based on sulfonated poly (phenylene oxide) (SPPO) as the top selective layer, and poly ethersulfone (PES) ultrafiltration membrane as the support layer, were prepared. It was found that the resistance to gas permeation imposed by the PES support layer increased significantly upon exposure to the solvent used in the coating solution. The polymer polarity and density of sulfonated poly (phenylene oxide) (SPPO) membranes were manipulated by exchanging the proton of the sulfonic groups with mono-, di-, and tri-valent metal cations. The performance of the composite membranes coated with ion-exchanged SPPO, toward the separation of CO_2/CH_4 and O_2/N_2 gas systems, was found to correlate with the location of the metal in the universal periodic table of the chemical elements. Altering the metal cation that replaces the proton of the sulfonic groups alters: the cross-linking forces, the hindrance effects due to the voluminous metal size, and the SO_3-metal groups polarity due to the change in the metal electronegativity.

4.1 Introduction

The trend in material development for better gas separation membranes is mainly toward improving the properties of existing polymers, which is attained via chemical and/or physical modification of the polymers to favor the transport properties of the gases of interest.

Poly (2,6-dimethyl-1,4-phenylene oxide) (PPO) possesses a linear structure with very low transition temperature assigned to the rotational motion of its phenyl ring [1]. PPO has the highest gas permeability among aromatic polymers with high glass transition temperature. The presence of ether linkages and the absence of polar groups suppress chain packing and densification. The methyl groups attached on both sides of the phenyl ring hinder the free rotation of the phenyl ring, resulting in moderate selectivity of PPO membranes [2]. Even though permeability of PPO to gases is high, its permselectivity is low compared to other glassy polymers [2-6].

A possible mode of improving the permselective property of a polymer is by introduction of polar groups inducing stronger interchain interactions. Chen and Martin [7] have obtained O_2/N_2 selectivity of 11.7 using sulfonated polystyrene. Improved gas transport properties of PPO were observed by Ghosal and Chern via aryl-nitration of the polymer [8]. Attempts to improve the permselectivity of PPO by sulfonation were made. Fu et al. [3] reported that the permeability ratio of O_2/N_2 increased while O_2 permeability decreased significantly by sulfonating PPO. Kruczek and Matsuura [9] reported a decrease in the permeability of gases upon increasing the degree of PPO sulfonation, while CO_2/CH_4 and O_2/N_2 permselectivities increased. In the same work, they reported the performances of sulfonated PPO with metal counter ions such as Na^+, Mg^{2+}, and Al^{3+}.

The high selectivity of Mg^{2+}-form was explained by the fact that Mg^{2+} cation would crosslink two sulfonate groups. Bikson and Nelson [10] reported O_2/N_2 separation factor of about 7.1 by using a composite membrane having separation layer comprised of SPPO in the lithium form. Polotskaya et al. [11] reported improved selectivity of SPPO compared to PPO. In their work, selectivity of SPPO for CO_2/N_2 was 86 compared to 15 for PPO.

In this work, composite membranes were prepared by coating polyethersulphone (PES) ultrafiltration flat sheet membranes with highly selective sulfonated polyphenylene oxide (SPPO). Selection of the support membrane depends on the pore size distribution and the compatibility with the solvent system used. The support membrane should not significantly contribute to the overall resistance to gas permeation. The effect of the pores and the pore size distribution of the microporous support on the final performance of the composite membranes have been addressed in the literature [10,12]. Some researchers [12] have addressed the problem of pore penetration (which results in a large effective thickness) by impregnating the support with a nonsolvent so as to achieve a thin, defect free skin layer of a glassy polymer. Rezac and Koros [13] showed that using high concentration of high molecular weight polymer in the coating solution could help in minimizing the polymer intrusion due to the interlock between the polymeric coils. They showed that a high molecular weight polymer along with a good solvent gives maximum hydrodynamic dimensions, which reduces the extent of pore penetration resulting in a thin top layer. Controlling the maximum pore size in the support, and the hydrodynamic volume of the polymer in the coating solution, stopped the intrusion of the coating polymer into the support pores [13].

This chapter is aiming mainly at studying the effect of the metal form of SPPO on the performance of the composite membrane. The effect of the metal form of SPPO on the density of the membranes and the sorption of gases in the membranes is investigated. The support membrane is assessed in order to determine the extent of interference by the support membrane in the overall performance of the composite membrane.

4.2 Experimental

4.2.1 Materials:

A sample of PPO (intrinsic viscosity in chloroform equal to 1.58 dL/g) was kindly supplied by General Electric Company, Selkirk, NY. All other chemicals used in the experiments were of reagent grade and were used without any further purification.

PPO was sulfonated to ion exchange capacity (IEC) equivalent to 1.73 meq/g. The process of sulfonation is detailed in the **General Experimental and Methods** chapter of this thesis report.

Commercial PES UF membrane (Osmonics HO51), having 12-kDalton molecular weight cut off (MWCO) was used as the support membrane.

4.2.2 Preparation of Composite Membranes

SPPO in the hydrogen form was dissolved in 2-ethoxyethanol to prepare a 4.0% (w/w) solution. The solution was then filtered through 3.0μm Teflon filters to remove impurities present in the solution. Prior to coating the porous PES substrate membranes, they were thoroughly washed in demineralized water. The substrate was dried for at least 12 hours in a vacuum oven at room temperature. Coating solution was spread over the porous substrate with a rounded tip dropper. The volume of SPPO solution coated on a unit surface area of PES substrate membrane was $0.017 cm^3/cm^2$. The coated substrate was kept in a preheated convection oven at 60^oC for 24 hours and then left to cool at ambient temperature. Then the composite membranes were soaked in the corresponding electrolyte solutions for cation exchange.

4.2.3 Preparation of Homogeneous Membranes

Dense homogeneous membranes were prepared by pouring 4.0% (w/w) polymer

solutions of SPPO into stainless steel metal rings. 2-Ethoxyethanol was used as a solvent. The metal rings, about 5.5 cm in diameter, were clamped onto the surface of a clean Pyrex glass plate. The polymer solution was poured into the rings; the polymer solution together with the glass plate was placed in a convection oven, which was heated to 60°C, for drying. Drying step lasted for 24 hours. Dense SPPO membranes then were soaked in the electrolyte solution to exchange the proton of the sulfonic group with the corresponding metal cation. Membranes were then stored in vacuum for at least 48 hours.

4.2.4 Cation Exchange

Aqueous solutions of $AlCl_3$, $BaCl_2$, $Ca(OH)_2$, $Mg(NO_3)_2$, CsCl, KCl and LiCl, of 1.0 N concentration were prepared with the exception of $Ca(OH)_2$ which was at saturation concentration (0.02 N). Membranes were kept for at least 4 days in the respective electrolyte solution (one week in case of $Ca(OH)_2$). Then they were removed and washed with demineralized water.

4.2.5 Gas Permeation Testing

Three membranes were installed and run simultaneously on the constant volume system. The feed pressure (absolute) was maintained at around 5250±50 mmHg (700.0 kPa) and the permeate pressure (absolute) cycle was maintained between 1 mmHg to 10 mmHg (0.133 to 1.333 kPa). Description of the constant volume system is found in the **General Experimental Methods** chapter.

4.2.6 Density and Sorption Measurements

Experimental procedure and calculations used in determining the density of the membranes, and the sorption of gases in the different membranes are detailed in the **General Experimental Methods** chapter.

4.2.6 Intrinsic Viscosity Measurements

Determination of the intrinsic viscosity of SPPO–2-Etoxyethanol solution is detailed in the **General Experimental Methods**. The efflux times of dilute SPPO–2-ethoxyethanol solutions were measured using capillary viscometer (Cannon-Fenske viscometer #100).

4.3 Results and Discussion

4.3.1 Effect of Composite Membranes Preparation Conditions on Support Membrane

The criteria for the choice of the porous substrate membrane should be a minimum resistance to the gases passing through it. A key factor to ensure that the support exhibits little resistance to the gas permeating through is to eliminate the penetration of the coating polymer into the pores of the substrate membrane. The mean pore size and the pores size distribution of the PES ultrafiltration membrane, HO51, were determined based on polyethylene glycol (PEG) separation experiments [14]. HO51 has a 12-kDalton

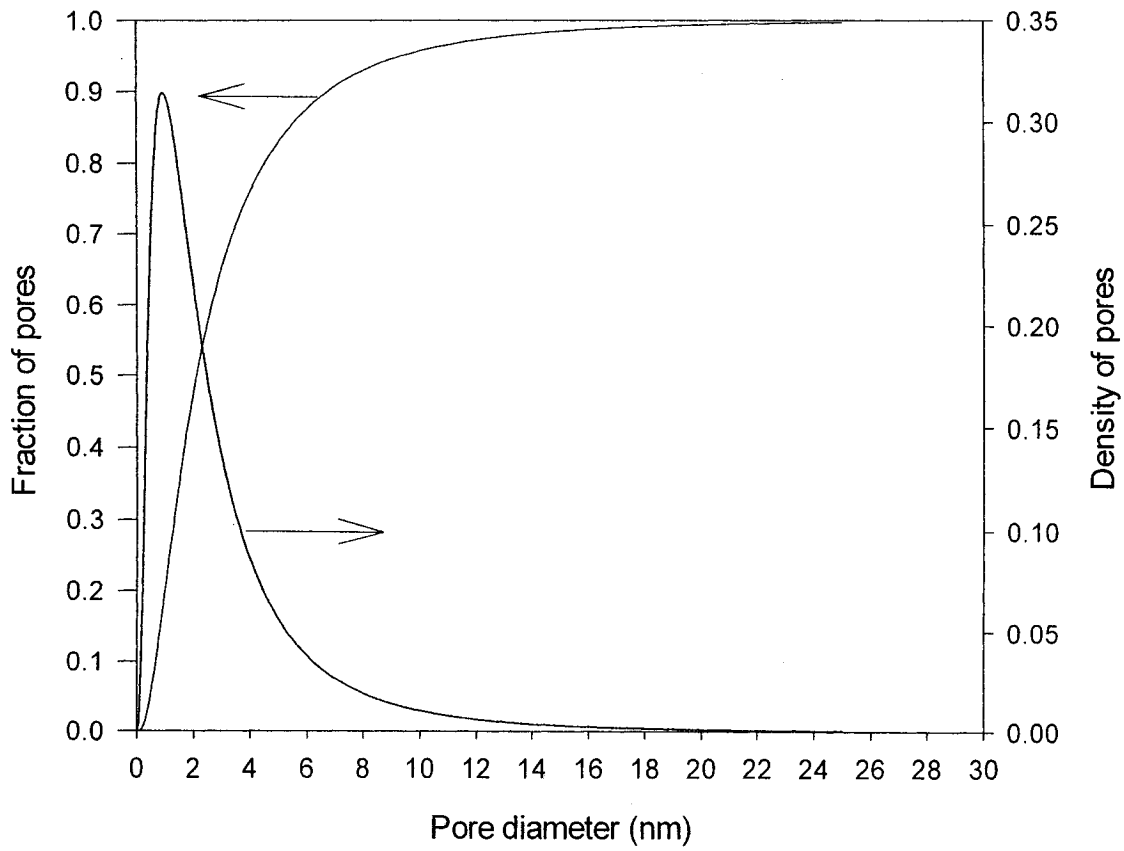

Fig. 4.1: Probability density function and cumulative distribution of pores size of PES (HO51) membranes.

molecular weight cut off (MWCO). Figure 4.1 shows the cumulative pore size distribution of HO51 substrates studied. Figure 4.1 indicates that 50% of the pores are less than 2.5 nm while the largest pore size is expected to be more than 28 nm. It should be noted that the pore size distribution given in Fig. 4.1 corresponds to that of a wet membrane.

It is important to consider that the process of preparing the composite membranes involved drying the water-wet porous substrate and exposing it to the solvent of the coating solution, followed by drying at 60°C. The pores may collapse as water within the membrane matrix is evaporated. Therefore, pores are expected to be smaller than those in the membranes before drying. In addition, the dried substrate membranes would undergo further change in their morphology when exposed to the solvent in the coating solution. This was evident from the comparison of gas permeation data of a dried substrate membrane; and a dried then solvent exposed then dried membrane. The data in Table 4.1 clearly indicate an increase (about 250%) in the resistance of the membranes that were exposed to solvent.

Table 4.1: Comparison of gas permeance of water-dried only and water-dried/ solvent-exposed/solvent-dried HO51 membranes.

	Gas permeance				Gas permeance ratio	
	CO_2	CH_4	O_2	N_2	CO_2/CH_4	O_2/N_2
Dried	94.7* (12.0%)**	134.2 (17.6%)	94.0 (9.4%)	103.0 (13.2%)	0.705	0.912
Dried / solvent exposed / dried	34.7 (8.0%)	52.3 (11.2%)	34.9 (8.1%)	38.5 (9.5%)	0.664	0.908

*Average permeance for 5 coupons.
**Variation in permeance of the 5 coupons = (standard deviation)/(average permeance).

4.3.2 Size of SPPO Macromolecules in Solution

The weight averaged molecular weight of PPO, M (g/mol), can be calculated from its intrinsic viscosity in chloroform according to the Mark-Houwink equation [15],

$$[\eta] = 0.00048\, M^{0.64} \qquad (1)$$

Since $[\eta]$ is known to be 1.58 dL/g before sulfonation, then M ≈ 316,400 g/mole.

The IEC value of SPPO used as the coating polymer in this work is 1.73 meq/g of dry polymer. This corresponds to 24.1% sulfonation of the repeat units of the PPO. Assuming there was no molecular cleavage during sulfonation, the molecular weight (weight average) of the sulfonated PPO is calculated as follows,

$$M_{SPPO} = \frac{316{,}400}{120}\left[(1\text{-}0.2409)\ 120 + (0.2409)\ 200\right] = 367{,}200 \text{ g/mole}$$

Figure 4.2 shows the plot of the reduced viscosity for dilute solutions of SPPO polymer in 2-ethoxyethanol. The reduced viscosity, η_{red}, is given by,

$$\eta_{red} = \frac{\nu - \nu_o}{C\ \nu_o} = \frac{K\ t - K\ t_o}{C\ K\ t_o} = \frac{t - t_o}{C\ t_o} \qquad (2)$$

where ν and ν_o are the kinematic viscosities of the polymer solution and the solvent, respectively.

Kinematic viscosities are related to the efflux time of the solution, t, and the solvent, t_o, by the viscometer capillary constant K in [cSt/s].

When the reduced viscosities of dilute solutions of a polymer are plotted versus their polymer concentrations in (g/dL), the data are usually represented by a straight line of a positive slope having a Y-axis intercept corresponding to the intrinsic viscosity of the polymer solution, [η]. However, this was not the case for SPPO with an IEC value of 1.73 meq/g when the solvent used was 2-ethoxyethanol. The reduced viscosity increased

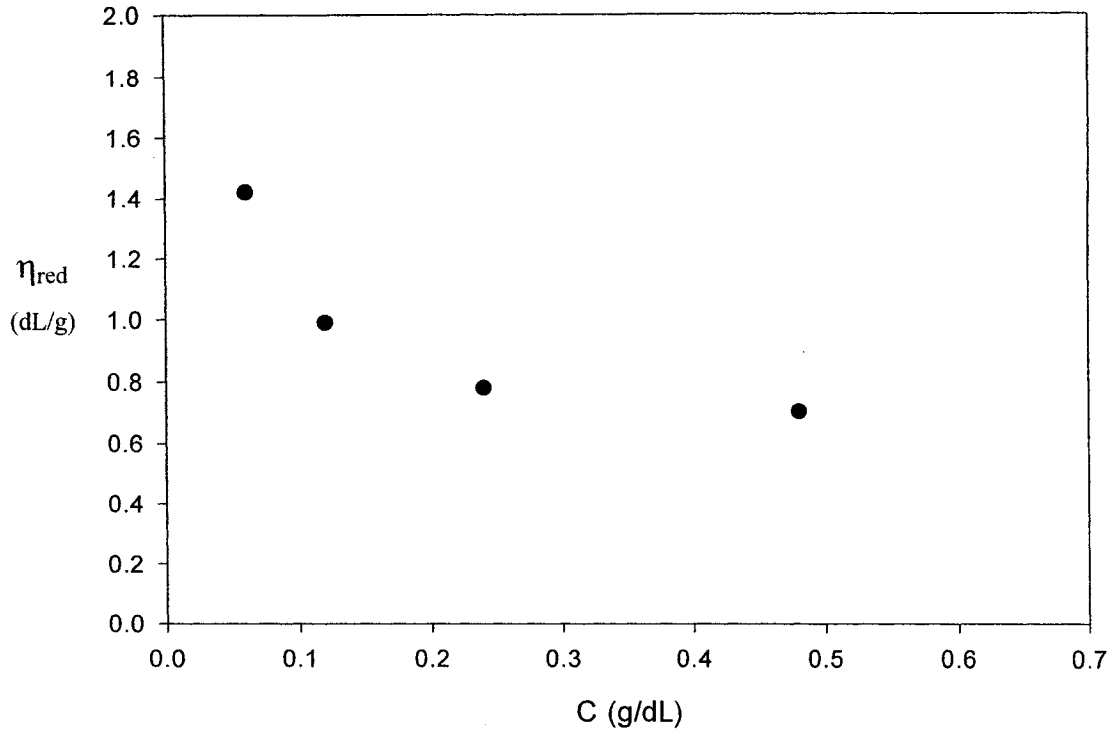

Fig. 4.2: Reduced viscosity of SPPO with an IEC of 1.73 meq/g in 2-ethoxyethanol (25°C).

with a decrease in the polymer concentration. This is often encountered when the polymer is a polyelectrolyte [13,15,16]. In dilute solutions of the ionic polymers, the reduced viscosity may reach a value many times over the actual intrinsic viscosity. At high concentrations, the behaviour of the polyelectrolytic polymer solution is normal as the molecules are in close contact and overlap one another.

The increase in the reduced viscosity upon dilution is due to an increase in the hydrodynamic volume of the polymer, which results from the action of expansive forces on the polymer. Polyelectrolytic molecules in dilute solutions can be imagined as a restraining cross-linked network of the polymer segments that can also be imagined as an elastic membrane [16]. The mobile counter ions can diffuse out of the polymer domain into the solvent domain leaving behind residual charges within the polymer domain so that the polymer should expand to minimize the repulsion forces. Another theory put

forward to explain this phenomenon is that in the case of equilibrium, the net repulsive forces due to the presence of charges within the polymer domain is equal to the osmotic forces resulting from the excess mobile cations within the polymer domain. Losing a part of the mobile counter-ions to the solvent domain would abrupt the equilibrium so that the polymer expands to bring the forces into balance again. Full extension configuration could be reached if a small net charge is developed. A charge as small as 1.0 electronic charge per 10 units of the polyelectrolyte molecule would be sufficient [16].

Experimental data showing the polyelectrolytic expansion trend can be well represented by an empirical relation [16],

$$\eta_{red} = \frac{A}{(1 + B\, C^{0.5})} \tag{3}$$

where A and B are constants. According to the above equation, a straight line is expected when $(1/\eta_{red})$ vs. $C^{0.5}$ is plotted. The intercept of this line is the inverse of the intrinsic viscosity.

The data in Fig. 4.2 were plotted in Fig. 4.3 according to equation (3). The best line fit representing the experimental data $(1/\eta_{red})$ vs. $C^{0.5}$ is

$$1/\eta_{red} = 1.5189\, C^{0.5} + 0.4281 \tag{4}$$

Therefore, $[\eta] = 1/0.4281 = 2.336$ dL/g.

The radius of gyration of a polymer (R_g), assuming the polymer molecules assume the spherical configuration in the solution, is related to the intrinsic viscosity of the polymer solution by the Einstein viscosity law for linear polymers [13,16]:

$$[\eta]\, M = \Phi\, (6R_g^2)^{3/2} \tag{5}$$

where $[\eta]$ is the intrinsic viscosity of the polymer solution in dL/g, M is the molecular

weight of the polymer and Φ is a universal constant equal to 2.8×10^{21}, which represents a frictional coefficient. In order for the polymer not to penetrate the pores of the substrate, the estimated dimension, R_g, should be larger than the maximum pore radius present such that the polymer is sieved on the surface of the support [12,13,17]. Based on equation (5), the size ($2R_g$) of the SPPO polymer in the coating solution was estimated to be about 55 nm. Therefore, the SPPO polymer coil in the coating solution is expected to retain on top of the support.

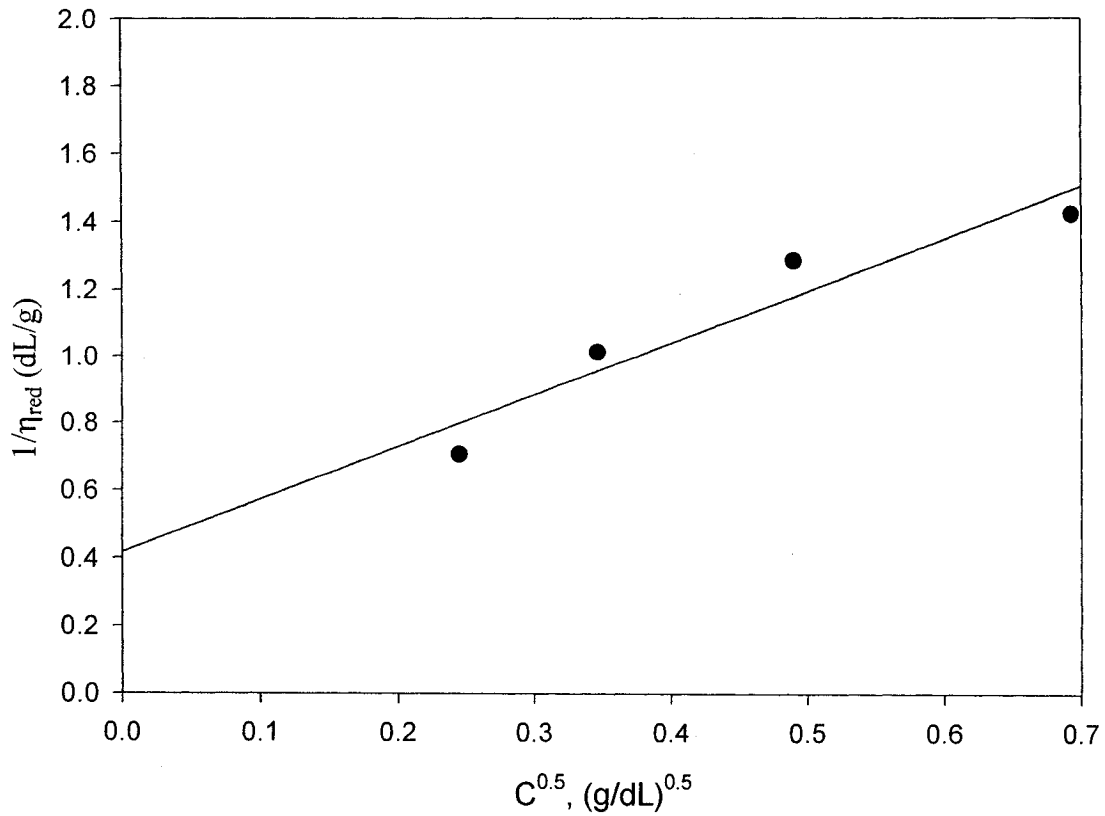

Fig. 4.3: Reduced viscosity of SPPO with an IEC of 1.73meq/g in 2-ethoxyethanol (25°C).

4.3.3 Assessment of the Interference of the Support Membrane in the Overall Performance of the Composite Membrane

Based on the assumption that the composite membranes have two distinct resistances acting in series, these resistances have been evaluated and the results are shown in Table 4.2. In order to assess the extent of interference the support layer is imposing on the gas permeation rates, the results of the least two permeable SPPO composite membranes (H- and Mg-form), and the results of the most permeable SPPO composite membrane (Al-form), are presented in Table 4.2. All data are based on pure gas permeation. The thickness of the coating layer was estimated to be 8.0μm with 1.3μm standard deviation. The thickness was estimated based on the measured thickness of dense homogeneous membranes prepared under the conditions similar to those used for coating the substrate membrane. The total resistance of a composite membrane is

$$R_T = \frac{1}{A\, p_T^*} \tag{6}$$

where A is the gas permeation area and p_T^* is the gas permeance obtained for the composite membrane in GPU[1]. The resistance of the uncoated support, R_S, is based on the gas permeance presented in Table 4.1 for the dried-solvent exposed-dried support,

$$R_S = \frac{1}{A\, p_S^*} \tag{7}$$

where p_S^* is the gas permeance of the uncoated support membrane in GPU. The resistance of the coated layer is therefore,

$$R_C = R_T - R_S \tag{8}$$

The permeability of the coated layer is then calculated based on R_C and the estimated thickness of the coated layer as follows,

---

[1] Gas permeation units, $1\text{GPU}=10^{-6}\ \frac{\text{cm}^3(\text{STP})}{\text{cm}^2.\text{s.cmHg}}=3.345\times10^{-12}\ \frac{\text{mol}}{\text{m}^2.\text{s.Pa}}$

$$p_C = \frac{\delta_C}{A\,R_C} \times 10^4 \qquad (9)$$

where δ_C is the thickness of the coated layer (cm) and p_C is the coating material permeability in Barrer. The intrinsic permeabilities so obtained were compared in Table 4.2 with those obtained from Kruczek [15] for SPPO with an IEC value of 1.8 meq/g. It is clear from Table 4.2 that the coating layer resistance is dominating the gas permeation, while the support membrane resistance becomes significant when the coating layer becomes more permeable to a gas. Since CO_2 has the highest permeability, the support resistance becomes appreciable for this gas.

It is worth mentioning that the effect of the cation is significant in the permeability data. The permeability of SPPO membrane increased almost by 75% upon exchanging the protons of sulfonic groups with Al^{3+} cations, while 34.6% drop in the gas permeance occurred when the Mg^{2+} cations replaced the protons of the sulfonic groups.

4.3.4 Effect of the Cation Form on the Performance of SPPO Composite Membranes

It is important to consider the differences in certain properties of the cations used in this work in order to correlate them with the experimental data obtained. Of these properties are the electronegativity of the atom and the atomic radii. Considering the periodic table of chemical elements; electronegativity increases from left to right within a period, while it decreases from top to bottom within a group. The atomic size follows an opposite trend; it decreases within a period from left to right while it increases from top to bottom within a group. Electronegativity is a measure of the electron withdrawal ability of the atom nucleus.

Table 4.2 Estimated resistances of the composite membranes, substrate membranes, and the coated layers.

1) **SPPO-H** Gas	CO_2	CH_4	O_2	N_2
Total permeance (GPU)	2.301	0.059	0.411	0.072
R_T (GPU.cm^2)$^{-1}$	0.045	1.763	0.253	1.444
R_S (GPU.cm^2)$^{-1}$	0.003	0.002	0.003	0.002
R_C (GPU.cm^2)$^{-1}$	0.043	1.761	0.250	1.442
(R_C / R_T) %	94.05	99.90	98.94	99.83
p_C (Barrer)[a]	19.520	0.470	3.310	0.580
Intrinsic permeability (Barrer) [15]	10.780	0.250	2.110	0.320
2) **SPPO-Mg** Gas	CO_2	CH_4	O_2	N_2
Total permeance (GPU)	1.536	0.023	0.251	0.029
R_T (GPU.cm^2)$^{-1}$	0.068	4.521	0.414	3.586
R_S (GPU.cm^2)$^{-1}$	0.003	0.002	0.003	0.002
R_C (GPU.cm^2)$^{-1}$	0.065	4.520	0.412	3.584
(R_C / R_T) %	96.03	99.96	99.35	99.93
p_C (Barrer)[a]	12.760	0.184	2.020	0.236
Intrinsic permeability (Barrer) [15]	11.980	0.220	2.330	0.270
3) **SPPO-Al** Gas	CO_2	CH_4	O_2	N_2
Total permeance (GPU)	3.844	0.126	0.657	0.116
R_T (GPU.cm^2)$^{-1}$	0.027	0.825	0.158	0.897
R_S (GPU.cm^2)$^{-1}$	0.003	0.002	0.003	0.002
R_C (GPU.cm^2)$^{-1}$	0.024	0.824	0.156	0.894
(R_C / R_T) %	90.06	99.78	98.31	99.73
p_C (Barrer)[a]	34.060	1.010	5.330	0.930

[a] Based on 8.0μm thickness of the coated layer.

If two atoms are different in their electronegativities and they are involved in a bond, then the electron pair constituting the bond spends more time about the more electronegative nucleus. Therefore, electronegativity difference between two atoms that are involved in a bond determines the polarity and the strength of the dipole developed between the two atoms [18,19]. Table 4.3 lists the atomic and ionic radii and the electronegativity of the different elements of concern in this study. Since all cations are attached to the same $-SO_3^-$ group, then differences in the performance of membranes in different cationic

forms are attributed to the different effects that have been brought about by the different cations replacing the proton of the sulfonic groups.

4.3.4.1 Monovalent Cation Form of SPPO Composite Membranes

Table 4.4 qualitatively ranks the polarity of the $-SO_3$-Me group. Tables 4.5 and 4.6 summarize the performance of SPPO composite membranes with the different monovalent cations. The effect of replacing the proton of the sulfonic group with a monovalent cation is very clear. From Tables 4.5 and 4.6, the following can be concluded. CO_2 permeance increases in the order SPPO-H < SPPO-Li < SPPO-K ≤ SPPO-Cs. However, the permeance of CH_4, O_2, and N_2 gases, follows the same trend, i.e. SPPO-Li >SPPO-K ≥SPPO-Cs > SPPO-H.

Table 4.3: Atomic radii, ionic radii and electronegativities of chemical elements of concern in this study.

Element (Cation)		Atomic radius[19] (A^o)	Ionic radius[19] (A^o)	Electronegativity[19] $(eV)^{1/2}$
H	(H^+)	0.37	-	2.1
Li	(Li^+)	1.52	0.74	1.0
K	(K^+)	2.31	1.38	0.8
Cs	(Cs^+)	2.62	1.7	0.7
Mg	(Mg^{2+})	1.6	0.72	1.2
Ca	(Ca^{2+})	1.97	1.00	1.0
Ba	(Ba^{2+})	2.17	1.36	0.9
Al	(Al^{3+})	1.43	0.53	1.5
O				3.5

Table 4.4: Expected polarity trend of $-SO_2$-O-Me group.

SO_2 - O- Me	E_O-E_{Me}*	Polarity rank
SO_2 - O- H	1.4	4
SO_2 - O- Li	2.5	3
SO_2 - O- K	2.7	2
SO_2 - O- Cs	2.8	1

* Electronegativity difference between oxygen and metal.

Table 4.5: Composite membranes performance with monovalent metal forms of SPPO coating: CO_2/CH_4.

	Pure gas			20/80 CO_2/CH_4 Gas mixture		
Cation Form	Permeance (GPU) CO_2	Permeance (GPU) CH_4	CO_2/CH_4	CO_2 (GPU)	F**	CO_2 % in permeate
H^+	2.3 (±9.8%)*	0.059 (±4.8%)	39.0	2.1 (±18.4%)	37.0	90.25 (±2.1%)
Li^+	2.6 (±9.0%)	0.16 (±17.7%)	16.9	2.9 (±23.2%)	21.6	84.4 (±2.1%)
K^+	2.9 (±0.6%)	0.094 (±17.3%)	30.7	2.8 (±6.4%)	25.8	86.6 (±1.3%)
Cs^+	2.9 (±11.0%)	0.1 (±1.1%)	28.9	2.7 (±0.3%)	32.2	89.0 (±1.7%)

*Variability
**Separation Factor

Table 4.6: Composite membranes performance with monovalent metal forms of SPPO coating: O_2/N_2.

	Pure gas			20/80 O_2/N_2 gas mixture		
Cation Form	Permeance (GPU) O_2	Permeance (GPU) N_2	O_2/N_2	O_2 (GPU)	F**	O_2 % in permeate
H^+	0.411 (±0.3%)*	0.072 (±3.4%)	5.7	0.45 (±4.9%)	6.8	63.1 (±1.7%)
Li^+	0.567 (±10.3%)	0.14 (±11.6%)	4.0	0.55 (±15.0%)	4.0	49.7 (±7.2%)
K^+	0.533 (±7.1%)	0.098 (±14.4%)	5.4	0.50 (±15.4%)	5.2	56.5 (±1.4%)
Cs^+	0.434 (±3.3%)	0.099 (±2.9%)	4.4	0.52 (±0.3%)	5.3	57.4 (±1.7%)

*Variability
**Separation Factor

Looking into the permeance ratio of both pure gas and gas mixture, the order in membrane selectivity for CO_2/CH_4 and O_2/N_2 gas pairs is SPPO-H> SPPO-Cs≥ SPPO-K> SPPO-Li.

It is noticeable that there is a significant increase in the permeance for all gases, while CO_2/CH_4 and O_2/N_2 selectivity drop, upon exchanging the proton of the sulfonic group

with Li^+. This result could be exploited by the fact that all metal atoms are much voluminous compared to the hydrogen atom and therefore all metal form membranes become less densely packed. The density data, shown in Table 4.7, support the fact that introducing a monovalent metal cation in place of the hydrogen atom results in less dense and less packed structure. In particular, a significant drop in the density of membranes is noticed from the H-form to the Li-form. Therefore, the low permeance and high separation obtained from the H-form membranes is due to the dense and tight structure. By going from the Li-form to Cs-form, the permeance keeps increasing in case of CO_2. This is believed to be due to the increase in sorption of CO_2 in the membranes.

Table 4.7: Density of the monovalent metal forms of SPPO homogeneous membranes.

Membrane	Density g/cm^3	Standard deviation g/cm^3
SPPO-H	1.293	0.006
SPPO-Li	1.234	0.027
SPPO-K	1.217	0.024
SPPO-Cs	1.220	0.004

The interaction between CO_2 and $-SO_3$-Me groups increases as the polarity of the latter group increases. According to Table 4.4, the polarity of $-SO_3$-Me group should increase from Li to Cs. Figure 4.4 clearly indicates an increase in the sorption of CO_2 in an order that is in agreement with the polarity rank order of the $-SO_3$-Me groups shown in Table 4.4. On the other hand, Fig. 4.4 indicates that sorption of CH_4 gas in the SPPO membranes has not significantly changed with the different monovalent metal forms. Chen and Martin [7] reported that CO_2 sorption increased with an increase in the sulfonation degree of polystyrene. However, sorption of gases such as CH_4, O_2 and N_2, was affected only slightly by the polarity change [7,20]. Gases such as O_2, N_2, and CH_4,

which have larger kinetic diameters than CO_2 (Table 4.8), are more affected by the hindrance produced because of the size of the metal cation that is replacing the proton of the sulfonic group. Therefore, the permeance of these gases decreases in the order of increasing metal cation size. The hindrance effect due to the metal cation size can be ordered as follows: $-SO_2-O-Cs > -SO_2-O-K > -SO_2-O-Li$.

Table 4.8: Kinetic (sieving) diameter of gases [21].

Gas	CO_2	O_2	N_2	CH_4
Kinetic Diameter (A^o)	3.3	3.46	3.64	3.8

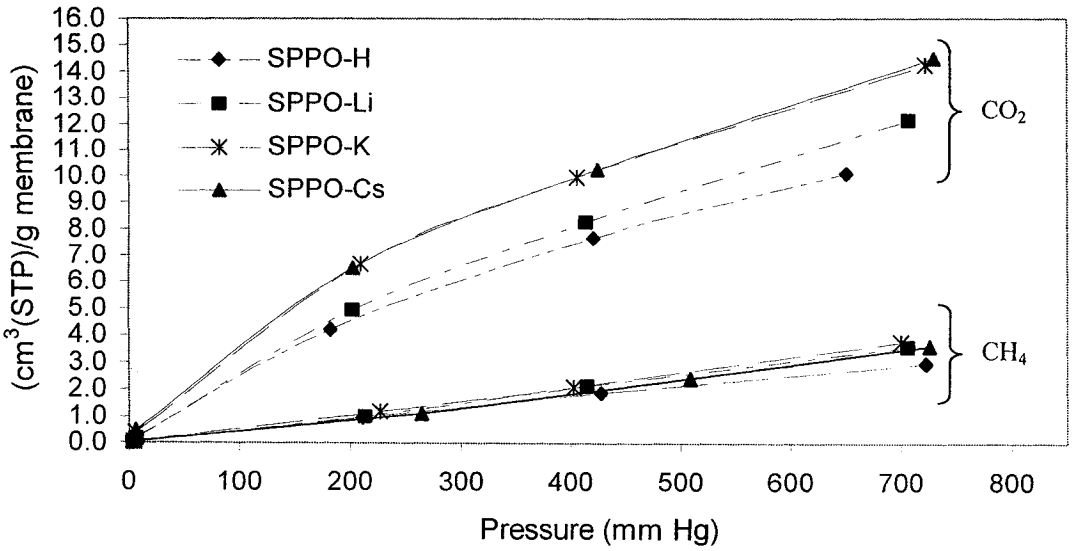

Fig. 4.4: Sorption of CO_2 and CH_4 in monovalent forms of SPPO membranes.

4.3.4.2 Divalent and Trivalent Metal Cation Form of SPPO TFC Membranes

Tables 4.9 and 4.10 show the performance of SPPO composite membranes in different divalent cation forms. In general, membranes in the divalent cation form showed higher selectivity and lower permeance for the gases tested when compared to membranes prepared from the monovalent cation form of the SPPO. These results can be interpreted in terms of the electrostatic bonding of the multivalent cations with more than one sulfonic group. The divalent cations are expected to be better cross-linking agents

Table 4.9: TFC membranes performance with divalent metal forms of SPPO coating: CO_2/CH_4.

	Pure gas			20/80 CO_2/CH_4 Gas mixture		
Cation form	Permeance (GPU) CO_2	Permeance (GPU) CH_4	CO_2/CH_4	CO_2 (GPU)	F**	CO_2 % in permeate
Mg^{2+}	1.54 (±12.2%)	0.023 (±16.2%)	67.0	1.69 (±9.6%)	48.6	92.4 (±1.8%)
Ca^{2+}	3.19 (±6.7%)	0.134 (±11.6%)	23.8	3.16 (±7.5%)	30.1	88.3 (±1.4%)
Ba^{2+}	2.83 (-)	0.077 (-)	36.7	2.76 (-)	31.6	88.8
Al^{3+}	3.84 (±6.3%)	0.126 (±12.7%)	30.5	4.02 (±8.3%)	41.0	91.2 (±0.88%)

*Variability
**Separation Factor

Table 4.10: TFC membranes performance with divalent metal forms of SPPO coating: O_2/N_2.

	Pure gas			20/80 O_2/N_2 gas mixture		
Cation form	Permeance (GPU) O_2	Permeance (GPU) N_2	O_2/N_2	O_2 (GPU)	F**	O_2 % in permeate
Mg^{2+}	0.251 (±12.2%)	0.029 (±15.0%)	8.6	0.26 (±8.6%)	7.4	65.1 (±1.3%)
Ca^{2+}	0.596 (±11.6%)	0.120 (±15.1%)	5.0	0.66 (±12.4%)	5.4	57.8 (±4.5%)
Ba^{2+}	0.527 (-)	0.103 (-)	5.1	0.50 (-)	5.0	55.8 (-)
Al^{3+}	0.657 (±3.6%)	0.116 (±10.4%)	5.7	0.72 (±8.3%)	5.9	59.7 (±7.1%)

*Variability
**Separation Factor

Table 4.11: Density of the multivalent metal forms of SPPO homogeneous membranes.

Membrane	Density g/cm^3	Standard Deviation g/cm^3
SPPO-Mg	1.430	0.007
SPPO-Ca	1.411	0.027
SPPO-Ba	1.390	0.013
SPPO-Al	1.300	0.010

compared to monovalent cations as they may bond with two $-SO_3^-$ groups. The Mg-form had the lowest gas permeance and the highest selectivity among the group. As a matter of fact, the Mg-form had the lowest gas permeance and the highest selectivity among all SPPO membrane forms without exception. Table 4.3 shows that Mg^{2+} is the smallest among the divalent metal cations used; therefore it is expected to give the tightest membrane structure. Density data in Table 4.11 agrees with this conclusion. Further, comparing the density data in Table 4.7 and Table 4.11, densities of SPPO membranes in

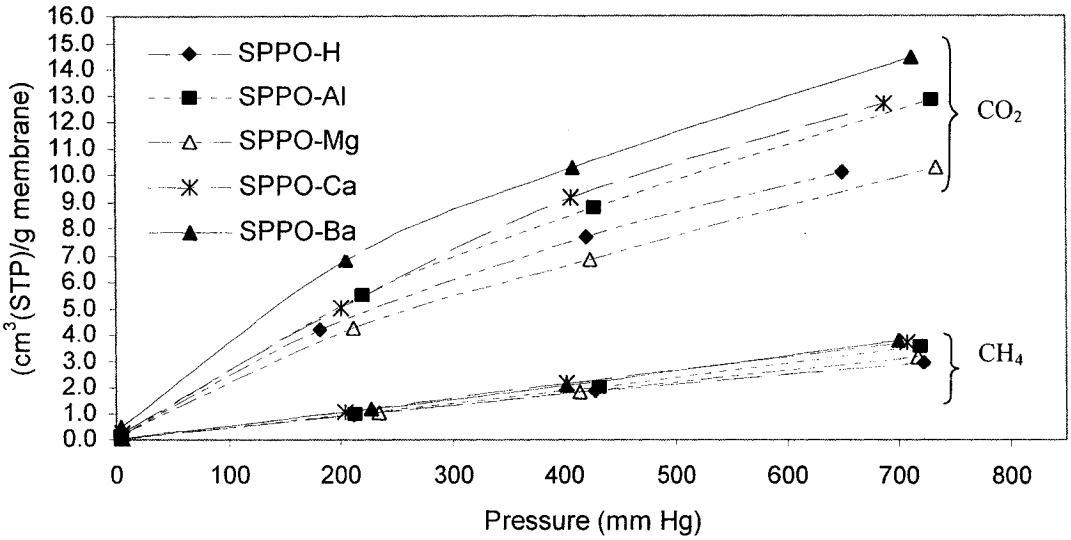

Fig. 4.5: Sorption of CO_2 and CH_4 in H-form and multivalent-forms of SPPO membranes.

the divalent cation forms are higher than those in the monovalent cation forms. This suggests that replacing the proton of the sulfonic groups with divalent cations leads to tighter structures. Sorption data for SPPO membranes with the divalent and trivalent cation forms are shown in Fig. 4.5. It is expected that the form of the divalent cation does not affect the sorption of CO_2 as the polarity of the ($-SO_3$-Me-SO_3-) does not change from a divalent cation form to another. This is explained based on the fact that the

two polar bonds, cross-linking the divalent cation (Me^{+2}) and the two $-SO_3^-$ groups, are two dipoles opposing each other, which will cancel the effect of each dipole. However, Fig. 4.5 shows that sorption of CO_2 in the Ca-and Ba-forms of SPPO membranes increased while the sorption of CO_2 in the Mg-form of SPPO membranes decreased in comparison to that of the H-form of SPPO membranes. This could be justified by the presence of some residual charge on the ($-SO_3$-Me-SO_3-) group, which increases as the size of the divalent cation increases. In the case of Ca- and Ba-forms, there is a residual charge on the ($-SO_3$-Me-SO_3-) groups resulting from non-aligned cross-linking, i.e. the dipoles of the two cross-linking bonds are not cancelled. This may be the reason for the stronger interaction of CO_2 with these membranes in comparison to that of the H-form of SPPO. However, in the case of the Mg-form, the cross-linking bonds are more aligned and have least residual charge, resulting in the weakest interaction of CO_2 with the membrane.

A noticeable trend in the performance of the membranes with divalent cation form is that the Ca-form has the highest permeance for all gases and the lowest selectivity. This could be the result of the superimposition of the cross-linking and the hindrance effects. Hindrance due to atomic size can be ordered as follows: Ba > Ca > Mg. Cross-linking becomes weaker as the atomic size increases, it follows the order: Mg > Ca > Ba. Increasing hindrance results in decreasing permeance while weakening cross-linking results in increasing permeance. The superimposition of these two conflicting effects resulted in a maximum permeance and a minimum selectivity for Ca-form membrane.

The performance of the Al-form membrane is quite unique. Its density is comparable to that of the H-form although Al atom is larger in size than H atom. One would expect that

Al^{3+} is associated with more than one $-SO_3^-$ group compared to Mg^{2+}, which may result in better cross-linking and tighter structure. However, the permeance data of the Al-form membranes are the highest among all forms of SPPO membranes. The selectivity data, on the other hand, are comparable to those of the H-form of SPPO membranes. The sorption of CO_2 gas in the Al-form is comparable to that of Li- or Ca-forms indicating a comparable polarity to these membranes. A possible justification of this unique performance is that Al^{3+} may be present in the film in a mixed salt form like $AlCl_2(SO_3)$ or $AlCl(SO_3)_2$.

4.4 Conclusions

1. The resistance for gas permeation through the PES ultrafiltration membrane used as a support substrate for SPPO coating, drastically increased upon drying and exposure to 2-ethoxyethanol solvent. This is probably due to the swelling of PES polymer and pore collapsing.
2. Commercial PES ultrafiltration membrane (HO51) having MWCO of 12 kDalton is appropriate for use as a support membrane for coating when the high molecular weight SPPO is coated. This is because the ultrafiltration membrane has pores that are small enough to retain SPPO molecules by sieving. HO51 membranes showed low resistance for gas permeance relative to coated layer. However, their resistance may become significant as the gas permeance through the coating increases.
3. Exchanging the proton of the sulfonic groups in a SPPO membrane with a monovalent metal cation decreases the membrane density as a result of the insertion of a much more voluminous cation. As a result, the permeance of SPPO membranes in monovalent metal cation form has increased with respect to all tested gases.

4. The permeance of O_2, N_2, and CH_4 gases, decreases as the atomic weight of the monovalent metal cation increases, i.e. by going down along the first group of the periodic table of the chemical elements. This is the result of increasing hindrance due to the increase in the size of the monovalent cation replacing the proton of the sulfonic groups. However, the permeance of CO_2 gas increases in the same direction as a result of an increase in the interaction of the gas with the membrane due to an increase in the polarity of the membrane. The electronegativity difference, between the metal atom and the oxygen atom in the sulfonate group, increases by going down along the group of the periodic table of the chemical elements.
5. Exchanging the proton of the sulfonic groups in SPPO membrane with divalent metal cations increases the density of the membrane as divalent cations can cross-link two SO_3^- groups. However, the residual charge increases as the size of the divalent metal cation increases, which results in an increase in CO_2 sorption, by going down along the second group of the periodic table of the chemical elements.
6. The permeance for all gases shows a maximum while the permselectivity shows a minimum at Ca^{+2} by going down the periodic table for divalent metals. This is mainly the result of two conflicting effects: the metal cation size and the cross-linking bond strength.
7. The highest permeance was obtained with the Al-form of SPPO with relatively high permselectivity and separation efficiency, although the membrane density was relatively low. It is believed that this is the result of having some salt complex formation of the electrolyte used with the sulfonate group such as: $AlCl(SO_3)_2$ or $AlCl_2SO_3$.

4.5 References

[1] D. Aycock: "*Poly(Phenylene Ether)*", Encyclopedia of Polymer Science and Technology, V 13, Interscience Publishers, NY (1974).

[2] S. Percec and G. Li: "*Chemical Modification of Poly(2,6-dimethyl-1,4-phenylene oxide) and Properties of the Resulting Polymers*", ACS Symposium Ser., 364, American Chemical Society, Washington DC (1988).

[3] H. Fu, L. Jia, and J. Xu: "*Studies on the Sulfonation of Polyphenylene Oxide and Permeation Behaviour of Gases and Water Vapor Through Sulfonated PPO Membranes. I. Sulfonation of PPO and Characterization of the Products. II. Permeation Behavior of Gases and Water Vapor Through Sulfonated Membranes*", J. Appl. Polym. Sci.,51, (1994) 1399-1409.

[4] B. Story and W. J. Koros: "*Sorption and Transport of CO_2 and CH_4 in Chemically Modified Poly (Phenylene Oxide)*", J. Membr. Sci., 67, (1992) 191-210.

[5] S. Mahajan: "*Structural Modification of Poly(2,6-Dimethyl-1,4-Phenylene Oxide)*", Polym.- Plast. Tech. Eng., 30, (1991) 1.

[6] R. T. Chern, F. R. Sheu, L. Jia, V. T. Stannett, and H. B. Hopfenberg: "*Transport of Gases in Unmodified and Aryl-Brominated Poly(2,6-Dimethyl-1,4-Phenylene Oxide)*", J. Membr. Sci., 35, (1987) 103-115.

[7] C. Chen and C. Martin: "*Gas-Transport Properties of Sulfonated Polystyrenes*", J. Membr. Sci, 95, (1994) 51-61.

[8] K. Ghosal and R. T. Chern: "*Aryl-Nitration of Poly (Phenylene Oxide) and Polysulfone. Structural Characterization and Gas Permeability*", J. Membr. Sci, 72, (1992) 91-97.

[9] B. Kruczek and T. Matsuura: "*Development and Characterization of Homogeneous*

Membranes from High Molecular Weight Sulfonated Poly (Phenylene Oxide)", J. Membr. Sci, 146, (1998) 263-275.

[10] B. Bikson and K. Nelson: "*Production and Use of Improved Composite Fluid Separation Membranes*", U.S. Patent 5,356,459 (1994).

[11] G. Polotskaya, S. Agranova, T. Antonov, and G. Elyashevich: "*Gas Transport and Structural Features of Sulfonated Poly(Phenylene Oxide)*", J. Appl. Polym. Sci., 66, (1997) 1439-1443.

[12] K. Ebert, A. Bezjak, K. Nijmeijer, M. Mulder, and H. Strathmann: *"The Preparation of Composite Membranes with a Glassy Top Layer"*, J. Appl. Polym. Sci., 46, (1992) 1927-1938.

[13] A. Rezac and J. Koros: *"Preparation of Polymer-Ceramic Composite Membranes with Thin defect-free Separating Layers"*, J. Appl. Polym. Sci., 46, (1992) 1927-1938.

[14] A. Michaels: "*Analysis and Prediction of Sieving Curves for Ultrafiltration Membranes: A Universal Correlation*", Sep. Sci. Tech., 15, (1980) 1305-1322.

[15] B. Kruczek: "*Development and Characterization of Dense Membranes for Gas Separation Made from High Molecular Weight Sulfonated Poly (Phenylene Oxide)*", Ph.D. Thesis, Chemical Engineering Department, U. of Ottawa, 1998.

[16] P. Flory: "*Principles of Polymer Chemistry*", George Banta Company, Mensha, Wisconsin (1953).

[17] Y. Yampol'skii and D. Paul: "*Polymeric Gas Separation Membranes*", CRC Press, Boca Raton (1994).

[18] A. Sharp: "*Inorganic Chemistry*", 2nd edn., Longman Scientific & Technical, U.K., (1981).

[19] K. Henold and F. Walmsley: "*Chemical Principles, Properties, and Reactions*", Addison-Wesley, California (1984).

[20] T. Sakai, H. Takenaka, and E. Tarikai: "*Gas Diffusion in the Dried and Hydrated Nafions*", J. Electrochem. Soc.: Electrochem. Sci. and Tech., 133, (1986) 88-92.

[21] J. Koros and G. Fleming: "*Membrane-Based Gas Separation*", J. Membr. Sci., 83, (1993) 1.

4.6 Nomenclature

A	Total membrane surface area, cm^2.
C	Concentration of polymer solution, g/dL.
F	Separation factor of membrane.
K	Viscometer capillary constant, cSt/s.
M	Molecular weight of polymer.
p_C	Gas permeability of coated layer, Barrer.
p_S^*	Gas permeance of the support layer, GPU.
p_T^*	Total gas permeance of the composite membrane, GPU.
R_C	Coated layer resistance to gas permeation, 1/ (cm^2 GPU).
R_g	Polymer coil radius of gyration, cm.
R_S	Resistance of the porous support to gas permeation, 1/ (cm^2 GPU).
R_T	Total resistance of composite membrane to gas permeation, 1/ (cm^2 GPU).
t_o, t	Elapsed time for solvent and solution, respectively, in capillary viscometer, s.
δ_C	Coated layer thickness, m.
Φ	Frictional coefficient, 2.8×10^{21}dL/(mol cm^3).
η	Reduced viscosity of solution, dL/g.
$[\eta]$	Intrinsic viscosity of polymer solution, dL/g.
v_o, v	Kinematic viscosity of solvent and polymer solution, respectively, cSt.

Appendix

4.A Averaging Separation Factor and Permeate Composition for More than One Membrane

The separation factor, F, is defined as:

$$F_{1/2} = \frac{\left(X_1 / X_2\right)_{Permeate}}{\left(X_1 / X_2\right)_{Feed}} \tag{A-1}$$

where X_1 and X_2 represents the mole fraction of gas 1 and gas 2, respectively. When several membranes of the same type, are tested separately for binary gas mixture separation, the average composition of the permeates is calculated using the following equation:

$$\overline{X}_1 = \frac{\sum_{i=1}^{n} J_i \left(X_{1i}\right)_{Permeate}}{\sum_{i=1}^{n} J_i} \tag{A-2}$$

where subscript i is membrane i. J is the gas flux and $\overline{X}_1$ is the average mole fraction of gas 1 in the permeate. Therefore, the separation factor can be rewritten as:

$$\overline{F}_{1/2} = \frac{\left(\overline{X}_1 / (1 - \overline{X}_1)\right)}{(X_1 / X_2)_{Feed}} \tag{A-3}$$

Chapter 5

Characterization of Gas Separation Membranes Prepared from Brominated Poly (Phenylene Oxide) by Infrared Spectroscopy

• Proceedings of the International Congress on Membranes and Membrane Processes (ICOM 2002), Desalination 148 (2002) 369–375.

Abstract

Infrared (IR) spectra of brominated high molecular weight PPO membranes revealed that brominating PPO at the phenyl ring results in decreasing both the C-O-C torsional motion, and the plane C-H bending, which are assigned respectively to the 1300 cm^{-1} and 1180 cm^{-1} bands in PPO. Splitting in the 1180 cm^{-1} band was observed at 37.4% bromination and higher, indicating different modes for C-H bending that occurred as a part of the methyl groups was hindered in their motion by adjacent bromine substituents. The permeability of gases in the brominated PPO membranes increased slightly in comparison to that of PPO as the degree of bromination was increased to 37.4%, however, the permeability of gases almost doubled at 60% bromination degree. The trend in the gas permeability data and the IR spectra obtained in this study support the mechanism proposed in the literature, i.e. higher degrees of bromination are needed to enhance the permeability of gases through stiffening the PPO backbone, which leads to an increase in the rate of diffusional jumps.

5.1 Introduction

Poly (2,6- dimethyl 1,4-diphenyl oxide) or PPO polymer possesses the highest gas permeability among the high glass transition temperature aromatic polymers with moderate gas selectivity. This stems from its chemical and conformational structure. PPO backbone has a kinked structure due to the nonlinear ether linkage. The absence of polar groups and the presence of the ether linkages have suppressed the chain packing and densification. The transition temperature assigned to the rotation of the phenyl ring around the ether linkage is very low [1,2]. The high free volume and the ease of the rotational motion of the phenyl rings have contributed to the high diffusivity and permeability of gases in PPO. The moderate gas selectivity partly comes from the moderate inhibition of the phenyl rings rotation as a result of the interference of the methyl groups with the hydrogen atoms on adjacent rings [3]. Chemical modification of PPO aims at enhancing the selectivity of the resulting polymer toward gases and (or) its permeability to gases. Bromination of PPO was studied by many researchers [2-7]. Percec and Li [2] brominated PPO to different degrees: 0, 6.5, 21.5, 46, 61, and 100%. The permeability of CO_2 reported was respectively: 64, 64, 67.2, 78.1, 99.8, and 158.1 barrer. The permselectivity of CO_2/CH_4 reported was respectively: 16.4, 16.7, 17.7, 19.4, 18.0, and 23.7. They concluded that bromination of PPO is effective only when higher degrees of bromination were achieved. They reported that bromination of PPO decreased the flexibility of the polymer chain which was evidenced by the increase in the glass transition temperature that reached 274°C at 100% bromination degree. Chern et al. [4,5] suggested that increasing the bromination degree resulted in increasing both the density and the glass transition temperature. They reported an increase in the permeability of CO_2 and CH_4 gases, with CO_2/CH_4 permselectivity in the range 17-20, as the degree of bromination was

increased. They reported that increasing the degree of bromination resulted in increasing the chain stiffness and decreasing the polymer packing. These two conflicting factors canceled each other at lower bromination degree (less than 36%), while at higher bromination levels (more than 36%); both CO_2 and CH_4 diffusivities increased as a result of decreasing the polymer packing that overwhelmed the effect of the chain stiffness [4]. However, Story and Koros [3] reported that bromination of PPO resulted in reducing the chain spacing and fractional free volume relative to PPO. They postulated that substituting a bulky group, like the bromine group, on the phenyl ring position resulted in stiffening the ether linkage due to interference with the two methyl groups on an adjacent ring. With higher bromination degrees, the phenyl rings would stiffen and lock in an orthogonal conformation. Higher bromination would increase the average length of the rotating segment, the diffusional jump length, resulting in increasing the diffusion of gases in the polymeric membrane [3].

In this chapter, we report the permeability, solubility and diffusivity of gases in high molecular weight PPO and its brominated derivatives: 20.0 %, 37.4%, and 60%. Infrared spectroscopic technique provides an insight about the effect of bromination on the vibration mode of the different bonds and chemical groups.

5.2 Experimental

5.2.1 Materials

A sample of PPO (intrinsic viscosity in chloroform equal to 1.58 dL/g) was kindly supplied by General Electric Company, Selkirk, NY. All other chemicals used in the experiments were of reagent grade and were used without any further purification.

PPO was brominated to three levels: 20%, 37.4% and 60%. Bromination process is described in detail in the **General Experimental and Methods** chapter of this thesis report.

5.2.2 Preparation of Homogeneous Membranes

Dense homogeneous membranes were prepared by pouring 2% (w/w) polymer solutions into stainless steel rings. The rings, about 5.5 cm in diameter, were clamped onto the surface of a clean Pyrex glass plate. Trichloroethylene was used as a solvent for both 20% and 37.4% brominated PPO, while 60% brominated PPO was dissolved in chloroform. Solvent was removed by drying at room temperature for 24 hours. Membranes were then stored in vacuum for at least 48 hours before testing.

5.2.3 Permeability Measurements

Three membranes were installed and run simultaneously on the constant volume system. The feed pressure (absolute) was maintained at around 5250±50 mmHg (700.0 kPa) and the permeate pressure (absolute) cycle was maintained between 1 mmHg to 750 mmHg (0.133 to 100.0 kPa). Description of the constant volume system is found in the **General Experimental Methods** chapter.

5.2.4 Density and Sorption Measurements

Experimental procedure and calculations used in determining the solubility of gases in the

different membranes are detailed in the **General Experimental Methods** chapter.

5.2.5 Infrared Measurements

The infrared setup and operation is explained and discussed in the **General Experimental Methods** chapter.

5.2 Results and Discussion

Figure 5.1 presents the plot of the density of the PPO based polymeric membranes as a function of the bromination degree. It can be seen that the density of the membranes increases with the increase in the degree of bromination (Br). Chern et al. [4,5,7] reported a linear increase in the density of the polymer with the degree of bromination (based on low molecular weight PPO); however, it leveled off at degrees of bromination higher than 91%. Table 5.1 reports the permeability and solubility of CO_2, CH_4, O_2, and N_2 gases in PPO and brominated PPO membranes. It is clear from this table that the permeability increased for all gases as the degree of bromination increased. The sorption of gases increased with the increase in the degree of bromination. However, the diffusivity decreased for all gases as the

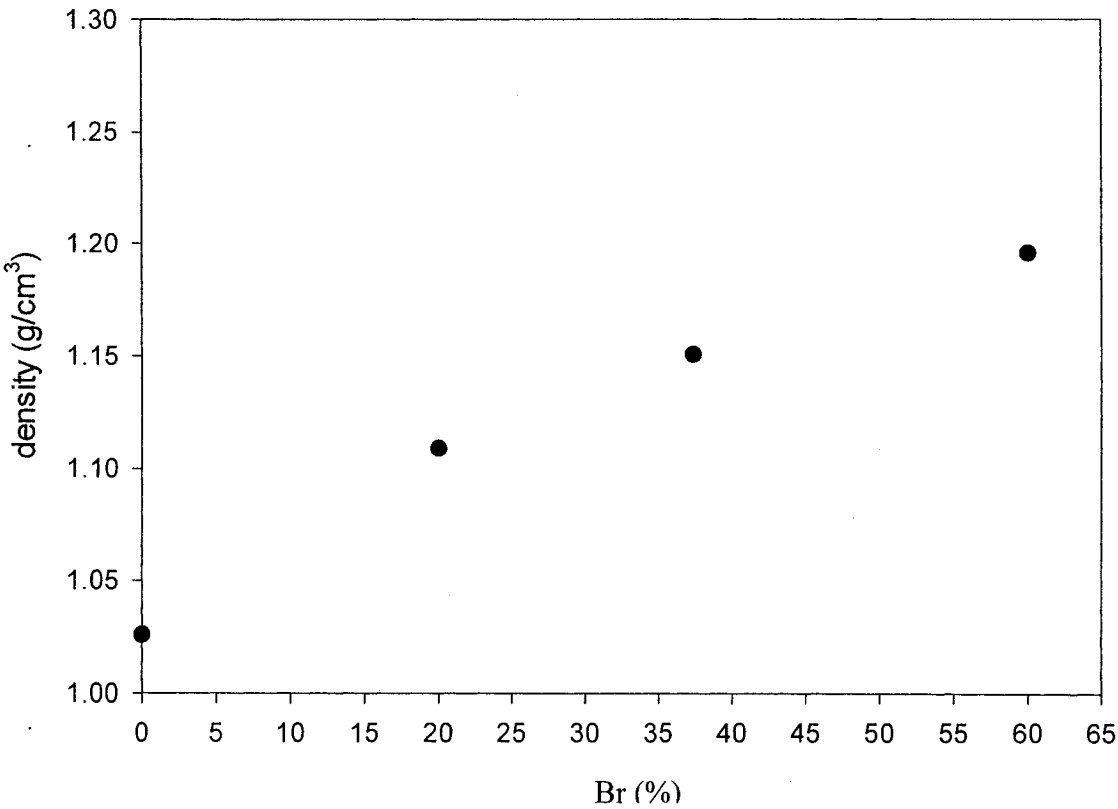

Fig. 5.1: Density of brominated PPO membranes as a function of the degree of bromination.

Table 5.1: Transport properties of PPO and brominated PPO membranes.

% Br[1]	Gas Permeability[2] (Barrer)				Sorption[3] (cm^3 (STP)/g)				Diffusivity[4] (10^{-8} cm^2/ sec)			
	CO_2	CH_4	O_2	N_2	CO_2	CH_4	O_2	N_2	CO_2	CH_4	O_2	N_2
0.0	90.0	5.4	16.7	3.7	7.1	2.3	0.4	0.4	9.1	1.7	34.4	7.6
20.0	93.6	4.9	18.8	3.8	7.4	2.5	0.9	0.6	8.6	1.3	14.2	4.1
37.4	97.1	5.4	17.7	3.7	8.4	2.7	1.1	0.8	7.9	1.4	11.0	3.0
60.0	159.9	9.1	36.7	8.0	8.0	2.8	1.3	1.1	13.6	2.2	19.9	5.2

[1]Degree of bromination
[2]Permeability obtained at 700 kPa (absolute) feed side and 100.0 kPa (absolute) permeate side.
[3]Sorption reported at pressure ≈ 100.0 kPa and 21.0°C.
[4]Diffusivity calculations are detailed in Appendix 6.A.

bromination level increased to 37.4%, and then it increased as the degree of bromination increased to 60%. The permeability of any gas has not effectively increased until high degree of bromination was achieved. Up to 37.4% bromination level, all gases have had little change in their permeability in comparison to PPO, while at 60% bromination level, the increase in the permeability of both O_2 and N_2 is about 120%, whilst the permeabilities of CO_2 and CH_4 are 70% higher than that in PPO membrane. The permeability ratios of CO_2/CH_4 and O_2/N_2 have not practically changed with the change in the bromination degree.

The data reported in Table 5.1 conform with the general trends reported in the literature for low molecular weight PPO, that the permeability of gases would be enhanced slightly by brominating PPO to degrees up to 36%. A significant increase in the permeability of all gases would be obtained at bromination degrees higher than 36% [3,6,7]. Although all the literature reported an increase in the solubility of gases in the polymer with the increase in the bromination degree, the main attribute to the significant jump in permeabilities when bromination degree was higher than 36%, is due to the significant increase in the diffusivities of these gases [3,7]. The increase in the degree of bromination results in stiffening the polymer backbone as evidenced by the increase in glass transition temperature measurements

[3-7]. The increase in the diffusion coefficients of the tested gases with the increase in the polymeric segments stiffness is indicative of the enhancement in the diffusional jumps rate [3]. Diffusional jumps rate is enhanced by an increase in the length of the polymeric segment that is involved in the diffusional jump. This is only possible when more than one phenyl ring is stiffened forming longer segments for rotation, which can be achieved with high degrees of bromination [3].

Figure 5.2-a shows the IR spectra of PPO membrane and Table 5.2 lists the possible IR frequency assigned to the different PPO bands. Figures 5.2-b to 5.2-d show the IR spectra of the brominated PPO membranes in helium gas. On comparing the IR spectrum of brominated PPO membranes to that of PPO membrane, it is noticed that bromination has caused some of the original PPO bands intensities to decrease and to broaden. In some cases, with 37.4% and 60% degrees of bromination, band splitting has occurred. Of particular interest are the 1300 cm^{-1} and the 1180 cm^{-1} bands which are assigned to the C-O-C bond, and the plane C-H bending, respectively. By brominating PPO at the phenyl ring, the bromine group, which is a bulky group, replaces the hydrogen atom, which is small in comparison to the bromine group. The bulky bromine group hinders the torsional motion of the phenyl ring around the ether linkage. As well, this bulky bromine group interferes with the vibration of the methyl groups on adjacent phenyl rings. This is reflected in the IR spectrum of the brominated PPO membranes. The decrease in the intensities of the bands with the increase in the degree of bromination indicates a decrease in the activity or vibration of these bands. For instance, the intensities of the bands at 1600 cm^{-1} and 1010 cm^{-1}, which are respectively assigned to aromatic C-C stretching and ring breathing, have decreased as the degree of bromination has increased.

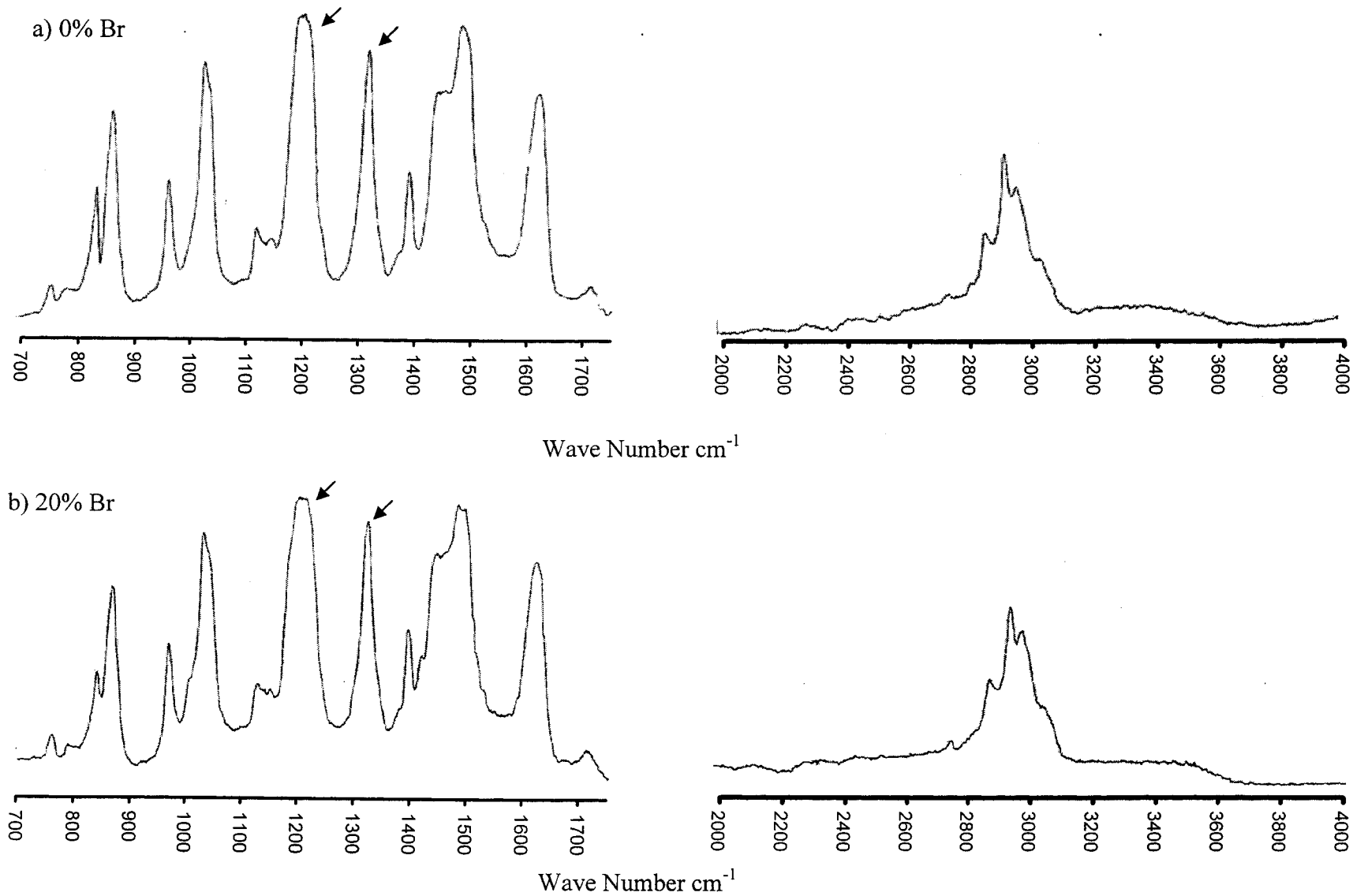

Fig. 5.2: IR spectra of HMW PPO based membranes: a) 0% Br; b) 20% Br; c) 37.4% Br; d) 60% Br.

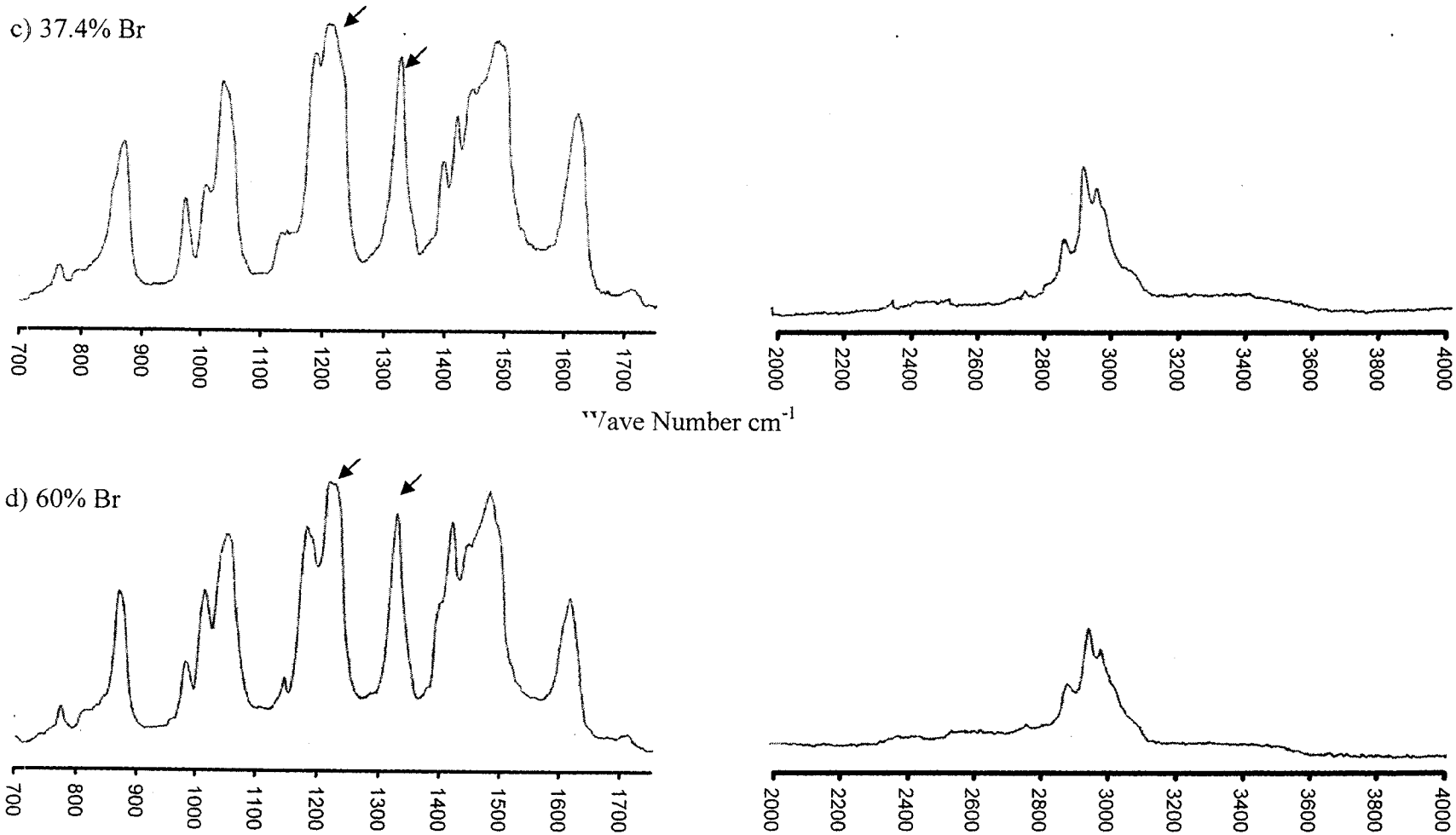

Fig. 5.2- continued.

Of particular interest are the 1300 and 1180 cm^{-1} bands. The decrease in the intensity of the 1300 cm^{-1} band that is assigned to the vibration of the C-O-C linkage is the result of the stiffening and reduction in the ether linkage torsional motion due to the presence of the bulky bromine on some of the phenyl rings. The decrease in the intensity of the 1180 cm^{-1} band, which is assigned to the plane C-H bending, as well as the splitting in this band, is indicative of the presence of different modes for C-H plane bending as a result of the induced hindrance by the bromine atom on the methyl groups of the adjacent phenyl ring.

Table 5.2: IR frequency assigned to PPO bands.

Frequency (cm^{-1})	Intensity	Vibration
3080-2800	Broad	Stretching alkane and aromatic C-H
1600	Sharp	C-C aromatic ring
1470	Sharp	Bending CH_2, anti-bending CH_3
1420-1450	Weak	Stretching CC aromatic
1380	Weak	Symmetric bending CH_3
1300	Sharp	C-O-C, C-C bridge bond
1180	Sharp	Plane CH bend
1120	Shoulder	Anti-stretching C-O-C
1010	Sharp	Trigonal ring breathing
950	Weak	Bending C-O-C
850	Sharp	Aromatic C-H out of plane bending
820	Sharp	Unknown

By compiling the IR observations and the gas transport data in the dense membranes as well as the information present in the literature [3-7]; the following is a postulation that is believed to explain the effect of bromination of PPO on the transport of gases in brominated PPO membranes. Bromination results generally in stiffening the polymer backbone, which reduces the diffusion of the gas molecules across the membrane in the intersegmental void space parallel to the polymer backbone. This is evidenced by the decrease in the diffusivity coefficient of all gases by brominating PPO up to 37.4% degree bromination. The decrease in the diffusivity is offset by the increase in the solubility of gases. At high degree of bromination, as in the case of 60% bromination degree, the length of the diffusional jump

segment is long enough, a result of stiffening more than one consecutive phenyl ring, to produce effective increase in the diffusional jump rate. This conforms to the postulation put by Story and Koros [3] that a high degree of bromination is needed to enhance the permeability of gases in the polymer in order to increase the interference of the bromine group with the methyl groups on the adjacent phenyl rings leading to some conformational interlock between stiffened phenyl rings and thus increasing the diffusional jump rate.

5.3 Conclusions

1. Brominating high molecular weight PPO increased the permeability of CO_2, CH_4, O_2, and N_2 gases. However, the permeability ratios CO_2/CH_4 and O_2/N_2 practically did not changed.
2. Increasing the bromination level of PPO results in increasing the solubility of gases.
3. Increasing the bromination level to a certain threshold value results in decreasing the gases diffusivity, when this threshold value is surpassed, a significant increase in the diffusivity of gases will be noticed. In this work, 37.4% brominated PPO membranes possessed the lowest diffusivity coefficients amongst the studied brominated PPO membranes (Br%: 0.0, 20, 37.4, 60).
4. IR spectra of the brominated PPO membranes have revealed that bromination results in reducing the vibrational activity of the ether linkage. As the degree of bromination increased, the splitting in the band assigned to the plane C-H bending increased while its intensity decreased as a result of the increase in the induced hindrance by the bromine groups on the methyl groups of adjacent phenyl rings.

5.4 References

[1] D. Aycock: "*Poly(Phenylene Ether), in Encyclopedia of Polymer Science and Technology*", V 13, Interscience Publishers, NY (1974).

[2] S. Percec and G. Li: "*Chemical modification of poly(2,6-dimethyl-1,4-phenylene oxide) and properties of the resulting polymers*", ACS Symposium Ser., 364, American Chemical Society, Washington DC (1988).

[3] B. Story and W. Koros: "*Sorption and transport of CO_2 and CH_4 in chemically modified poly (phenylene oxide)*", J. Membr. Sci., 67, (1992) 191-210.

[4] R. Chern, F. Sheu, L. Jia, V. Stannet and H. Hopfenberg: "*Transport of gases in unmodified and aryl-brominated 2,6-dimethyl-1,4-poly (phenylene oxide)*", J. Membr. Sci., 35, (1987) 103-115.

[5] R. Chern, L. Jia, S. Shimoda, and H. Hopfenberg: "*A note on the effects of mono- and di-bromination on the transport properties of poly(2,6-dimethylphenylene oxide*", J. Membr. Sci., 48, (1990) 333-341.

[6] C. Bonfanti, L. Lanzini, A. Roggero, and R. Sisto: "Chemical modification of poly (2,6-dimethyl-1,4-phenylene oxide) by bromination-alkynylation", J. Poly. Sci.: Part A: Polymer Chemistry, 32, (1994) 1361-1369.

[7] J. Lianda, F. Sheu, R. Chern, and H. Hopfenberg: "Gas sorption and transport in poly (phenylene oxide) (PPO) and aryl-brominated PPO membranes", Chinese J. Poly. Sci., 7, (4), (1989) 306-314.

Chapter 6

Gas Separation Performance of Membranes Made from Sulfonated Brominated Poly (Phenylene Oxide)

- Submitted to Journal of Membrane Science

Abstract

High molecular weight PPO was brominated to three levels of degree of bromination. Each brominated PPO was further sulfonated to three levels of degree of sulfonation. Membranes were prepared from these sulfonated brominated PPO and the transport properties of CO_2, CH_4, O_2, and N_2 gases in these membranes were characterized.

The main effect of bromination of PPO is to increase the permeability of gases while maintaining the same permselectivity. The main effect of simultaneous sulfonation and bromination of PPO is: (i) to increase the gas permeability, and to decrease the gas permeability ratio, in comparison to sulfonated-only PPO, while on the other hand, (ii) to decrease the gas permeability, and to increase the gas permeability ratio, in comparison to brominated only PPO. A noticeable trend in sulfonated brominated PPO membranes, when the degree of bromination is increased while the same degree of sulfonation is maintained, is the occurrence of a minimum in both gas permeability and diffusivity at 37.4% degree of bromination. All these effects produced by sulfonation of PPO, or bromination of PPO, or simultaneous sulfonation and bromination of PPO, are believed to be the direct result of the manipulation in the polymer backbone stiffness, membranes density, and membranes packing and free volume fraction.

6.1 Introduction

The trend in material development for better gas separation membranes is mainly toward improving the properties of existing polymers, which is attained via chemical and/or physical modification of the polymers to favor the transport properties of the gases of interest. Although there are no quantitative relationships to guide membrane structure-performance optimization, simple rules have emerged that currently offer the most reliable guide for understanding membrane structure-performance relation. According to these rules, the structure of the polymer repeat unit can be manipulated to achieve the most favorable balance of transport properties [1,3,4].

Poly (2,6-dimethyl-1,4-phenyl oxide) (PPO) belongs to the thermally-stable glassy polymers having a high glass transition temperature [2]. A very attractive characteristic of PPO is its high permeability to gases. It possesses gas permeabilities that are superior to other known glassy polymers such as polysulfones and polycarbonates. A major disadvantage of PPO as a gas separation membrane is its comparatively lower gas selectivity [3,4].

A number of electrophilic substitution reactions have been conducted on PPO to improve the gas separation characteristics. A possible mode of improving the permselective property of a polymer is by introduction of polar groups to induce stronger interchain interactions. Sakai et al. [5] studied the gas transport characteristics of Nafion, a sulfonated polymer. They have shown that the sulfonated fluorocarbon ionomer has improved gas selectivity. Chen and Martin [6] obtained O_2/N_2 selectivity of 11.7 using sulfonated polystyrene. Attempts were made to sulfonate PPO in order to improve the permselectivity of PPO. Fu et al. [7] reported that the permeability ratio of O_2/N_2

increased while O_2 permeability decreased significantly by sulfonation of PPO. Kruczek and Matsuura [8] showed that by sulfonating PPO, the permeability of gases would decrease while the permselectivity would increase. They obtained a CO_2/CH_4 permeability ratio of 43 while CO_2 permeability went down to 11 Barrer by sulfonating PPO [8].

Bromination of PPO at the aryl positions has been extensively studied. Most researchers studied the effect of bromination of low molecular weight PPO on gas separation performance [9-11]. Hamad et al. [12] studied brominated PPO having high molecular weight. The main effect of bromination is to increase the permeability of gases without sacrificing the parent PPO polymer permselectivity. Story and Koros [10] postulated that substituting a bulky group, like the bromine group, on the phenyl position resulted in stiffening the ether linkage due to interference with the two methyl groups on an adjacent ring. With higher bromination degrees, the phenyl rings would stiffen and lock in an orthogonal conformation. Higher bromination would increase the average length of the rotating segment, the diffusional jump length, resulting in increasing the diffusion of gases in the polymeric membrane [10]. Infrared (IR) study by Hamad et al. [12] on brominated PPO of high molecular weight supports the postulation of Story and Koros [10]. They added that low levels of bromination (20% and 37.4% bromination degrees) led to loss of diffusivity of gases as a result of stiffening of the polymer backbone, while at higher bromination levels, the permeability of gases increased significantly as a result of the increase in the diffusional jumps rate. The IR spectra of brominated PPO membranes revealed that brominating PPO at the phenyl ring resulted in decreasing both the C-O-C torsional motion, and the plane C-H bending. Splitting of the 1180 cm^{-1} band was observed at 37.4% and 60.0% bromination, which indicated that different modes for

alkane C-H bending occurred since the methyl groups were hindered by adjacent bromine substituents [12].

Chowdhury et al. [13] studied the effect of simultaneous bromination and sulfonation of high molecular weight PPO; they prepared three sulfonated brominated PPO polymers designated as SPPOBr20-1.78, SPPOBr40-1.47, and SPPOBr60-1.01. The abbreviation SPPOBr stands for sulfonated (S) brominated (Br) PPO; the first number following the abbreviation indicates the degree of bromination, e.g. 20, 40, or 60, while the second number indicates the ion exchange capacity (IEC), e.g. 1.78, 1.47, or 1.01 meq/g. They reported the permeability of gases in sulfonated brominated PPO membranes exhibited a minimum when the degree of bromination was about 40% [13]. As well, they reported the gas permeability of sulfonated PPO, with 1.8 meq/g IEC, for CO_2 and O_2 to be 14.1 and 2.38, respectively. The gas permeability ratio obtained for CO_2/CH_4 and O_2/N_2 were 50.4 and 5.8, respectively [13].

In this work, a thorough study is conducted on the effect of simultaneous sulfonation and bromination. In particular, focus was placed on:

1. Gas separation performance of the membranes, including the permeability of CO_2, CH_4, O_2 and N_2 gases, and the corresponding permselectivities.
2. Solubility and diffusivity of gases in the membranes.
3. Density and free volume fraction in the membranes.

The following notation will be used in while presenting results and discussion:

- Brominated PPO: PPOBr.
- Sulfonated PPO: SPPO.
- Sulfonated brominated PPO: SPPOBr.

6.2 Experimental

6.2.1 Materials

A sample of PPO (intrinsic viscosity in chloroform equal to 1.58 dL/g) was kindly supplied by General Electric Company, Selkirk, NY. All other chemicals used in the experiments were of reagent grade and were used without any further purification.

PPO was first brominated to three levels: 20%, 37.4% and 60%. Bromination process is described in detail in the **General Experimental Methods** chapter of this thesis report. Furthermore, the brominated PPO was sulfonated to three target IEC levels (see Table 6.1) for each level of bromination. The process of sulfonation is detailed in the **General Experimental Methods** chapter of this thesis report.

6.2.2 Preparation of Homogeneous Membranes

Dense homogeneous membranes were prepared by pouring 4% (w/w) polymer solution into stainless steel rings. The rings, about 5.5 cm in diameter, were clamped onto the surface of a clean Pyrex glass plate. After the polymer solution was poured into the rings, the polymer solution together with the glass plate was placed in a convection oven, which was heated to a predetermined temperature, for a predetermined period of time for drying. Table 6.1 details the solvent systems used to prepare the respective polymer solutions of the different membranes. Membranes were then stored in vacuum for at least 48 hours.

6.2.3 Permeability Measurements

Three membranes were installed and run simultaneously on the constant volume system. The feed pressure (absolute) was maintained at around 5250±50 mmHg (700.0 kPa) and the permeate pressure (absolute) cycle was maintained between 1 mmHg to 750 mmHg

(0.133 to 100.0 kPa). Description of the constant volume system is found in the **General Experimental Methods** chapter.

6.2.4 Density and solubility measurements

Experimental procedure and calculations used in determining the density of the membranes, and the solubility of gases in the different membranes are detailed in the **General Experimental Methods** chapter.

Table 6.1: Solvent systems and preparation conditions used to prepare the sulfonated brominated dense membranes.

%DBr[1]	%DSul[2] (IEC)[3]	Solvent system (w/w)	Evaporation	
			Temperature (°C)	Time (hours)
20.0	0.0	TCE[4]	Room	24
20.0	10.0 (0.7)	TCE/NMP (60/40)	60	24
20.0	19.7 (1.3)	TCE/NMP[5] (40/60)	60	24
20.0	26.7 (1.7)	TCE/NMP (20/80)	60	24
37.4	0.0	TCE	Room	24
37.4	7.8 (0.5)	NMP/Xylene (30/70)	70	24
37.4	18.0 (1.1)	NMP/Xylene (50/50)	70	24
37.4	25.5 (1.5)	NMP/Xylene (70/30)	70	24
60.0	0.0	Chloroform	Room	24
60.0	8.7 (0.5)	MtEt[6]/NMP (20/80)	70	24
60.0	20.2 (1.1)	MtEt/NMP (10/90)	70	24
60.0	32.9 (1.7)	NMP	70	24

[1] Degree of bromination.

[2] Degree of sulfonation.

[3] Ion exchange capacity (meq/g dry polymer).

[4] Trichloroethylene

[5] N-methyl-2-pyrrolidone

[6] 2-Methoxyethanol

6.3 Results and Discussion

Figure 6.1 presents the density of sulfonated brominated PPO membranes as a function of the total degree of chemical substitution (TSub). The degree of sulfonation (DSul) can be obtained from Fig. 6.1 by subtracting the degree of bromination (DBr) from TSub. The solid lines correspond to polymers having the same degree of bromination but different sulfonation degrees, while the dashed lines correspond to polymers of similar sulfonation degree but different bromination degrees. Since the solid lines are steeper than the dashed lines, it can be concluded that sulfonation has stronger influence on the density of the membranes than bromination. Sulfonic groups are strong polar groups that induce interchain interaction, which increases as the degree of sulfonation increases [1,7,8].

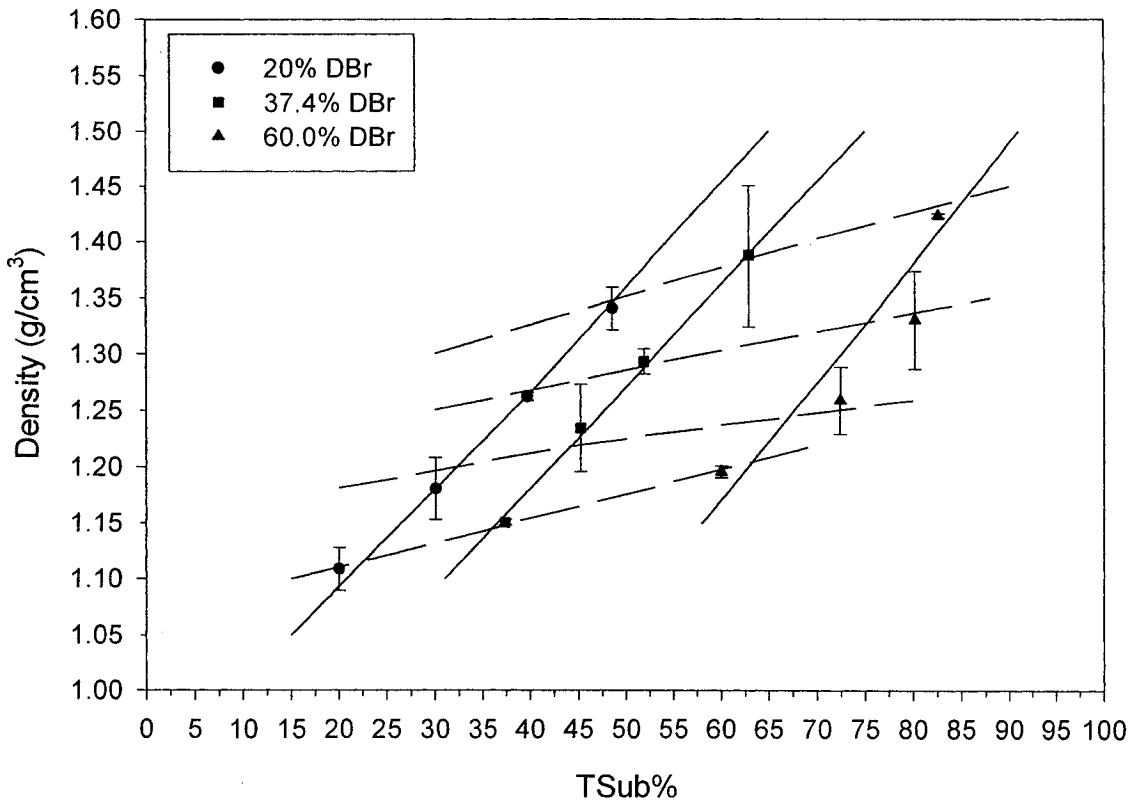

Fig. 6.1: Density of membranes made from sulfonated brominated PPO.

Table 6.2 details the performance of the membranes made from sulfonated brominated PPO. The following points can be deduced from Table 6.2:

1- All PPOBr membranes have higher gas permeability than PPO membranes, while they maintained the permselectivity of the parent PPO.

2- Increasing DSul while maintaining the same DBr in SPPOBr membranes results in decreasing gas permeability while gas permselectivity increases.

3- Generally, SPPOBr membranes have higher gas permeability when compared to SPPO membranes having the same DSul.

Table 6.2: Performance of sulfonated brominated PPO membranes.

%DBr	%DSul (IEC)	Gas permeability (Barrer)[1]				Permselectivity	
		CO_2	CH_4	O_2	N_2	CO_2/CH_4	O_2/N_2
0.0	0.0	90.0	5.4	16.7	3.7	16.7	4.5
20.0	0.0	93.6	5.4	16.7	3.7	17.3	4.5
20.0	10.0 (0.7)	84	3.15	13.6	3.3	26.7	4.1
20.0	19.7 (1.3)	58.8	1.77	9.9	1.5	33.2	6.6
20.0	26.7 (1.7)	40	0.96	7.5	1.2	41.7	6.4
37.4	0.0	97.1	5.4	17.5	3.8	18.0	4.6
37.4	7.8 (0.5)	62.5	2.8	10.2	2.4	22.3	4.3
37.4	18.0 (1.1)	40.8	1.44	4.1	0.8	28.3	5.1
37.4	25.5 (1.5)	24.3	0.6	3.6	0.6	40.5	6.0
60.0	0.0	159.9	9.1	36.7	8.0	17.6	4.6
60.0	8.7 (0.5)	147.2	8.5	27.0	6.0	17.3	4.5
60.0	20.2 (1.1)	84.8	2.3	14.0	2.0	36.9	7.0
60.0	32.9 (1.7)	76.4	1.8	12.6	1.7	42.4	7.4

[1]Reported permeabilities at permeate pressure (absolute)~ 100.0 kPa.

4- When DBr of SPPOBr membranes is increased while maintaining the same DSul, gas permeability exhibits a minimum at DBr = 37.4%. For example, for SPPOBr membranes having DSul ≈ 18.0%, the permeability of CO_2 drops from 58.8 Barrer, at DBr =20.0%, to 40.8 Barrer, at DBr =37.4%, then it increases to 84.8 Barrer, at DBr= 60.0%.

Figures 6.2 through 6.4 show the sorption of CO_2, CH_4, O_2, and N_2 gases, in SPPOBr membranes. Figures 6.2 through 6.4 show that for any DBr, sorption of CH_4, O_2, and N_2 gases have not changed significantly with the increase in DSul, while a significant increase, as expected, is noticed with the increase in DSul in the case of CO_2 gas.

Figure 6.5 presents the calculated diffusivity of the different gases in the sulfonated brominated PPO membranes (see appendix 6.A), as a function of DSul for the three-bromination levels: 20.0%, 37.4% and 60.0%. It should be noted that the diffusivity data correspond to gas pressure of 700 mmHg (93.3 kPa). It is clearly noticed in Fig. 6.5 that the lowest diffusivity coefficients were obtained for all gases when DBr was 37.4%. Figure 6.6 plots the free volume fraction as a function of DSul for the three levels of DBr. It can be concluded from Fig 6.6 that an increase in DSul results in decreasing the free volume fraction, which is the direct result of the increase in the interchain interaction (hydrogen bonding). The effect of bromination is generally to increase the free volume fraction when DSul=0. However, in the case of SPPOBr membranes, for any particular DSul (DSul> 0), increasing DBr from 20% to 37.4% produced no significant change in the free volume fraction, while increasing DBr to 60% produced a significant increase in the free volume fraction.

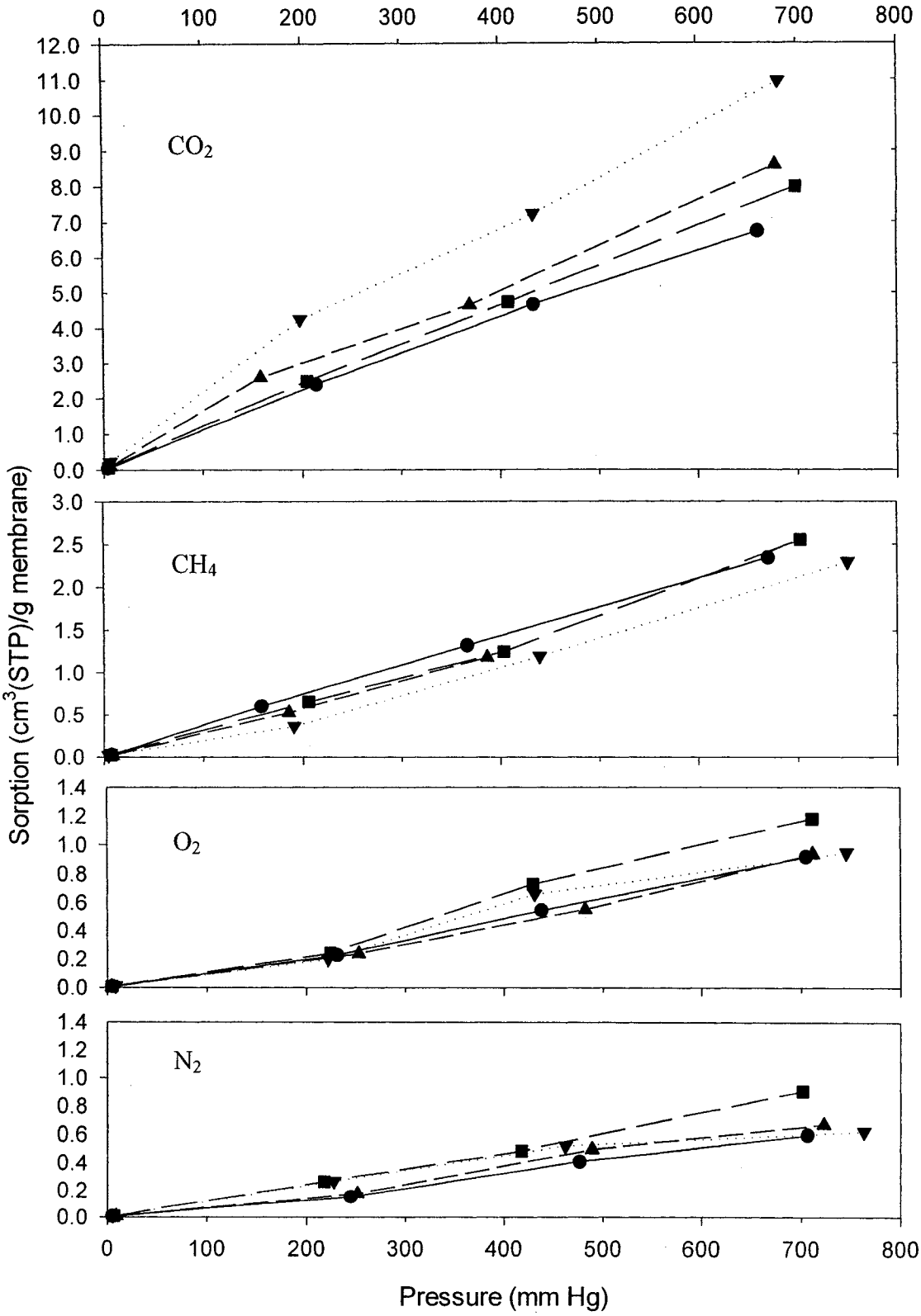

Fig 6.2: Sorption of CO_2, CH_4, O_2, and N_2 gases in 20% Brominated PPO sulfonated to different DSul (%): (●) 0.0, (■) 10.0, (▲) 19.7, and (▼) 26.7.

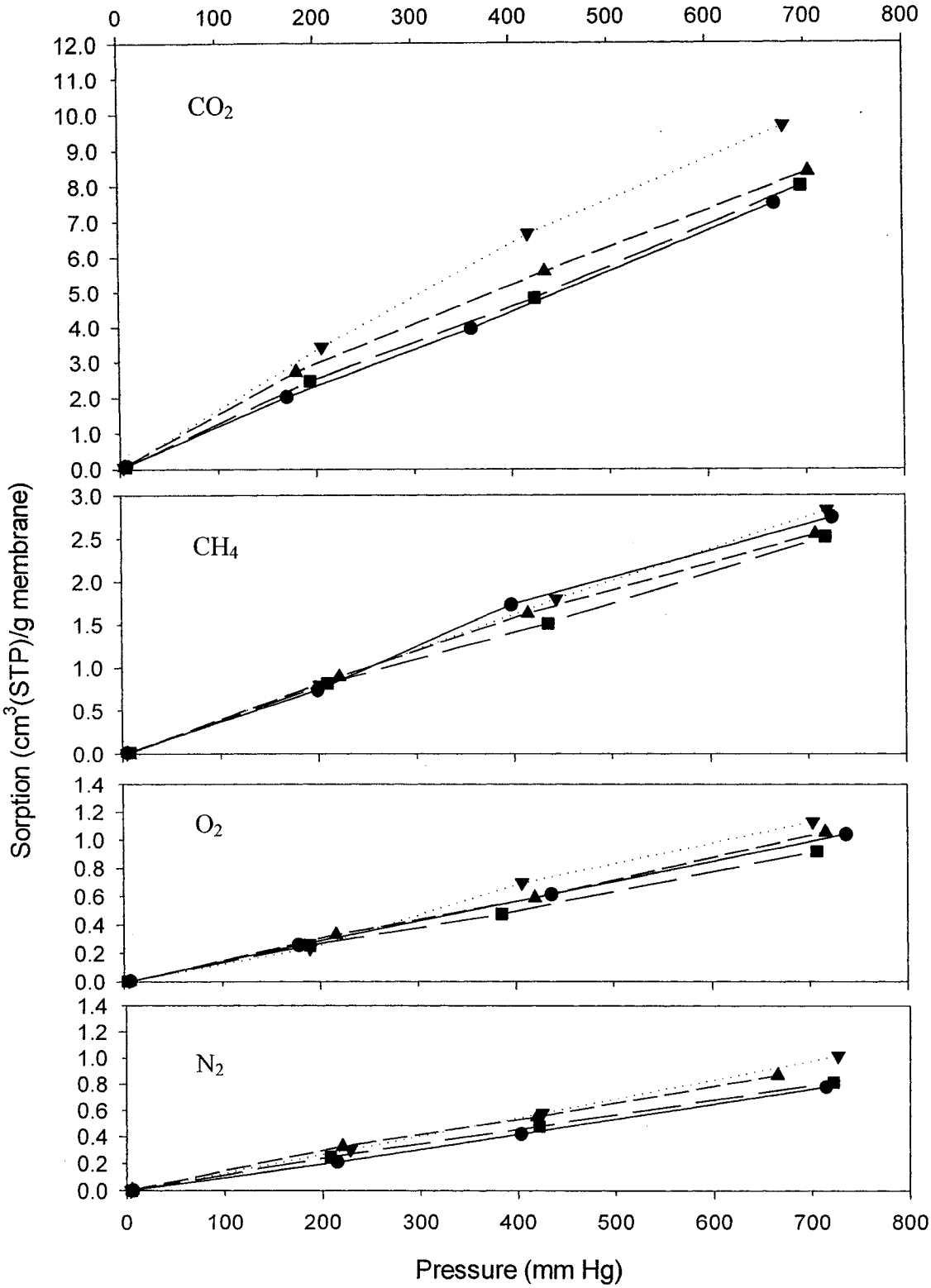

Fig. 6.3: Sorption of CO_2, CH_4, O_2, and N_2 gases in 37.4% Brominated PPO sulfonated to different DSul (%): (●) 0.0, (■) 7.8, (▲) 18.0, and (▼) 25.5.

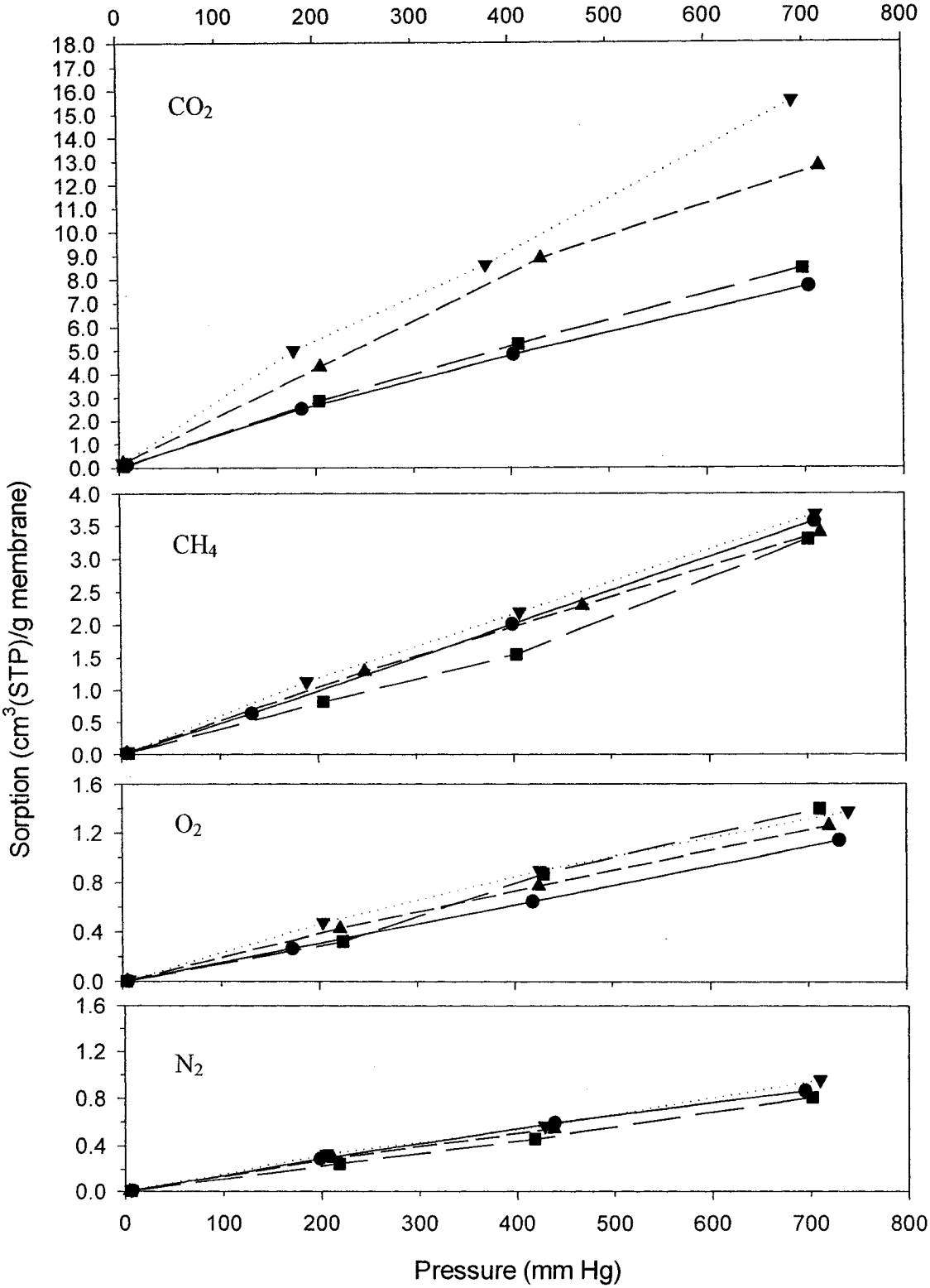

Fig. 6.4: Sorption of CO_2, CH_4, O_2, and N_2 gases in 60.0% Brominated PPO sulfonated to different DSul (%): (●) 0.0, (■) 8.7, (▲) 20.2, and (▼) 32.9.

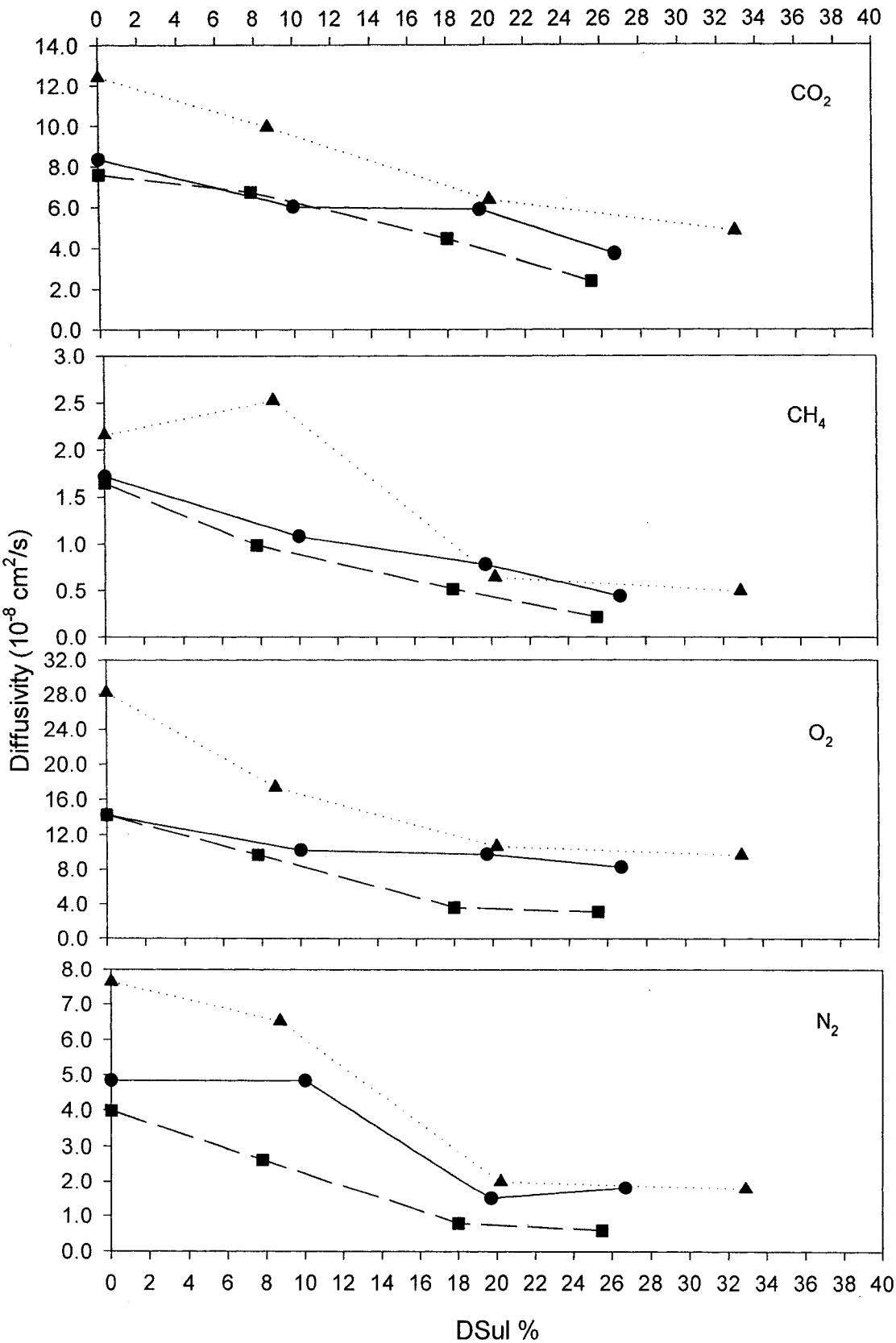

Fig. 6.5: Gas diffusivity in sulfonated brominated PPO membranes calculated at pressures ~ 700 mmHg: (●) 20.0% Br, (■) 37.4% Br, and (▲) 60.0% Br.

Revisiting the discussion presented in chapter (5) on the effect of bromination of PPO, in light of the free volume fraction data presented in this chapter. For PPOBr membranes, increasing DBr results in increasing the free volume fraction, however, gas diffusivity exhibits a minimum at DBr= 37.4% (data corresponding to DSul=0 in Figs. 6.5 and 6.6). This confirms the fact that the polymer backbone is more stiffened as DBr is increased to 37.4%, resulting in reduction in the rate of diffusion along the intersegmental void space parallel to the polymer backbone. Further increase in DBr results in enhancement in the diffusion rate, which could be the result of two factors: the increase in the free volume fraction and the increase in the diffusional jumps rate [10,12].

The trend in gas diffusivity in SPPOBr membranes (having the same DSul), is similar to

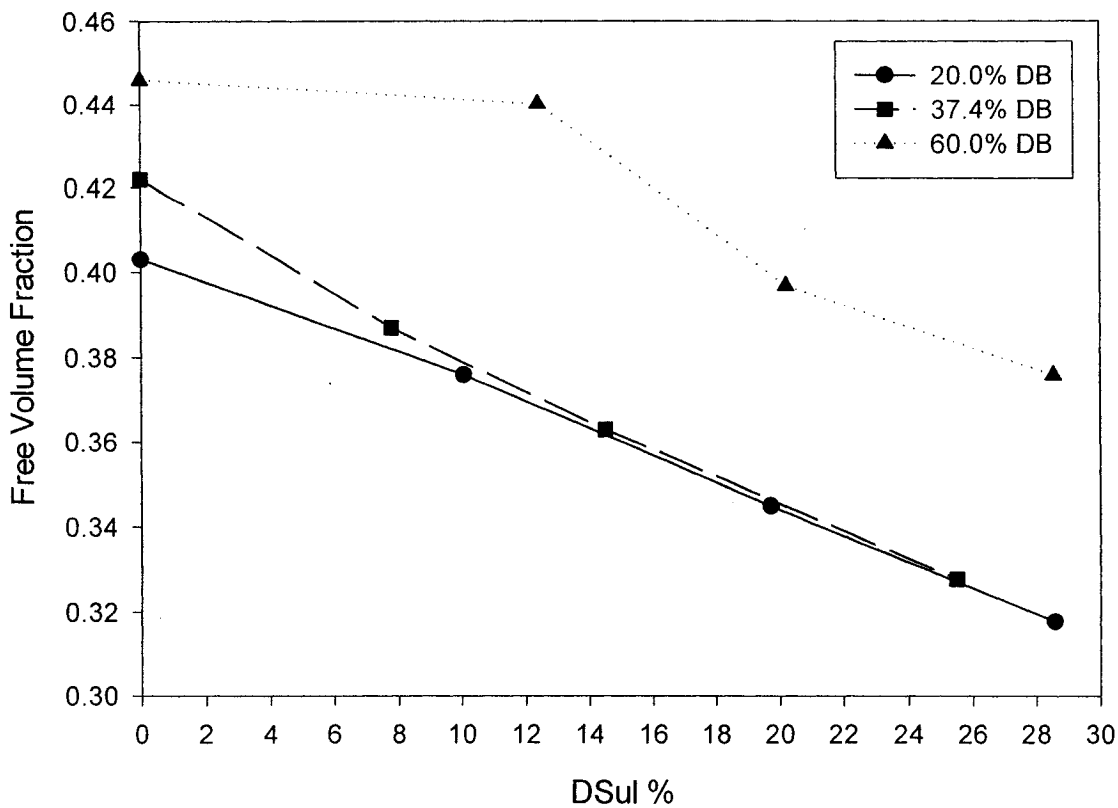

Fig. 6.6: Free volume fraction of sulfonated brominated PPO.

that in PPOBr membranes; i.e. the gas diffusivity exhibits a minimum at DBr= 37.4%. This is believed to be due to stiffening the polymer backbone, caused by both bromination and sulfonation, without any significant increase in the free volume fraction (see Fig. 6.6). However, increasing DBr to 60.0% has resulted in a significant increase in the free volume fraction, in addition to the increase in the diffusional jumps rate, which has consequently increased the gas diffusivity.

6.4 Conclusions

1. The higher the degree of sulfonation, the denser and more packed (lesser free volume) the membrane is. Bromination, on the other hand, produces less increase in the density of the membrane, while the free volume fraction increases.
2. For a given degree of sulfonation, SPPOBr membranes have higher gas permeability, but lower gas permeability ratio, in comparison to sulfonated-only PPO membranes.
3. For a given degree of bromination, the permeability and diffusivity of gases in SPPOBr membranes decrease as the degree of sulfonation increases.
4. In SPPOBr membranes, with increasing the degree of bromination while maintaining the same degree of sulfonation, the gas diffusivity and permeability will decrease until a threshold value is reached, after which both the gas diffusivity and permeability will increase. This is mainly the result of the manipulation in the polymer backbone stiffness, membranes density, and membranes packing or free volume fraction.

6.5 References

[1] J. Koros and G. Fleming: "*Membrane-Based Gas Separation*", J. Membr. Sci., 83, (1993) 1-80.

[2] D. Aycock: "*Poly(Phenylene Ether)*", Encyclopedia of Polymer Science and Technology, V 13, Interscience Publishers, NY (1974).

[3] R. Kesting and A. Fritzche: "*Polymeric Gas Separation Membranes*", Wiley Interscience, NY (1993).

[4] D. R. Paul and Y. Yampol'skii: "*Polymeric Gas Separation Membranes*", CRC Press, Boca Raton (1994).

[5] T. Sakai, H. Takenaka, and E. Tarikai: "*Gas Diffusion in the Dried and Hydrated Nafions*", J. Electrochem. Soc.: Electrochem. Sci. and Tech., 133, 88-92 (1986).

[6] C. Chen and C. Martin: "*Gas-Transport Properties of Sulfonated Polystyrenes*", J. Membr. Sci., 95, (1994) 51-61.

[7] H. Fu, L. Jia, and J. Xu: "*Studies on the Sulfonation of Polyphenylene Oxide and Permeation Behaviour of Gases and Water Vapor through Sulfonated PPO Membranes. I. Sulfonation of PPO and Characterization of the Products. II. Permeation Behaviour of Gases and Water vapor through Sulfonated Membranes*", J. Appl. Polym. Sci., 51, (1994) 1399-1409.

[8] B. Kruczek and T. Matsuura: "*Development and Characterization of Homogeneous Membranes from High Molecular Weight Sulfonated Poly (Phenylene Oxide)*", J. Membr. Sci, 146, (1998) 263-275.

[9] R. Chern, L. Jia, S. Shimoda, and H. Hopfenberg: "*A Note on the Effects of Mono- and Di-Bromination on the Transport Properties of Poly (2,6-Dimethylphenylene*

Oxide", J. Membr. Sci., 48, (1990) 333-341.

[10] B. Story and W. Koros: *"Sorption and Transport of CO_2 and CH_4 in Chemically Modified Poly (Phenylene Oxide)"*, J. Membr. Sci., 67, (1992) 191-210.

[11] R. Chern, F. Sheu, L. Jia, V. Stannet, and H. Hopfenberg: *"Transport of Gases in Unmodified and Aryl-Brominated on Poly (2,6-Dimethyl-1,4-Phenylene Oxide)"*, J. Membr. Sci., 35, (1987) 103-115.

[12] F. Hamad, K. Khulbe, and T. Matsuura: *"Characterization of Gas Separation Membranes Prepared from Brominated Poly (Phenylene Oxide) by Infrared Spectroscopy"*, Desalination, 148, (2002) 369–375.

[13] G. Chowdhury, R. Vujosevic, T. Matsuura, and B. Laverty: *"Effects of polymer molecular weight and chemical modification on the gas transport properties of poly (2,6-dimethyl-1,4-phenylene oxide"*, J. Polym. Sci., 77, (2000) 1137-1143.

[14] D.W. Krevelen: "Properties of Polymers", 3rd Ed., Elsevier, Amesterdam, (1990).

[15] F. Hamad, G. Chowdhury, and T. Matsuura: "*Development of sulfonated poly phenylene oxide- polyethersulfone thin-film composite membranes for gas separation: study on the effect of counter-cations on the gas transport properties*", J. Membr. Sci., 191 (1-2), (2001) 71-83.

6.6 Nomenclature

C	Concentration of adsorbed gas in the membrane, $cm^3(STP)/(cm^3_{membrane})$.
D	Gas diffusivity of the membrane, cm^2/s.
DBr	Degree of bromination, %.
DSul	Degree of sulfonation, %.
FVF	Free volume fraction.
IEC	Ion exchange capacity, meq/g.
M	Polymer molecular weight, g/mol.
p	Gas permeability of the membrane, Barrer.
S	Gas solubility of the membrane, $cm^3(STP)/(cmHg\ cm^3_{membrane})$.
TSub	Total degree of chemical substitution, %.
V_w	Van der Waals molar volume, cm^3/mol.
ρ	Membrane density, g/cm^3.

Appendix

6.A Diffusivity Calculations

The intrinsic gas permeability (p) is the product of two coefficients, the solubility of the gas in the membrane (S) and the diffusivity coefficient (D) [1,3,4]:

$$p = S \cdot D \rightarrow D = \frac{p}{S}$$

For example, for sulfonated brominated PPO (20.2% DSul and 60% DBr) membranes, which have a density of 1.331 g/cm^3:

$$p_{CO_2} = 84.8 \text{ (Barrer)} \times 10^{-10} \frac{\text{cm}^3\text{(STP).cm}}{\text{cm}^2\text{.s.cmHg}}$$

$$C_{CO_2} = 12.75 \frac{\text{cm}^3\text{(STP)}}{\text{g membrane}} = 9.6 \frac{\text{cm}^3\text{(STP)}}{\text{cm}^3\text{membrane}} \text{ (at pressure} \approx 716 \text{ mmHg)}$$

$$S_{CO_2} = 9.6 \frac{\text{cm}^3\text{(STP)}}{\text{cm}^3\text{membrane}} \times \frac{10 \text{ mmHg}}{1 \text{ cm Hg}} \times \frac{1}{716 \text{ mmHg}} = 0.134 \frac{\text{cm}^3\text{(STP)}}{\text{cm}^3\text{membrane.cmHg}}$$

$$D_{CO_2} = \frac{84.6 \times 10^{-10}}{9.6/(716/10)} = 6.33 \times 10^{-8} \frac{\text{cm}^2}{\text{s}}$$

6.B Free Volume Fraction Calculations

The molar volume of the polymer molecules is calculated based on the Van der Waals structural groups contribution. The free volume fraction (FVF) is calculated according to the following equation [14]:

$$FVF = 1 - \frac{V_w \rho}{M}$$

where V_w is the Van der Waals molar volume of the polymer, M is the molecular weight of the polymer, and ρ is the corresponding membrane density. Table 6.B.1 summarizes the results of the free volume fraction calculations.

The basic structure of PPO is shown in Fig. 6.B.1, where group A represents an atom or a substituent group attached to the aromatic carbon. In the case of sulfonated brominated PPO polymer, *A* could be (H) atom, or bromine (Br) atom, or sulfonic (SO_3H) group. Table 6.B.1 lists the Van der Waals volume of the different groups constituting the repeat units of sulfonated brominated PPO. Accordingly, the Van der Waals volume of the phenyl ring is: 71.1 cm^3/mol when *A*= H, 81.7 cm^3/mol when *A*= Br, and 96.0 cm^3/mol when *A*= SO_3H.

For unmodified PPO, the molecular weight of the repeat unit structure is 120 g/mol. The weight average of the molecular weight of the unmodified PPO used in this study (intrinsic viscosity in chloroform = 1.57 dL/g) is 316400 g/mol [15]. The following equations are used to calculate the molecular weight and molar volume of the chemically modified PPO polymer:

$$V_w = \frac{316400}{120.0}\left[71.1\left(1 - \frac{DSul}{100} - \frac{DBr}{100}\right) + 81.7\frac{DBr}{100} + 96.0\frac{DSul}{100}\right]$$

$$M = \frac{316400}{120.0}\left[120.0\left(1 - \frac{DSul}{100} - \frac{DBr}{100}\right) + 198.9\frac{DBr}{100} + 200.1\frac{DSul}{100}\right]$$

The free volume fractions were calculated based on membranes densities shown in Fig. 6.1, which are summarized in Table 6.B.1.

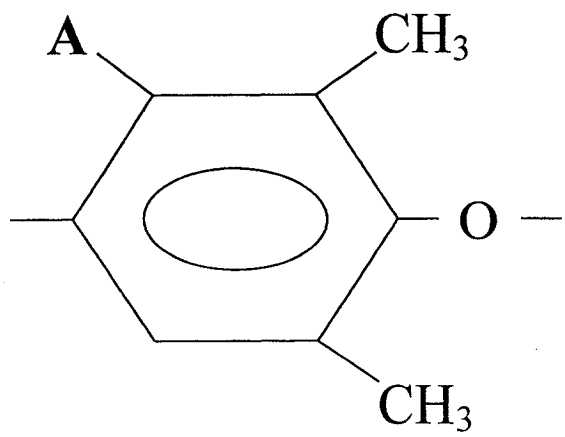

Fig. 6.B.1: Basic structure of a repeat unit of sulfonated brominated PPO. A= H, Br, SO_3H.

Table 6.B.1: Molecular weight, Van der Waals molar volume, and the free volume fraction of sulfonated brominated PPO membranes.

DSul (%)	DBr (%)	Density (g/cm^3)	V_w (cm^3/mol)	M (g/mol)	FVF
0.0	0.0	1.026	187467	316400	0.392
20.0	0.0	1.109	193057	358007	0.402
20.0	10.0	1.181	200570	379272	0.375
20.0	19.7	1.263	207756	399612	0.343
20.0	26.7	1.341	214368	418324	0.313
37.4	0.0	1.151	197920	394204	0.422
37.4	7.8	1.235	203731	410652	0.387
37.4	18.0	1.294	208742	424834	0.361
37.4	25.5	1.388	216940	448040	0.328
60.0	0.0	1.196	204236	441220	0.446
60.0	8.7	1.225	213499	467436	0.440
60.0	20.2	1.331	219302	483862	0.397
60.0	32.9	1.387	225528	501483	0.376

Table 6.B.2: Van der Waals molar volume and molecular weight of chemical groups forming the repeat units of sulfonated brominated PPO [14].

#	Chemical Group	V_w (cm^3/mol)	M (g/mol)
1	-H	3.44	1.0
2	-Br	14.0	79.9
3	$-SO_2-$*	20.3	64.1
4	-OH*	8	17.0
5	-O-	5.5	16.0
6	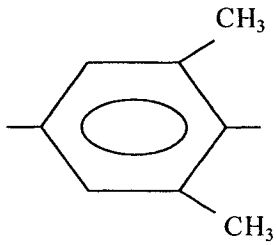	65.6	104
7*	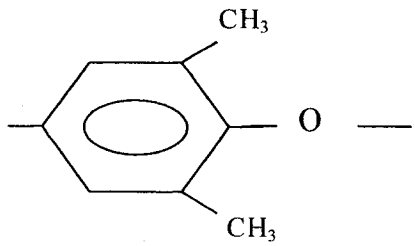	71.1	120.0
8*	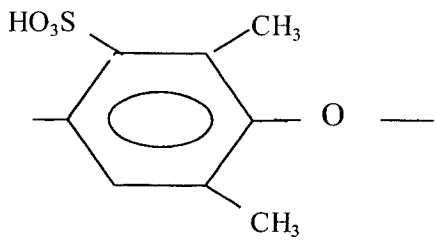	81.7	198.9
9*	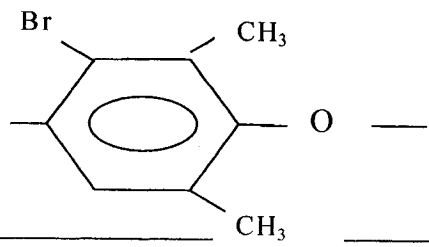	96.0	200.1

* $-SO_3H = -SO_2- + -OH$

*Entries 7 to 9 are calculated based on entries 1 to 6.

Chapter 7

Comparison of Gas Separation Performance and Morphology of Homogeneous and Composite PPO Membranes

• Submitted to Journal of Membrane Science

Abstract

Composite membranes, prepared by coating PPO on top of a 12-kDa MWCO ultrafiltration membrane (Osmonics-HO51), showed enhanced gas permeability ratio and separation factor for CO_2/CH_4 gas system, as well as some decrease in the permeability of CO_2 gas, in comparison to the dense homogeneous PPO membrane. Permeability ratios, CO_2/CH_4, obtained for composite and homogeneous PPO membranes were 37 and 17, respectively. The CO_2 permeabilities obtained for composite and homogeneous PPO membranes were 80 and 92 Barrer, respectively.

AFM observations showed that the coated layer of the composite membrane possessed graded compactness across the depth, rough and large polymer aggregates on top surface while smooth and fine polymer aggregates on bottom surface. This morphology profile was opposite to that observed for the dense homogeneous membrane.

Based on AFM observations and solvent evaporation kinetics, it is postulated that the enhancement in the selectivity and the drop in the gas permeability of the coated layer, in comparison to that of the dense homogeneous membrane, is due to the densification and compaction of the polymer adjacent to the support membrane interface. This is the direct result of the migration of solvent toward the support membrane and the partial draw of the solvent into the support membrane pores. This has produced a smoother bottom surface as a result of (i) the formation of small nodules, and (ii) the fusion of these small nodules by the compressive forces that have developed due to the shrinkage of the swollen support substrate. These compressive forces have caused the bottom surface to wrinkle.

7.1 Introduction

Composite membranes basically consist of one or more polymeric layers coated over a porous substrate that can be either an inorganic or a polymeric membrane. Ideally, the deposited layer, which is usually an expensive high performance polymer, controls the flux and selectivity of the composite membrane. The porous support membrane is to provide the mechanical strength for the selective layer in high operational pressures, and ideally should not contribute to the transport of the gas. The most attractive aspect of composite structures is the potential for minimizing cost because only small quantities of the high performance polymer are utilized for their formation.

The effect of the pores and the pore size distribution of the microporous support on the final performance of the TFC membranes have been mentioned in the literature [1]. Some authors [2] have addressed the problem of pore penetration (which results in a large effective thickness) by impregnating the support with a nonsolvent so as to achieve a thin, defect free skin layer of a glassy polymer. They have also shown that a high molecular weight polymer, along with a good solvent, has given maximum hydrodynamic dimensions reducing the extent of pore penetration, which further has resulted in a thin top layer. Rezac and Koros [1] showed that proper selection of the pore size distribution, the polymer molecular weight and solvent system, might eliminate the pore intrusion problem, rendering the polymer coil dimensions in the coating solution larger than the biggest pore of the support. Using high concentration solution of high molecular weight polymer minimizes the intrusion of the polymer into the pores due to the interlock between the polymeric coils. Other treatments that are found in the literature include heat treatment or annealing [3], pre-coating the support with a gutter layer [4,5].

Kesting and Fritzsche [6] stated that no generalization could be drawn about the effect of polymer-solvent and polymer-polymer interaction on the density and the order of the dense films. The relation between the reduced viscosity and the concentration of polymer in solution evidences this. Polymers are more extended and swollen in strong solvents than in weak solvents, reflected in higher reduced viscosities for the same concentration in the case of stronger solvents. However, this picture is reversed at high polymer concentrations due to increasing polymer segments entanglement. Nevertheless, the kinetic of dissolvation is expected to significantly influence the packing density of the membrane, which is affected by the temperature of the dissolvation and the volatility of the solvent. The packing density of the membrane is influenced by the stiffness of the polymer chain that is further influenced by the polymer-solvent interaction in a manner that is similar to the effect of the molecular weight.

Khulbe et al. [7] showed that the morphology of the top and bottom surfaces of poly (phenylene oxide) (PPO) membranes, as well as the gas permeability and CO_2/CH_4 permeability ratio, depended on the preparation temperature. The roughness of the top surface increased as the preparation temperature decreased. The nodule size on the top surface increased as the preparation temperature decreased. The permeability of gases increased while the CO_2/CH_4 permeability ratio decreased as the preparation temperature decreased.

The permeability and permselectivity of the coated layer of composite membrane is usually considered to be equal to those of a dense homogeneous membrane prepared from the same polymeric material. This is based on the argument that the coated layer of a TFC membrane and the dense homogeneous membrane has identical physical and

morphological characteristics.

Alsdeg et al. [8] observed an increase in the surface roughness and depressions, an increase in the molecular weigh cut off (MWCO), and an increase in the product rate; as the rate of solvent exchange during the phase inversion process was increased. Gildert et al. [9] showed that as the self-diffusivity coefficient, which is defined as the product of activity and diffusivity coefficient, of water in the gelation medium decreased, the solute separation coefficient increased and the product rate of the membrane decreased. Decreasing the self-diffusivity coefficient resulted in decreasing the rate of non-solvent (water) penetration into the incipient membrane phase during gelation; therefore, finer polymer aggregates would precipitate, resulting in a denser skin layer, smoother surface, and smaller effective pores size [9].

In this chapter, the performance of PPO composite membranes is investigated and compared to that based on dense PPO membranes. The comparison is carried out in terms of:

1. Gas permeation and separation performance.
2. Morphology of top and bottom surfaces of the dense homogeneous membrane and coated layer.
3. Kinetics of solvent evaporation.

7.2 Experimental

7.2.1 Materials:

A sample of PPO (intrinsic viscosity in chloroform equal to 1.58 dL/g) was kindly supplied by General Electric Company, Selkirk, NY. All other chemicals used in the experiments were of reagent grade and were used without any further purification.

Commercial unltrafiltration (UF) polyethersulfone (PES) membrane (Osmonics HO51), having 12-kDalton molecular weight cut off (MWCO) was used as the support membrane.

7.2.2 Preparation of Composite Membranes

PPO was dissolved in trichloroethylene (TCE) to prepare a 3.0% (w/w) solution. The solution was then filtered through 3.0μm teflon filter to remove impurities present in the solution. Prior to coating, the porous PES substrate membranes were thoroughly washed in demineralized water. Fresh UF membrane coupons were randomly cut, then soaked in distilled water for 24 hours and left to dry at room temperature in the fumehood for 24 hours. Coating solution was spread over the PES substrate membrane with a rounded tip dropper. The volume of PPO solution coated on a unit surface area of PES substrate membrane was 0.045 cm^3/cm^2.

The coated PPO layer could be easily peeled, which made determination of the coated layer thickness possible. The coated layer could be peeled when PPO concentration in the coating solution was 1.0% (w/w) and higher.

7.2.3 Preparation of Homogeneous Membranes

Dense homogeneous PPO membranes were prepared by pouring 3.0% (w/w) PPO-TCE polymer solution into stainless steel metal rings. The metal rings, about 5.5 cm in

diameter, were fixed on the surface of a clean Pyrex glass plate. The polymer solution together with the glass plate was placed in the fumehood at room temperature for 24 hours.

7.2.4 Gas Permeation Testing

Three membranes (dense homogeneous or composite) were installed and run simultaneously on the constant volume system. The feed pressure was maintained at around 5250 mmHg (700.0 kPa absolute) and the permeate pressure cycle was maintained between 1 mmHg to 750 mmHg (0.133 to 100.0 kPa absolute). Description of the constant volume system is found in the **General Experimental Methods** chapter.

7.2.5 Intrinsic Viscosity Measurements

Determination of the intrinsic viscosity of PPO–TCE solution is detailed in the **General Experimental Methods**. The efflux times of dilute PPO–TCE solutions were measured using capillary viscometer (Cannon-Fenske viscometer #100).

7.2.6 Solvent Weight Loss

A specially fabricated mold set, composed of a stainless steel square frame and a glass plate, was used to prepare the homogeneous and composite membranes. A predetermined amount of 3% (w/w) PPO-TCE solution was used to prepare the dense homogeneous membrane or to coat the substrate membrane. To prepare the composite membrane, a piece of the support membrane, cut to the area of the glass plate, was held firmly between the glass plate and the metallic frame. When the homogeneous membrane was prepared, a piece of the support membrane was cut according to the shape and dimensions of the frame, in order to be used as a gasket between the glass plate and the frame to prevent any seeping of the polymer solution. The mold set was fixed on the tray of a four-

decimal-digits digital-balance. The weight of the mold set is tared. Then the polymer solution was spread over the glass plate, or the support membrane, using a round tip dropper. Timer was set on the instant of applying the solution. The weight of solution was recorded versus time. Schematic of the glass and frame set is shown in Fig. 7.1.

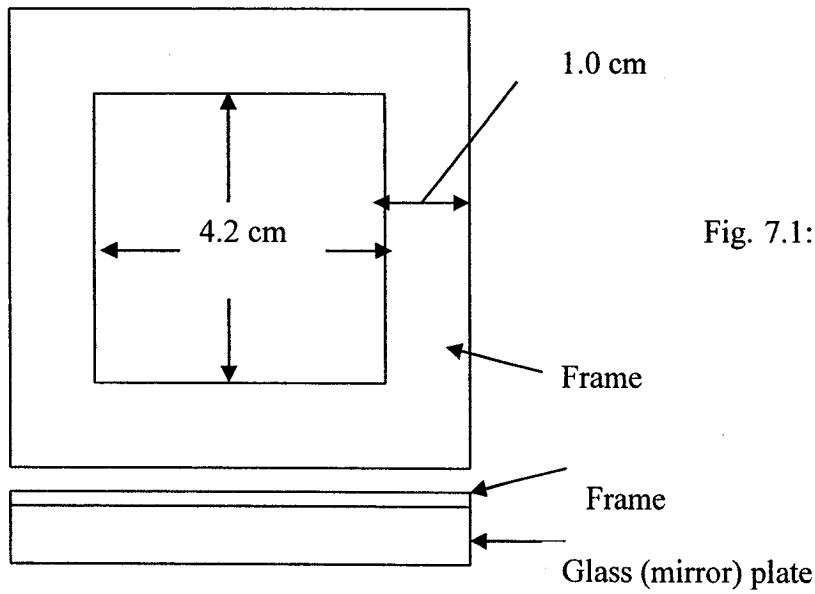

Fig. 7.1: Plate and frame set used to prepare the homogeneous and composite membranes.

7.2.7 Atomic Force Microscopy

Images of the surfaces of the membranes were taken using the tapping mode (TM) atomic force microscopy (AFM) on a Nanoscope III equipped with a 1553D scanner from Digital Instruments, which is available at the Industrial Membrane Research Institute (Chem. Eng. Dept./ U. of Ottawa). It is known that the resolution of any surface image by TM AFM depends on the size and curvature of the tip. Surface roughness parameters are affected, in addition to the tip size and curvature, by the treatment of the surface data captured (flattening, filtering, etc.). In this work, all surface images were taken with the same tip and treated in the same way [10].

The mean roughness (R_a) of the captured surface was calculated (built-in facility in AFM

software) based on the following equation:

$$R_a = \frac{1}{L_x L_y} \int_0^{L_x} \int_0^{L_y} |F(x,y)|\, dx\, dy$$

where $F(x,y)$ is the surface relative to the center plane, and L_x and L_y are the dimensions of the surface. The center plane is the plane at which the volumes enclosed by the image above and below of it, are equal [10].

7.3 Results and Discussion

7.3.1 Performance of PPO Dense and Composite Membranes

Figures 7.2 to 7.4 present the performance of the homogeneous and composite PPO membranes, based on pure CO_2 and CH_4 gas permeation experiments. Figure 7.5 and 7.6 compare the performance of the homogeneous and composite PPO membranes, based on CO_2/CH_4 (20/80 mol/mol) gas mixture permeation experiments. The gas permeability of the composite membrane is based on the thickness of the coated layer, which was measured after the permeation experiments were over.

It is clearly noticed that the separation efficiency of the composite membrane, indicated by both permselectivity and the separation factor, has overwhelmingly over-performed

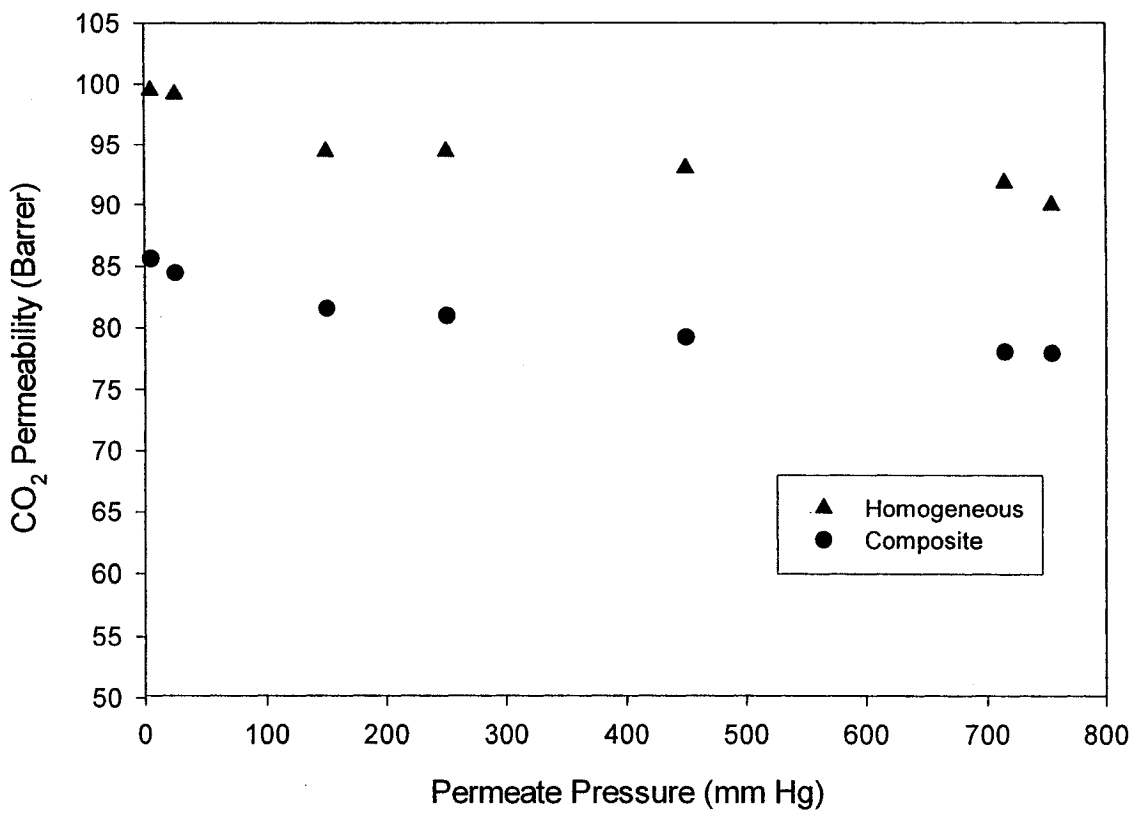

Fig. 7.2: Permeability of CO_2 in homogeneous and composite membranes.

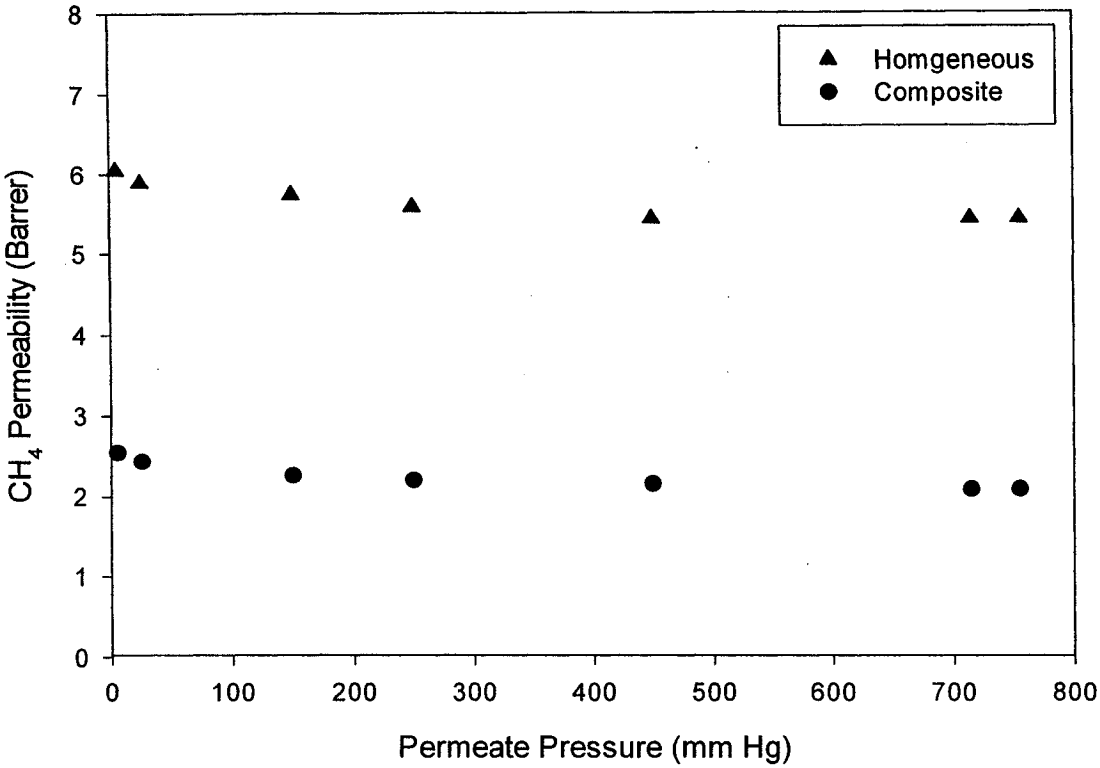

Fig. 7.3: Permeability of CH_4 in homogeneous and composite membranes.

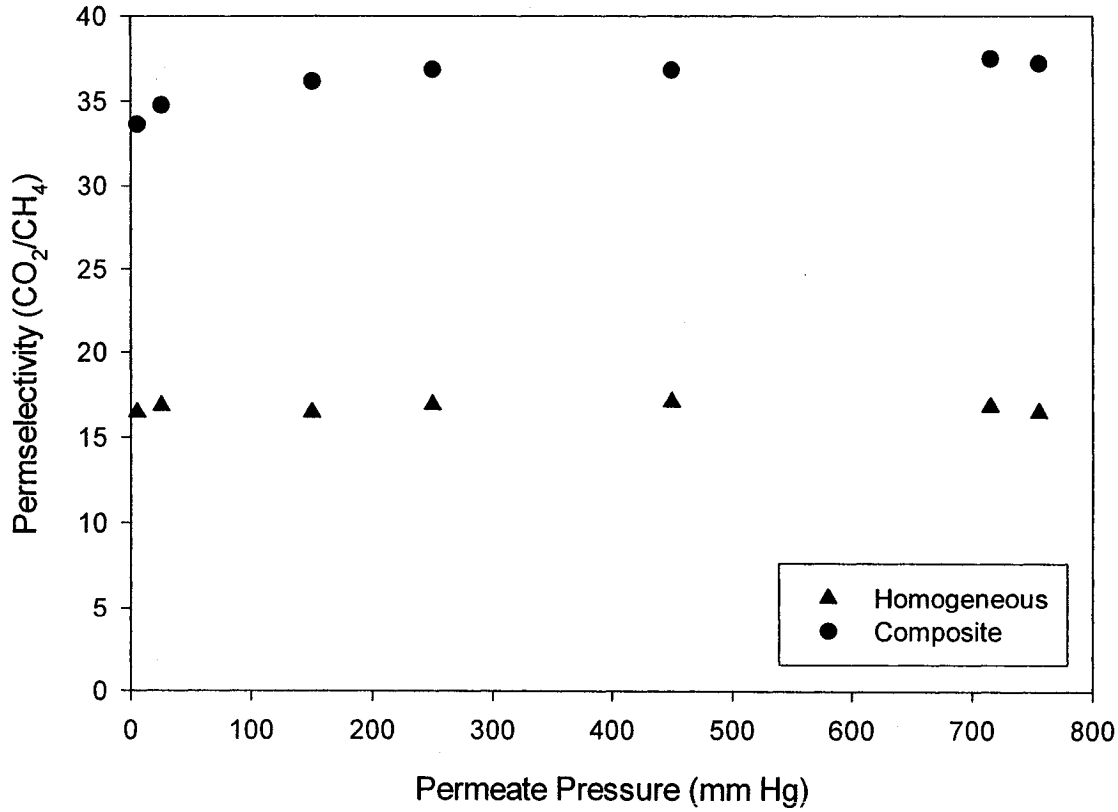

Fig. 7.4: Permeability ratio, CO_2/CH_4, in homogeneous and composite membranes.

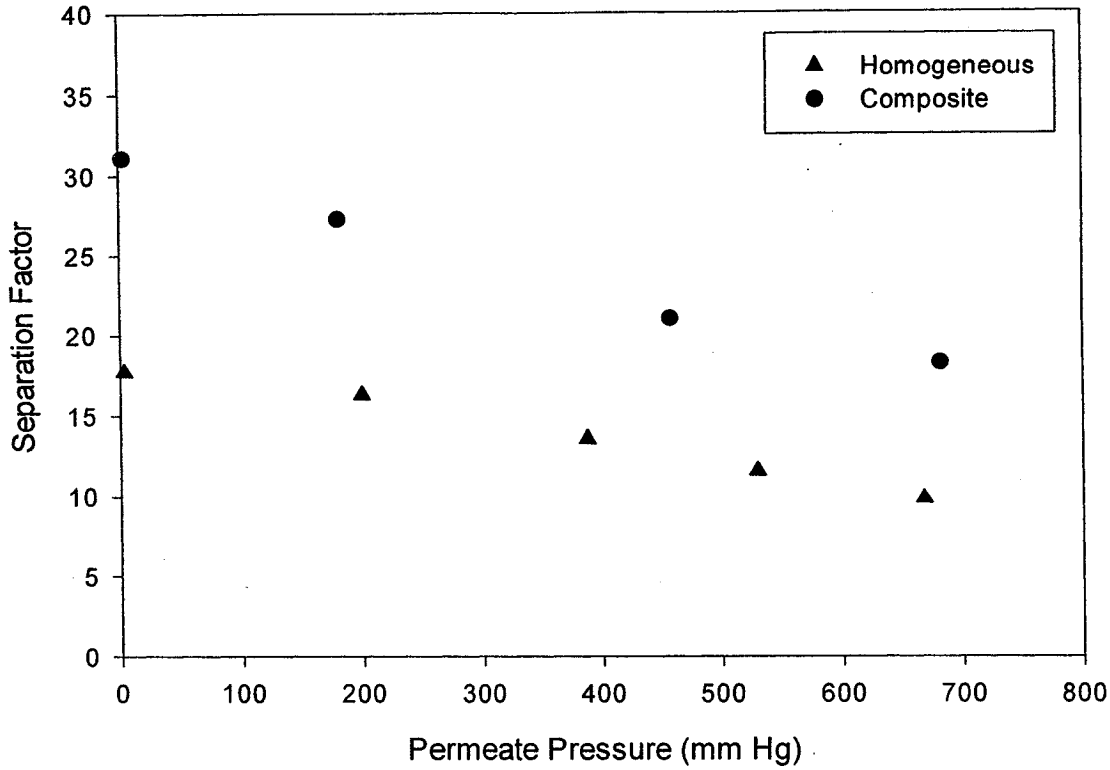

Fig. 7.5: Separation factor for (20/80) CO_2/CH_4 gas mixture feed in homogeneous and composite PPO membranes.

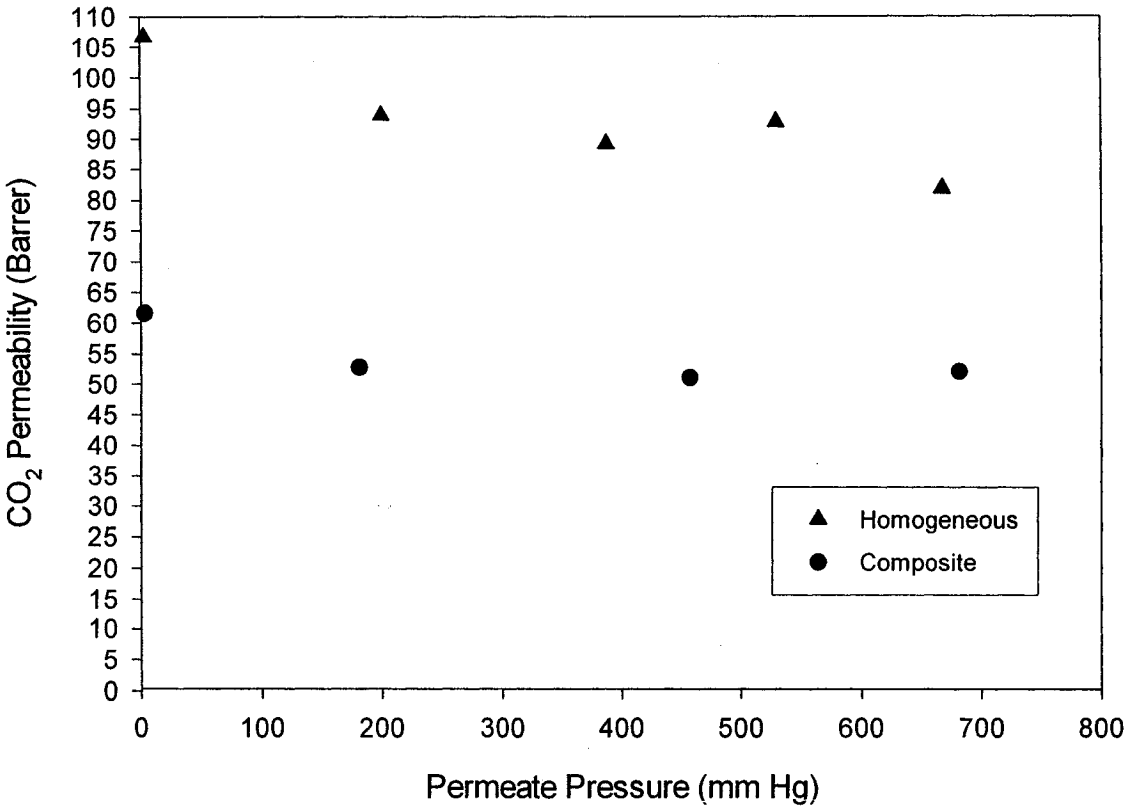

Fig. 7.6: Permeability of CO_2, based on feed gas mixture (20/80 CO_2/CH_4), of homogeneous and composite PPO membranes.

that of the homogeneous membrane. The increase in the separation efficiency is accompanied by a decrease in the gas permeability of the membrane for both CO_2 and CH_4.

CO_2 permeability of PES is 2.8 Barrer with CO_2/CH_4 permeability ratio equal to 30 [6,11]. Compared to the data given in Table 7.1 for PPO, CO_2 permeability of PES is much lower and CO_2/CH_4 permeability ratio is much higher. The possibility of the selectivity of the composite membrane to approach that of the PES, as a result of the intrusion of the coating polymer into the pores of the support membrane, is examined in the following.

The resistance model is utilized to assess the effect of the intrusion of the coating polymer into the pores of the support membrane on the overall performance of the composite membrane [4,6]. It is important to notice that the resistance model that is applied here does not account for any resistance imposed by an empty pore. The pore flow mechanisms prevailing in the pore size range available are Knudson and slip flow mechanisms [4,6]. These mechanisms if contributing to the overall performance of the composite membrane, work to undermine the permselectivity of the composite membrane.

Table 7.1 gives definitions and values of parameters required in the resistance model equations. The resistance model assumes that the polymer that has penetrated into the pores of the substrate has the same intrinsic permeability as that of the coating polymer. The depth of penetration is assumed to be equal to the thickness of the support membrane skin layer. Note that a wide range is given to penetration depth, set equal to δ_S, and surface porosity, f, for the test calculation. The actual δ_S and f are supposed to be well

Table 7.1: Definition of variables and parameters used in the resistance model.

Variable/Parameter	Definition	Value
δ_C	Coating thickness	13×10^{-4} cm (assumed)
δ_S	Support membrane dense layer thickness	0.0012×10^{-4} to 6.0×10^{-4} cm (assumed)
f	Fraction of pores area on the support membrane surface (surface porosity)	10^{-5} to 50% (assumed)
p_C	Coating polymer permeability (Set equal to intrinsic value of the dense homogeneous membrane)	CO_2= 92.0 Barrer
	Coating polymer permeability ratio (Set equal to intrinsic value of the dense homogeneous membrane)	CO_2/CH_4=17
p_S	Support membrane polymer (PES) intrinsic permeability [6,11]	CO_2= 2.8 Barrer
	Support membrane polymer (PES) intrinsic permeability ratio [6,11]	CO_2/CH_4=30

within these ranges. The component resistances, that are expected to contribute to the overall resistance of the composite membrane, are shown in Fig. 7.7, and are defined by the following equations.

$$R_C = \frac{\delta_C}{A_C p_C} \quad (1)$$

$$R_P = \frac{\delta_S}{A_C f p_C} \quad (2)$$

$$R_S = \frac{\delta_S}{A_C (1-f) p_S} \quad (3)$$

The overall resistance, R_T, is composed of the coating layer resistance, R_C, followed (in series) by two parallel resistances: the coated polymer intruded into part of the support membrane pores, R_P, and the support membrane skin layer polymer matrix, R_S.

Therefore, R_T is given by:

$$R_T = R_C + \frac{R_S R_P}{R_S + R_P} \tag{4}$$

The overall permeability is given by,

$$p_T = \frac{\delta_C + \delta_S}{A_C R_T} \tag{5}$$

where A_C is the membrane area.

Figure 7.8 shows the performance envelope produced by solving the resistance model for CO_2 permeability and ideal permselectivity. The envelope covers the many combinations of penetration depths and surface porosities in the ranges listed in Table 7.1. It is clear from Fig. 7.8 that the actual performance of the PPO composite membranes is far from the envelope. This indicates that the enhanced selectivity is most likely inherent to the coating layer.

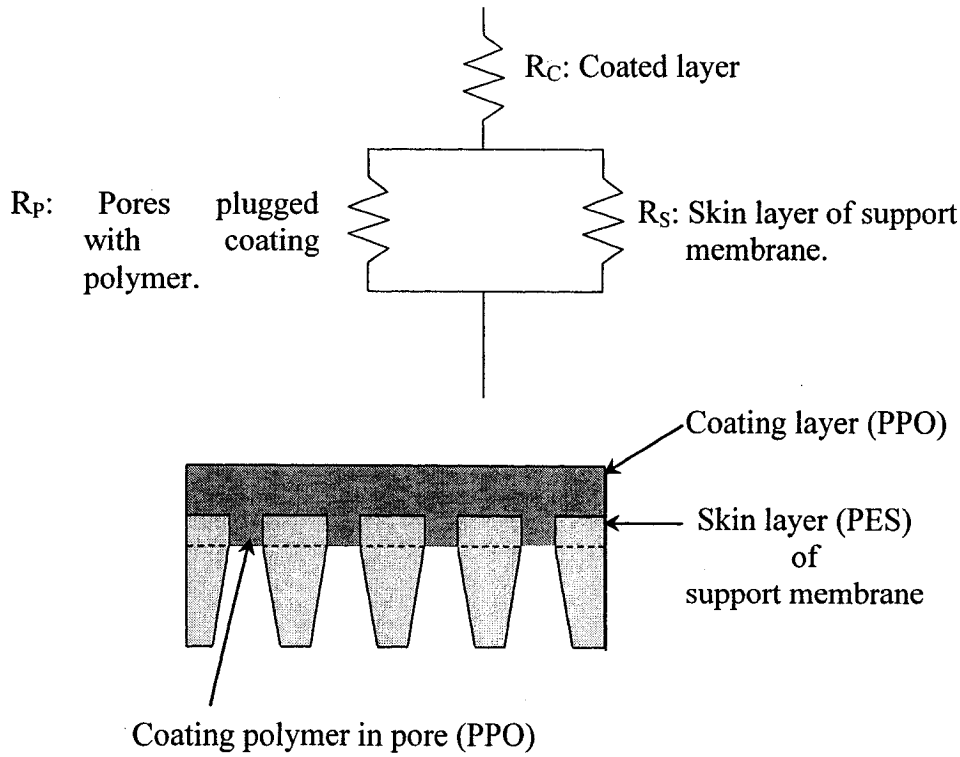

Fig. 7.7: Schematic of the composite membrane acting resistances.

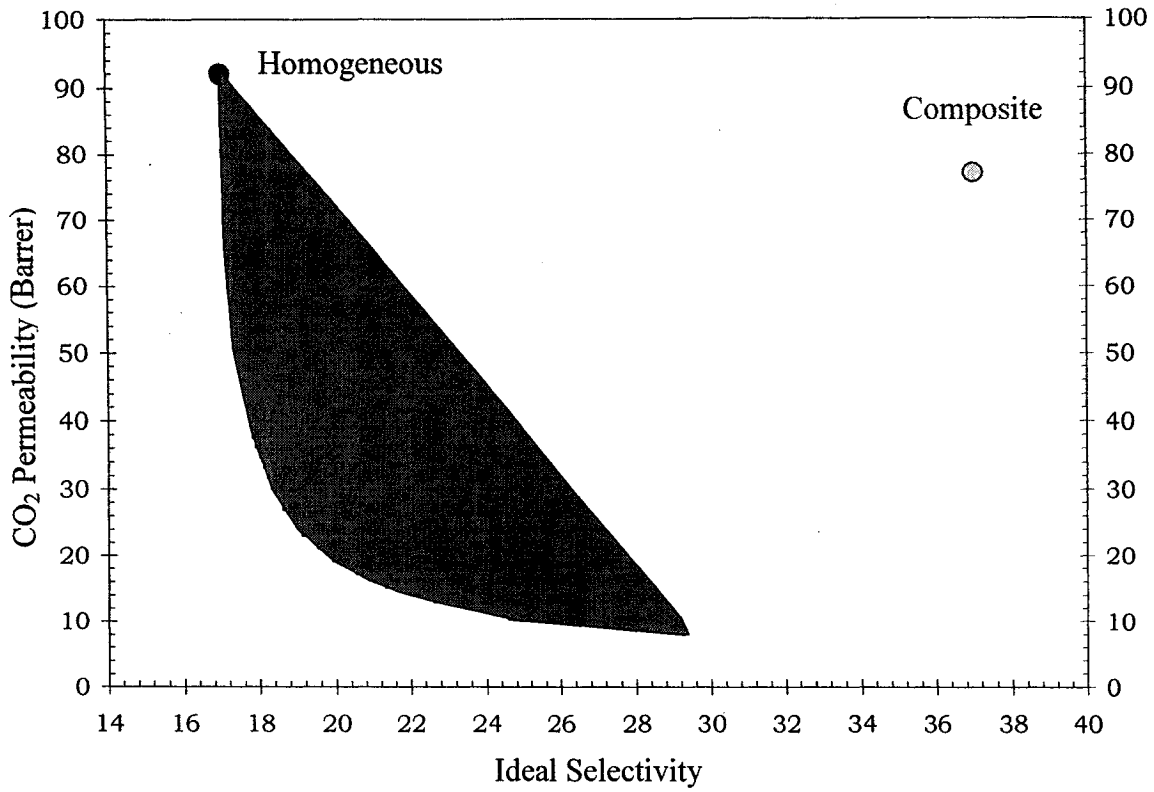

Fig. 7.8: Resistance model prediction in comparison to the actual performance of dense and composite PPO membranes.

In fact, there is least possibility for the penetration of coating polymer in the support membrane pores. Figure 7.9 represents the cumulative pore size distribution of the UF PES membrane, HO51, used as the support membrane [12]. The largest pore size is expected to be about 30 nm. The diameter of the PPO polymeric coil at infinite dilution in TCE, assuming it is spherical, is 42 nm. This is based on intrinsic viscosity of PPO in TCE solutions of 1.282 (dL/g). More details about PPO coil size determination will be given in the next chapter. Thus, the PPO polymer coil in TCE solution is large enough to be retained on top of the pore of the support membrane [1].

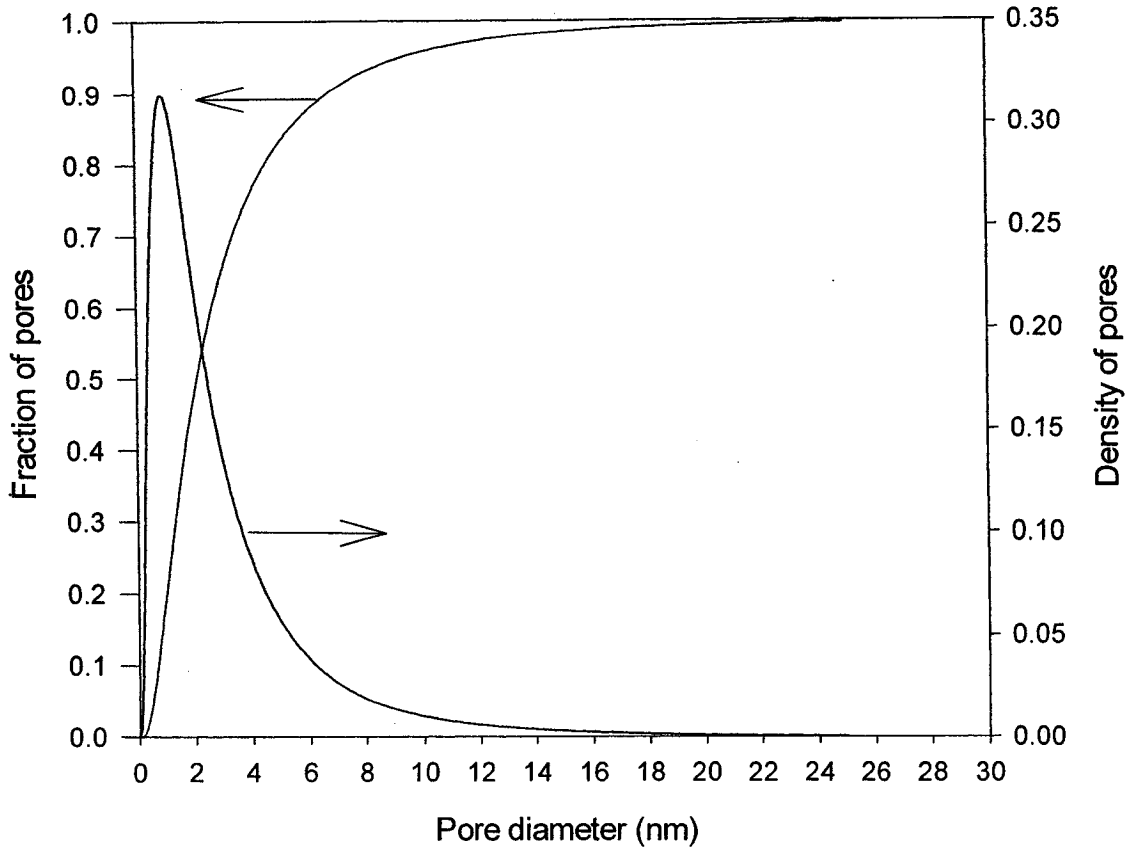

Fig. 7.9: Probability density function and cumulative distribution of pores size of PES (HO51) membranes.

7.3.2 Solvent Evaporation During the Preparation of Composite and Homogeneous PPO Membranes

Figure 7.10 shows the change of the ratio of the membrane weight, W, to the weight of solution initially added to mold set (Fig. 7.1), W_o, with time. Figure 7.10 shows that the weight of the solution decreases with time due the loss of solvent by evaporation. The figure shows also that the rate of solvent evaporation is different for homogeneous and composite membranes. Since the starting PPO concentration in PPO-TCE solution was 3% (w/w), the curves approach the 3.0% at infinite time. The amount of solution used to prepare the coated layer of the composite membrane and the dense membrane was about 1.350 g.

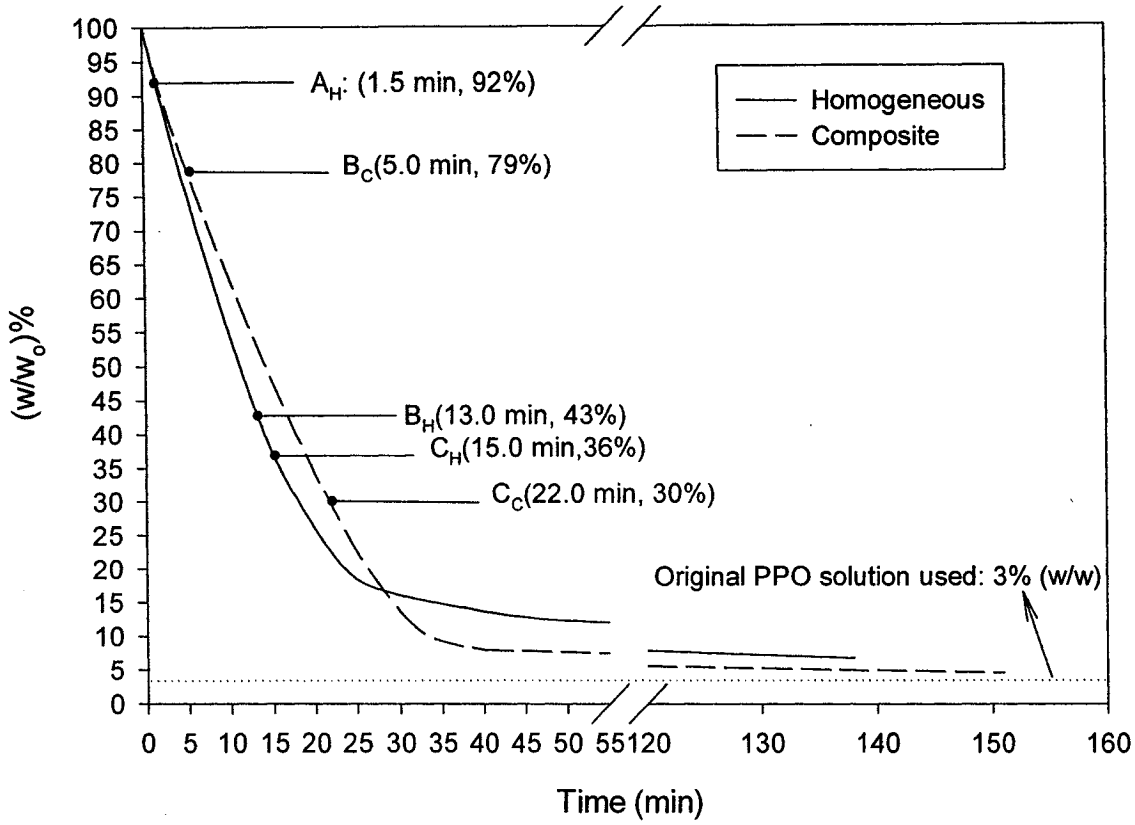

Fig. 7.10: Ratio of membrane weight to the initial solution weight used to prepare the membrane, as a function of drying time.

The plot of the rate of liquid evaporation vs. the liquid to solid weight ratio, in drying wet solid, is characterized by three main stages [13]:

- First phase: The evaporation rate is constant. This stage is controlled by the loss of the liquid from a completely wet surface (liquid-air interface).
- Second phase: The evaporation rate decreases consistently. This stage is controlled mainly by the evaporation of liquid at the air-interface; however, the decreasing evaporation rate is the result of the appearance of dry spots.
- Third phase: The drying process is controlled by the movement of the liquid through the solid layer as a result of the concentration gradient between the deeper parts and the surface. As the liquid concentration decreases, the rate of internal solvent movement

decreases.

- Other phases may exist as a result of the presence of different mass transfer resistances within the solid layer. In some cases evaporation may take place beneath the surface forming a receding liquid zone.

The above theory is applied to the evaporation of solvent from the solvent (TCE)/ polymer (PPO) solution. From Fig. 7.10, evaporation rate was calculated, which was plotted versus TCE/PPO weight ratio in Fig. 7.11. The weight ratio of TCE solvent to PPO starts from 32.33 (g/g), i.e. the weight ratio of TCE to PPO in the original solution used to prepare the membranes. As evaporation proceeds, the polymer concentrates and the solvent to polymer ratio decreases. Note that the evaporation procedure is split into 4

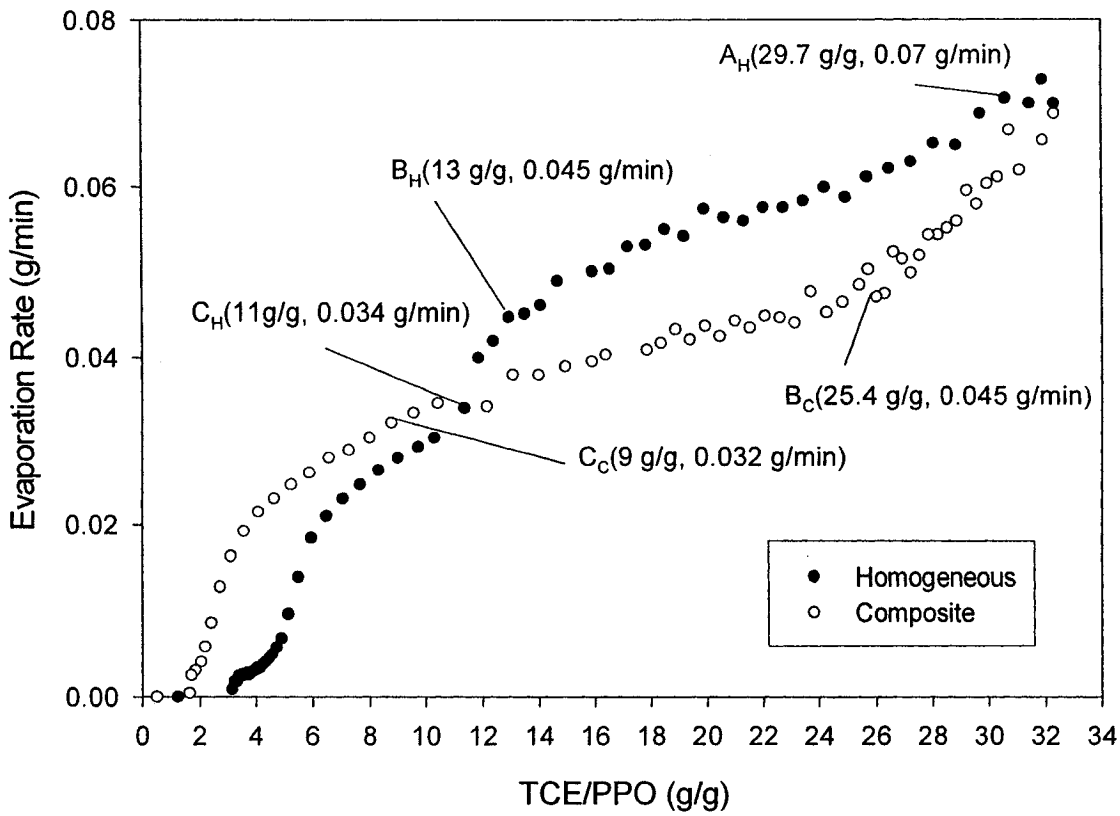

Fig. 7.11: Evaporation rate of TCE solvent as a function of (TCE/PPO) weight ratio, during the preparation of dense homogeneous and composite PPO membranes.

stages according to the theory described above. Note also that the end of stages 1,2 and 3 are indicated by letters A, B, and C respectively, with subscripts H and C, indicating homogeneous and composite membranes, respectively.

Looking into Fig. 7.11, the first phase characterized by a constant evaporation rate appears for homogeneous membrane but is missing for the composite membrane. The second phase is much shorter for the composite than the homogeneous membrane, but the evaporation rate at the end of the second phase is 0.045g/min for both. This is followed by a much longer third phase for the composite membrane than the homogeneous membrane.

These two different modes of solvent evaporation can be explained by assuming that solvent evaporation took place unidirectionally from the bottom side of the cast film to the air in the case of the homogeneous membrane, while in the case of the composite membrane, a part of the solvent moved initially to the other direction, i.e. from the top to the bottom side of the cast film, due to the draining action of the pores of the support membrane surface. The solvent is retained in the pores for some time before moving back to the top surface of the cast film. The amount of solvent at the top surface of the cast film is therefore much smaller in the beginning of the solvent evaporation for the composite membrane. Thus, the first and the second stages will become shorter. But the third stage, which reflects the movement of solvent from deep inside of the cast film to the top surface, becomes much longer for the composite membrane.

7.3.3 Morphology of Top and Bottom Surfaces of Dense Homogeneous and Composite PPO Membranes

Figure 7.12-a and –b are scanning electron microscope (SEM) images for the top (air-

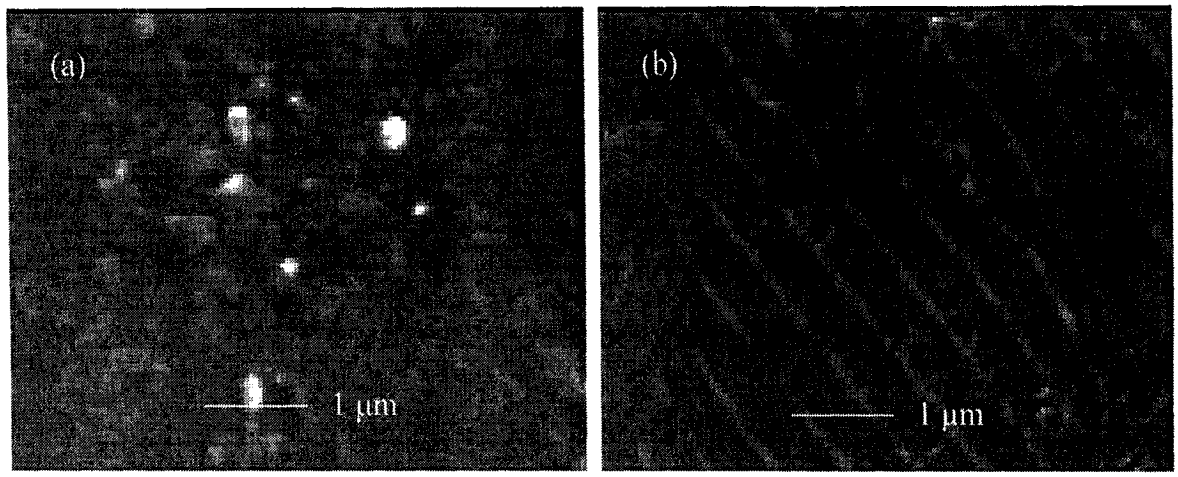

Fig. 7.12: SEM pictures of the top (a) and bottom (b) surfaces of a peeled-off PPO layer coated on PES HO51 UF membrane.

interface) and bottom (support-interface) surfaces, respectively, of a peeled-off coated layer of a composite PPO membrane.

It can be noticed that the top surface of the coated layer is rough and contains big nodule aggregates, while on the other hand; the bottom surface is smoother than the top surface with the appearance of an organized pattern. These observations on the coated layer surface morphology were further confirmed by the atomic force microscope (AFM) images. Figures 7.13 and 7.14 show the AFM images of the top and bottom surfaces of the homogeneous and peeled-off coated layer of composite PPO membranes. Table 7.2 summarizes the main morphological features of the top and bottom surfaces for these membranes.

In Table 7.2 and Figs. 7.13 and 7.14, we can observe:

1. For the homogeneous membrane, roughness increased from top to the bottom surface. Similarly, the nodule size increased from the top to the bottom side. On the contrary, both roughness and the nodule size decreased from the top to the bottom side for the composite membrane. Therefore, an inversion in the order of the nodule size and roughness was observed.

2. The surface of the homogeneous membrane is relatively smooth and no pattern lines were observed, unlike on the surface of the composite membrane.

Table 7.2: Comparison of the main morphological features on top and bottom surfaces of homogeneous and peeled-off coated layer of PPO composite membranes.

Membrane	Roughness		Remarks
	Top (nm)	Bottom (nm)	
Homogeneous	0.6	1.3	Uniform nodules (15-20 nm) on top surface. Nodules on bottom surface (20-25 nm).
Composite	4.2	1.2*	Top surface: presence of big nodules (~45 nm) and aggregates of nodules ranging from 90 to 250 nm. Bottom surface: presence of pattern with wide smooth surface in between the pattern lines. Nodule size ~25 nm.

*This corresponds to the roughness of the surface between the pattern lines.

The increase in the roughness and the nodule size from the top to the bottom of the homogeneous membrane is a norm [7]. But the decrease in the roughness and the nodule size from the top to the bottom of the coated layer of the composite membrane needs some explanation. It was suggested in the foregoing section that the solvent was drawn into the pores of the substrate membrane by the capillary action and then gradually moved back to the coated film as more solvent evaporated into the air from the top surface of the coated film. While the solvent is drawn into the pores of the substrate membrane, the surface of the membrane will swell, which will be followed by the shrinkage of the surface as the solvent moves back to the coated film. During the latter shrinkage period, a compressive force will work at the bottom of the coating film, bringing the nodules compactly together. Thus, several nodules are fused, leading to a decrease in the roughness. The compressive force can be so strong that wrinkling may

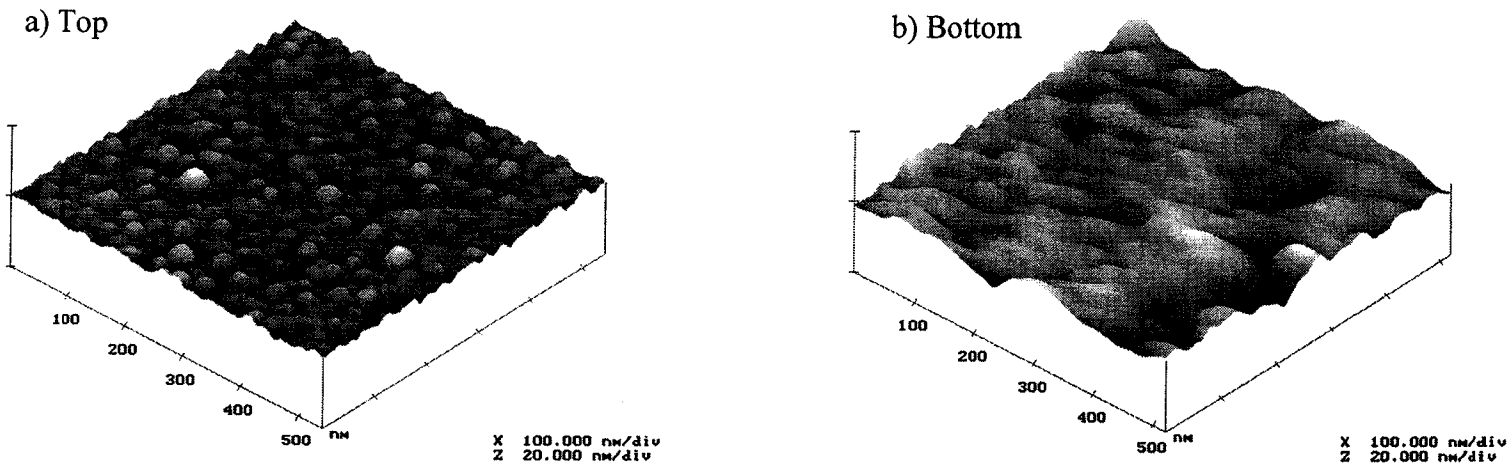

Fig. 7.13: AFM images for top (a) and bottom (b) surfaces of a homogeneous PPO membrane.

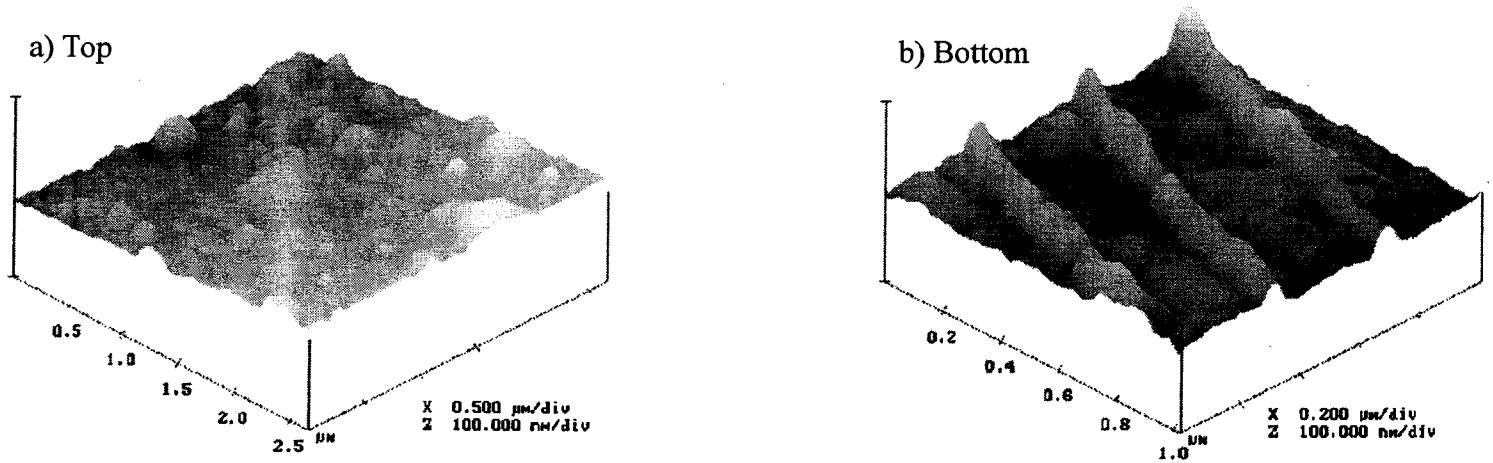

Fig. 7.14: AFM images for top (a) and bottom (b) surfaces of a peeled-off coated layer of composite PPO membrane.

start to occur at the bottom surface of the coated layer.

It is believed that the interstitial void space between nodules causes the leakage of gas mixture and hence lowers the selectivity of the membrane. The fusion of the nodules will stop the gas leakage through the interstitial void space. Hence it is natural that composite membranes have higher selectivity than homogeneous membrane as shown in Figs. 7.4 and 7.5.

Asakawa et al. [14] reported an increase in the separation factor, for O_2/N_2 mixtures, of composite membranes that consisted of laminated thin poly [1-(trimethylsilyl)-1-propyne] (PMSP) on porous polypropylene, Duragard 2400. They found, in the case of multi-layered PMSP, that the separation factor for the PMSP layer interfacing the support membrane to be as twice as that of the upper PMSP layers. They referred this enhancement in the separation factor to the possibility of the presence of dense layer in the intersurface between the PMSP and Duragard.

7.4 Conclusions

1. Composite PPO membranes prepared by coating 3% PPO-TCE solution on top of UF PES HO51 membrane, showed enhanced selectivity toward CO_2/CH_4 gas system. The gas permeability ratio, CO_2/CH_4, of the composite PPO membrane was 37, compared to 17 for the homogeneous PPO membrane.
2. The partial drainage of the solvent into the support membrane matrix caused the coated layer to have graded morphology, which was opposite to that observed for the homogeneous membrane, across it: rough top surface (air-interface) and smooth bottom surface (support-interface).
3. It is believed that compressive forces were developed at the bottom surface of the coated

film as a result of the shrinkage of the swollen support. These forces were responsible for the compactness and fusion of the nodules, which consequently resulted in enhanced selectivity of the coated film. The compressive forces were strong enough to wrinkle the bottom surface of the coated layer.

7.5 References

[1] J. Koros and A. Rezac: *"Preparation of Polymer-Ceramic Composite Membranes with Thin defect-free Separating Layers"*, J. Appl. Polym. Sci., 46, (1992) 1927-1938.

[2] Ebert, A. Bezjak, K. Nijmeijer, M. Mulder, and H. Strathmann: *"The Preparation of Composite Membranes with a Glassy Top Layer"*, J. Appl. Polym. Sci., 46, (1992) 1927-1938.

[3] J. Nelson: "*Composite membranes, their manufacture and use*", US patent 4,822,382 (1989).

[4] T. Matsuura: "*Synthetic Membranes and Membrane Separation Processes*", CRC Press, NY (1994).

[5] K Kimmerle, T. Hofmann, and H. Strathmann: "*Analysis of gas permeation through composite membranes*", J. Membr. Sci., 61, (1991) 1.

[6] R. Kesting and A. Fritzsche: "*Polymeric Gas Separation Membranes*", Wiley Interscience, NY (1993).

[7] K.C. Khulbe, G. Chowdhury, B. Kruczek, R. Vujosevic, T. Matsuura, and G. Lamarche: "*Characterization of the PPO Dense Membrane Prepared at Different Temperatures by ESR, Atmoic Force Microscope and Gas Permeation*", J. Membr. Sci., 126, (1997) 115-122.

[8] A. Alsari, K. Khulbe, and T. Matsuura: "*The Effect of Sodium Dodecyl Sulfate Solutions as*

Gelation Media on the Formation of PES Membranes", J. Membr. Sci., 188, (2001) 279-293.

[9] G. Gildert, T. Matsuura, and S. Sourirajan: "*Effect of Different Alcohol-Water Mixtures as Gelation Mediums During the Formation of Cellulose Acetate Reverse Osmosis Membranes*", J. Appl. Polym. Sci., 24, (1979) 305.

[10] Digital Instruments Inc., "Nanoscope III, Control System Manual", Santa Barbara, CA., 1993.

[11] D.R. Paul and Y.P. Yampol'skii: " *Polymeric Gas Separation Membranes*", CRC press, Boca Raton , Florida (1994).

[12] Final Report on "*Development of Thin Film Composite Membranes for Nanofiltration*" submitted by Industrial Membrane Research Institute to Zenon Environmental Inc, Burlington, Canada, 1999.

[13] R. E.Traybal: "*Mass-Transfer Operations*", McGraw-Hill Inc., 1981.

[14] S. Asakawa, Y. Saito, K. Waragi, and T. Nakagawa, Gas Sep. Purif., 2,3,1988.

7.6 Nomenclature

A_C	Membrane area, cm^2.
$F(x,y)$	Function describing surface topography of membrane relative to the center plane of the captured AFM image, nm.
f	Fraction of pores area on the support membrane surface (surface porosity).
L_x , L_y	Dimensions of the captured membrane surface image, nm.
p_C	Coated polymer permeability, Barrer.
p_S	Support membrane polymer (PES) permeability, Barrer.
R_a	Mean roughness of the captured membrane surface, nm.

R_C Coated layer resistance to gas permeation, cm/(cm^2 Barrer).

R_P Gas permeation resistance of the support membrane pores, which were plugged by the intruded coating polymer, cm/(cm^2 Barrer).

R_S Resistance of the support membrane skin layer matrix to gas permeation, cm/(cm^2 Barrer).

R_T Overall resistance of the composite membrane, cm/(cm^2 Barrer).

δ_C Coated layer thickness, cm.

δ_S Porous support membrane skin layer thickness, cm.

Chapter 8

Prediction of Gas Separation Performance of Thin Film Composite Membranes

• Submitted to the American Institute of Chemical Engineering (AIChE) Journal.

Abstract

Some morphological parameters of a commercial ultrafiltration membrane (HW31 of Osmonics) were obtained based on pure gas permeation experiments. These parameters are: the number of pores, the pore size and pore size distribution, and the dense layer thickness.

As well, prediction of the thin film composite membranes performance prepared by coating poly (phenylene oxide) (PPO) over HW31 support substrates, was attempted given the morphological parameters that describe the porous support membrane, along with the gas permeability of the polymers that constitute the coating layer and the dense layer of the support membrane. This study compared the experimental performance of the TFC membranes with the simulation results based on three scenarios: (i) total plugging of the support membrane pores by the coating polymer, (ii) partial plugging, and (iii) no-plugging of the support membrane pores.

The experimental membrane performance was presented best by the partial plugging of pores model at low coating polymer solution, while the no pore plugging model presented best the experimental performance of the TFC membranes at high coating polymer concentration.

The mathematical simulation showed that it is very important to optimize the morphological parameters of the support membrane when polymer intrusion into the pores of the support occurs.

8.1 Introduction

Composite membranes basically consist of one or more polymeric layers deposited over a porous substrate that can be either inorganic or polymeric membrane. Standard bi-layer composite membranes offer a compromise between the high selectivity of the coating polymer, which is usually expensive, and the high productivity of the porous support. Therefore, the performance of composite membranes needs to be optimized by individually optimizing the coating and the support layers. Minimizing the coating layer thickness is an economic need as well. The support substrate, on the other hand, should show least resistance to the permeating gases, should be insoluble in coating solution, and inexpensive [1,2,3].

A key issue in thin film composite membranes (TFC) preparation that always has been addressed is the requirement to avoid the intrusion of the coating polymer into the pores of the support [4,5,6]. This requirement puts a constraint on the support maximum pore size, which should not be larger than the hydrodynamic diameter of the polymer coil in the coating solution [4]. Of course, polymer intrusion into the support pores would sacrifice the supports surface porosity and thus its productivity. Some treatments are found in the literature to minimize this phenomenon, which include heat treatment or annealing [5] or pre-coating the support with silicon rubber to form a gutter layer [3,6]. Higher concentration of high molecular weight polymer in the coating solution can help in minimizing the polymer intrusion due to the interlock between the polymeric coils. On the other hand, this is not desirable as it results in thick coating layer [4]. However, the need to virtually evaluate the combination of a coating polymer and a porous support membrane is never been addressed. The inevitable pore intrusion should be accounted for

and the performance of the resulting TFC could be judged.

Many techniques exist that deal with characterizing the pores size and pores size distribution. These techniques include mercury porosimetry, bubble point, solute transport, gas permeation and many others [7,8,9,10]. In the solute transport technique, the separation of the solute is related to the size distribution of the pores assuming that the sieving process is solely due to size exclusion. Michaels found that the sieving coefficients of biological and synthetic ultrafiltration (UF) membranes in relation to the solute size fit to a log-normal probability distribution [8]. In the gas permeation technique, the concept of flow through porous media is used taking into account the contribution of the different pore flow mechanisms: Knudsen, slip, viscous, and surface transport. However, the contribution of the polymer matrix of the dense layer has not been accounted for. The whole gas permeation is considered as the result of flow through the pores in the dense layer [10].

In this work, gas permeation data are used to characterize UF membranes in terms of the total number of pores; the pores size distribution, and the dense layer thickness. The contribution of the polymer matrix of the dense layer is accounted for. An attempt to predict the gas separation performance of a TFC is carried out; given (1) the physical parameters that describe the porous support layer, which are the number of pores, pores size distribution, and the dense layer thickness, and (2) the gases permeability in the support and coating polymers.

8.2 Experimental

8.2.1 Support membrane testing

Ultrafiltration (UF) flat sheet membrane (PES HW31) provided by Osmonics Inc. was used as the support substrate for the thin film composite (TFC) membranes. Coupons were randomly cut from a fresh HW31 sheet. Coupons were soaked in distilled water for 24 hours then dried at ambient conditions for 24 hours. Each coupon then was exposed to trichloroethylene (TCE), which is the solvent of the coating polymer (PPO). The amount of TCE per unit area used was 0.025 cm^3/cm^2, i.e. 0.5 cm^3 of TCE was spread over an area having a 5.0 cm diameter. The substrate was left to dry at room temperature in the fumehood for 24 hours before testing. Testing the substrate was carried out with two gases, CO_2 and CH_4, using a constant pressure system. Four pressures were used at the feed side: 50, 100, 150, and 200 psig, while the permeate side was open to atmospheric conditions, i.e. permeate side pressure was atmospheric.

8.3.2 Thin film composite membrane (TFC) preparation and testing

Fresh UF membrane coupons were randomly cut, and then soaked in distilled water for 24 hours before being dried at room temperature in the fumehood. The substrate was then coated with poly (phenylene oxide) (PPO)-TCE solution. The coating solution was spread over the substrate with a round tip dropper. The amount of coating solution applied was 0.025 cm^3/cm^2. The coated membrane was left to dry at room temperature in the fumehood for 24 hours before testing. The PPO-TCE solutions, which were used for coating, were prepared with the following concentrations (W/W) %: 4, 2, 1, 0.5, 0.1, 0.05, and 0.01%.

Testing of the composite membranes was carried out in a constant volume system [11].

Feed pressure was maintained at 5250 torr (700 kPa absolute) and permeate pressure cycle was from 2 to 800 torr (0.266 to 106 kPa absolute). All reported TFC results in this work are at 760 torr absolute permeate pressure.

Determining the coating layer thickness is necessary for the simulation of the TFC performance. The coating layer thickness of the TFC membranes prepared from high PPO concentrations (4, 2, 1%) was measured after peeling it off the support. The thickness of the coating layer of the TFC membranes prepared from low concentrations (0.5, 0.1, 0.05, 0.01%) was calculated based on the thickness of the coating layer corresponding to the 1.0% PPO. The thickness was assumed to be proportional to the concentration of PPO in the coating solution. Choice of the 1.0% PPO concentration as a reference for the thickness calculations stemmed from the fact that it had the lowest variation in coating layer measurements, as seen in Table 8.1. The variation in the coating layer thickness measurements partly resulted from the swelling of the support substrate upon exposure to the solvent. The main factor for the variation in the thickness measurements is believed to be the high viscosity of the 2 and 4% coating solutions. The solution spread-ability over the substrate was not as smooth as it was in the case of 1% PPO solution. Table 8.1 lists the measured and the expected coating layer thickness of the TFC membranes.

Table 8.1: Estimated thickness of coating layer

PPO %	Measured (Variability) (μm)	Calculated (μm)
4	16.0 (1.5)	
2	9.5 (1.3)	
1	6.0 (0.6)	
0.5		3.0
0.1		0.6
0.05		0.3
0.01		0.06

8.3 Theoretical

8.3.1 Polymer size determination

The hydrodynamic volume of a polymer in the solution is related to the intrinsic viscosity of the polymer solution by the Einstein viscosity law [12]:

$$[\eta]\, M = K\, V \tag{1}$$

where $[\eta]$ is the intrinsic viscosity of the polymer solution in dL/g, M is the molecular weight of the polymer and V is the hydrodynamic volume of the polymer coil in the solution. K is a universal constant and independent of the chemical nature of the polymer. For linear polymers, equation 1 can be rewritten as:

$$[\eta]\, M = \Phi\, (h^2)^{3/2} \tag{2}$$

where h is the root mean-square end-to-end distance of the polymer coil and Φ is the universal constant equivalent to 2.8×10^{21} which represents a frictional coefficient. If the polymer molecules assume the spherical configuration in the solution, then the radius of the sphere can be estimated in relation to the coiled polymer root-mean-square end-to-end distance as,

$$R_g = \sqrt{\frac{h^2}{6}} \tag{3}$$

where R_g is the radius of gyration of the polymer coil.

For the PPO used in this work, M =316,400. The intrinsic viscosity for PPO in TCE is evaluated to be 1.28 dL/g. Thus, using equations 2 and 3, R_g is calculated to be 21nm.

8.3.2 Determination of UF membrane parameters

The mechanism of gas transport through pores is controlled by the pore size relative to the mean free path of the permeating gas, λ:

$$\lambda = \frac{RT}{\left(\sqrt{2}\pi d_g^2 N_{av} \overline{P}\right)} \tag{4}$$

where R is the universal gas constant, T is the absolute temperature, d_g is the gas molecule diameter, N_{av} is Avogadro's number, and $\overline{P}$ is the average pressure in the pore. For a pore of radius R_b, the following pore flow mechanisms are possible [2,3,10]:

a) Knudsen flow mechanism ($R_b \leq 0.05\lambda$):

$$q_k = \left(\frac{32\pi}{9M_A RT}\right)^{\frac{1}{2}} R_b^3 \frac{\Delta P}{\delta} \tag{5}$$

where M_A is the molecular weight of the gas, and δ is the pore length.

b) Slip flow mechanism ($0.05\lambda < R_b \leq 50\lambda$):

$$q_s = \left(\frac{\pi}{M_A \bar{C}}\right) R_b^3 \frac{\Delta P}{\delta} \tag{6}$$

where $$\bar{C} = \left(\frac{8RT}{\pi M_A}\right)^{\frac{1}{2}} \tag{7}$$

c) Viscous flow mechanism ($R_b > 50\lambda$):

$$q_v = \left(\frac{\pi}{8\eta RT}\right) R_b^4 \overline{P} \frac{\Delta P}{\delta} \tag{8}$$

where η is the gas viscosity. There is a fourth transport mechanism known as the surface flow resulting from gas adsorbed on the pore wall to form a mono-layer of condensed gas. Therefore, for a surface flow to exist, R_b should be larger than d_g [10]. For the other pore flow mechanisms to occur, the minimum pore size should accommodate two monolayers of condensed gas and one gas molecule in the core of the pore. Therefore, the

minimum pore size, in which surface flow in addition to any other pore flow mechanism may occur, is equivalent to three times the gas molecule diameter, or R_b>1.5d_g. It is necessary to correct the above equations for the presence of the adsorbed monolayer that reduces the actual pore size available for the flow of gas molecules, as well to accommodate for the superimposed surface flow by adding the following equation to equations 5,6, and 8:

$$q_{sf} = \left(\frac{\pi RT\left(2R_b d_g - d_g^2\right)^2 d_g}{8\mu R_b} \right) k_H^2 \frac{\Delta P^2}{\delta} \tag{9}$$

where k_H is Henry's constant, and μ is the viscosity of the adsorbed gas layer. The adsorbed gas layer is considered to have the properties of the condensed gas at the working temperature. Thus equations 5, 6 and 8 become:

$$\bar{q}_k = \left(\frac{32\pi}{9M_A RT} \right)^{\frac{1}{2}} \left(R_b - d_g\right)^3 \frac{\Delta P}{\delta} + \left(\frac{\pi RT\left(2R_b d_g - d_g^2\right)^2 d_g}{8\mu R_b} \right) k_H^2 \frac{\Delta P^2}{\delta} \tag{5-a}$$

$$\bar{q}_s = \left(\frac{\pi}{M_A \bar{C}} \right) \left(R_b - d_g\right)^3 \frac{\Delta P}{\delta} + \left(\frac{\pi RT\left(2R_b d_g - d_g^2\right)^2 d_g}{8\mu R_b} \right) k_H^2 \frac{\Delta P^2}{\delta} \tag{6-a}$$

$$\bar{q}_v = \left(\frac{\pi}{8\eta RT} \right) \left(R_b - d_g\right)^4 \bar{P} \frac{\Delta P}{\delta} + \left(\frac{\pi RT\left(2R_b d_g - d_g^2\right)^2 d_g}{8\mu R_b} \right) k_H^2 \frac{\Delta P^2}{\delta} \tag{8-a}$$

The above equations are developed for a single pore. However, as mentioned previously, pores in UF membranes follow a log-normal distribution as shown in the following equation:

$$\frac{df}{dR_b} = \frac{1}{R_b \ln\sigma\sqrt{2\pi}} e^{\left[-\frac{\left(\ln 2R_b - \ln\bar{d}\right)^2}{2(\ln\sigma)^2}\right]} \tag{10}$$

where $\bar{d}$ is the geometric mean pore size, and σ is the geometric standard deviation of pore sizes around the geometric mean, and $\frac{df}{dR_b}$ represents the density function of the pore size distribution.

Let N_t be total number of pores in the dense layer of the UF membrane existing within an area of diameter D_m, then the total contribution of the pores within the UF substrate is given by:

$$Q = N_t\left(\int_{d_g}^{1.5d_g} q_{sf}df + \int_{1.5d_g}^{0.05\lambda} \bar{q}_k df + \int_{0.05\lambda}^{50\lambda} \bar{q}_s df + \int_{50\lambda}^{\infty} \bar{q}_v df\right) \tag{11}$$

When there is a transmembrane pressure difference across a UF membrane, then the total gas flux is the resultant of the simultaneous transport of gas through pores and through the polymer matrix of the dense layer of the UF membrane, which can be described by the solution-diffusion mechanism.

Assuming that the thickness of the dense layer is equivalent to the pore length δ, then the total flux through a UF membrane can be derived as follows:

$$AJ_g = A_m p_{gm}\frac{\Delta P}{\delta} + Q \tag{12}$$

where A is the total apparent membrane area, A_m is the area of the non-porous portion of the membrane surface. J_g is the flux of gas through the membrane, and p_{gm} is the intrinsic gas permeability of the UF membrane material. Dividing equation 12 by A, and noticing

that:

$$\frac{A_m}{A} = 1 - \varepsilon \tag{13}$$

where ε is the total surface porosity that can be defined as follows:

$$\varepsilon = \frac{N_t \int_{d_g}^{\infty} \pi R_b^2 \mathrm{d}f}{\pi D_m^2 / 4} \tag{14}$$

thus equation 12 becomes:

$$J_g = (1 - \varepsilon) p_{gm} \frac{\Delta P}{\delta} + \frac{Q}{A} \tag{15}$$

Equation 15 contains four variables that describe the UF substrate, which are: $\bar{d}$,σ, N_t, and δ. The gas permeation data obtained for UF membranes are used to determine these four parameters using a grid technique according to the flowchart in Fig. 8.1.

8.3.3 Simulation of TFC Membranes Performance

In order to simulate the performance of the TFC, it is necessary to consider a simple rule to judge the possibility of having polymer intruded into the pores of the UF substrate. In this work, the radius of gyration is considered as the characteristic dimension for the polymer in the coating solution by which pores are judged as being plugged by the intruded coating polymer, i.e. all pores that are larger than $2R_g$ are considered as plugged pores. Figure 8.2 shows a schematic for the resistance model applied to simulate the overall performance of the TFC. It is assumed in this model that the depth to which the polymer has intruded to, is equivalent to the dense layer thickness, δ. It is assumed that the gas permeating the coated layer is well mixed between the coated layer and the substrate, which implies that the gas exiting the coating layer exerts a uniform

intermediate pressure (P_m) on the substrate.

Let ε_{ep} be the surface porosity resembling the unplugged pores, which can be defined as:

$$\varepsilon_{ep} = \frac{N_t \int_{d_g}^{R_g} \pi R_b^2 \mathrm{d}f}{\pi D_m^2 / 4} \tag{16}$$

therefore, the portion of porosity that is plugged by the coating polymer, ε_{pp}:

$$\varepsilon_{pp} = \varepsilon - \varepsilon_{ep} \tag{17}$$

where ε is defined in equation 14. Based on the assumptions and argument just presented,

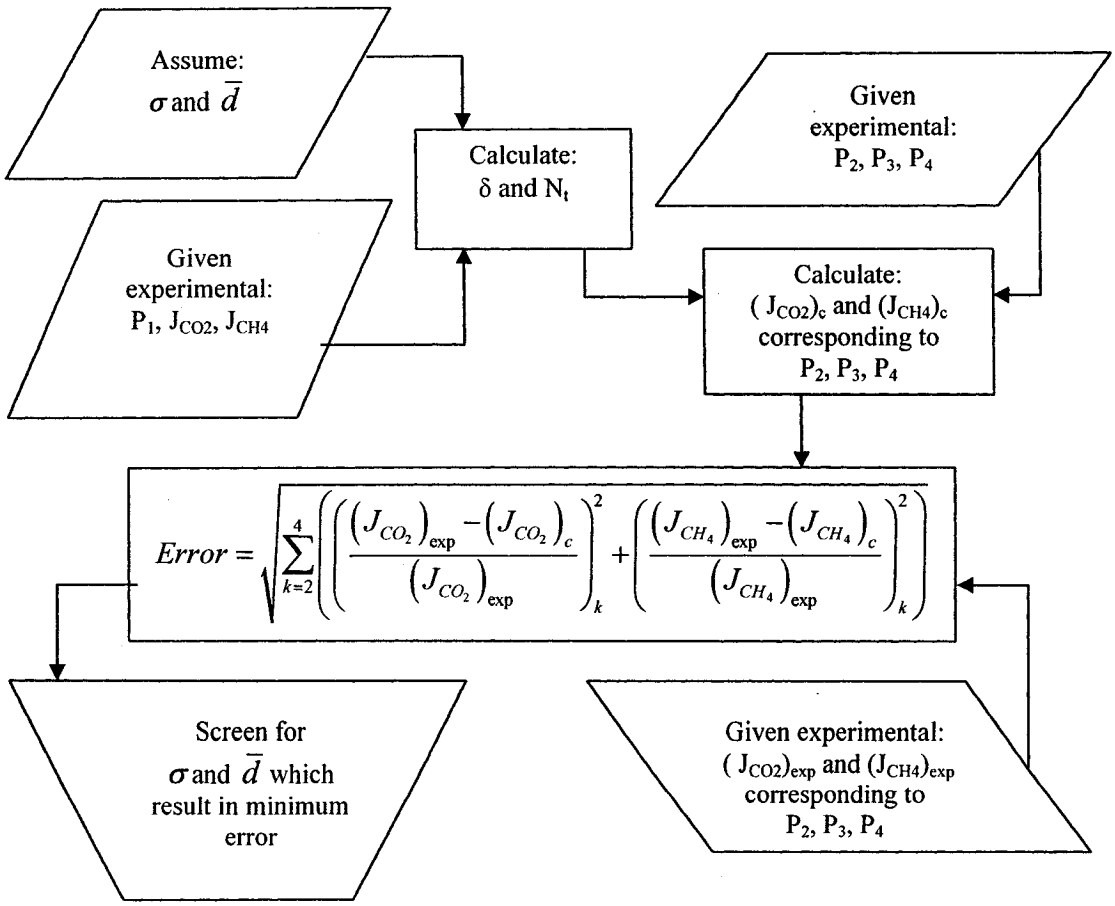

Fig. 8.1: Flow chart of solution to screen for optimum physical characteristic parameters of the UF porous substrate based on experimental gas permeation data.

the total flow through empty pores will be:

$$Q_{ep} = N_t \left(\int_{d_g}^{R_g} q \mathrm{d}f \right) \tag{18}$$

where q is the combination of pore flow mechanisms that dominate in the range of pores having radii between d_g and R_g. The pore flow mechanism combination is determined based

on the mean free path of the permeating gas, λ, evaluated at an average pressure:

$$\bar{P} = \frac{P_m + P_d}{2} \tag{19}$$

The total flow permeating through the coated layer:

$$Q_c = A\, p_{gc} \frac{(P_u - P_m)}{\delta_c} \tag{20}$$

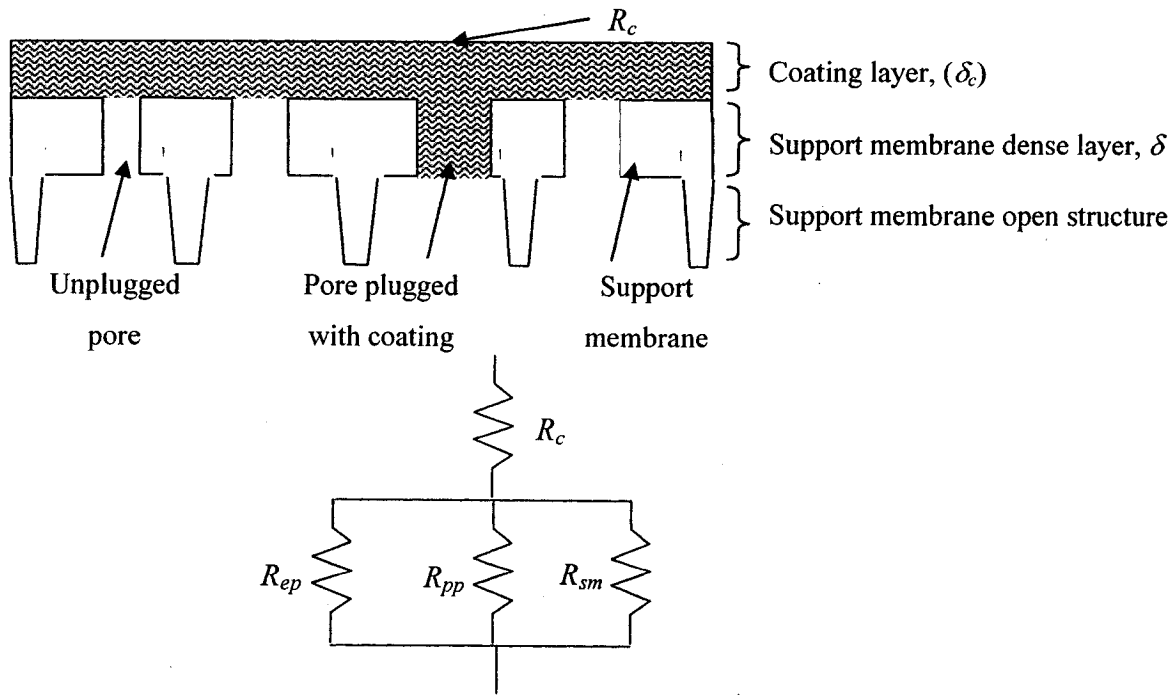

Fig. 8.2: Schematic of the resistance model used to simulate the TFC performance.

where p_{gc} is the intrinsic gas permeability of the coating material. Q_c should be equal to the total flow through the coated substrate, Q_s:

$$Q_s = Q_{sm} + Q_{ep} + Q_{pp} \tag{21}$$

Q_{ep} is defined in equation 18. Q_{sm} and Q_{pp} are defined as:

$$Q_{sm} = (1-\varepsilon) A\, p_{gm} \frac{(P_m - P_d)}{\delta} \tag{22}$$

$$Q_{pp} = (\varepsilon - \varepsilon_{ep}) A\, p_{gc} \frac{(P_m - P_d)}{\delta} \tag{23}$$

where Q_{sm}, Q_{ep}, and Q_{pp}, are the gas flow through the support material, empty pores, and plugged pores, respectively. P_m can be solved for by equating equations 20 and 21. Once P_m is calculated, two approaches can be followed to calculate the gas permeance through the TFC:

1. Using Q_c calculated in equation 20:

$$p_g^* = \frac{Q_c}{A(P_u - P_d)} \tag{24}$$

where p_g^* is the gas permeance of the TFC.

2. Using the resistance model as shown in Fig. 8.2:

$$R_c = \frac{\delta_c}{A\, p_{gc}} \tag{25}$$

$$R_{sm} = \frac{\delta}{(1-\varepsilon) A\, p_{gm}} \tag{26}$$

$$R_{pp} = \frac{\delta}{(\varepsilon - \varepsilon_{ep}) A\, p_{gc}} \tag{27}$$

equation (18) can be modified further to find the gas permeance coefficient through the empty pores:

$$Q_{ep} = \varepsilon_{ep} A\, p_{gp} \left(P_m - P_d\right) = N_t \left(\int_{d_g}^{R_g} q \mathrm{d}f \right) \tag{28}$$

$$p_{gp} = \frac{N_t \left(\int_{d_g}^{R_g} q \mathrm{d}f \right)}{\varepsilon_{ep} A \left(P_m - P_d\right)} \tag{29}$$

$$R_{ep} = \frac{1}{\varepsilon_{ep} A\, p_{gp}} \tag{30}$$

The total resistance imposed by the TFC is:

$$R_T = R_c + \frac{R_{sm} R_{ep} R_{pp}}{R_{sm} R_{ep} + R_{ep} R_{pp} + R_{sm} R_{pp}} \tag{31}$$

Thus, the total gas permeance in the TFC is:

$$p_g^* = \frac{1}{A R_T} \tag{31}$$

The ideal gas selectivity of the TFC, α, is defined as:

$$\alpha_{1,2} = \frac{\left(p_g^*\right)_1}{\left(p_g^*\right)_2} \tag{32}$$

Table 8.2 lists the physical properties of CO_2 and CH_4 needed in the simulation. It is worthy to mention that the permeability of CO_2 and CH_4 in the PPO coated layer that is used in this simulation is 78 and 2.0 Barrer, respectively; although the intrinsic permeability of CO_2 and CH_4 in PPO (high molecular weight PPO) are reported to be 90 and 5.6 Barrer, respectively [15]. This decrease in the permeability of CO_2 and CH_4,

while the gas ratio CO_2/CH_4 was increased from 16 to about 39, is believed to be the result of alteration in the coating layer morphology. The gas permeability for CO_2 and CH_4 in the PPO coating layer was obtained from pure gas permeation experiment for composite membranes with a 20.0 μm thick-coated layers prepared from 4% (W/W) PPO-TCE solution. This difference in the performance of dense PPO membrane and PPO composite membrane is the subject of the previous chapter of this thesis report.

The surface viscosity represents the viscosity of the adsorbed gas layer on the pore wall surface. This layer is looked at as condensate [10]. Therefore, the surface viscosity listed in Table 8.2 is the corresponding liquid viscosity at the given temperature.

Table 8.2: Properties of CO_2 and CH_4 used in this work (estimated at 294 K).

Parameter	Gas		Unit	Reference
	CO_2	CH_4		
M_A	44	16	g/mol	
μ	7.1×10^{-5}	2.0×10^{-5}	Pa.s	[13]
η	1.2×10^{-5}	9.5×10^{-6}	Pa.s	[13]
k_H	2.5×10^{-5}	0.1×10^{-5}	$mol/m^3/Pa$	[14]
d_g	3.3×10^{-10}	3.8×10^{-10}	m	[1]
p_{gm}	9.37×10^{-16}	3.35×10^{-17}	$mol.m/m^2/s/Pa$	[1]
p_{gc}	2.61×10^{-14}	0.669×10^{-15}	$mol.m/m^2/s/Pa$	

8.4 Results and Discussion:

8.4.1 Performance of TCE-treated UF membranes:

Figures 8.3 and 8.4 show the permeance of CO_2 and CH_4 gases in the TCE treated porous PES UF membranes (HW31). These UF coupons take the numbers 1 to 9 in the following discussion. The scatter in the permeance data is the result of the variability in the physical parameters of the UF membrane coupons tested. These physical parameters are: number of pores, pores size distribution, dense layer thickness. The number of pores and the pore size distribution determine the total surface porosity. The higher the number of pores is, and the bigger the pores are, the higher the permeance is. As well, the thinner the dense layer is, the higher the permeance is. Of course these physical parameters are varied due to variable conditions existing in the manufacturing process (the phase inversion process). Therefore, when these factors collectively work, the performance of the UF membrane coupons tested is expected to vary.

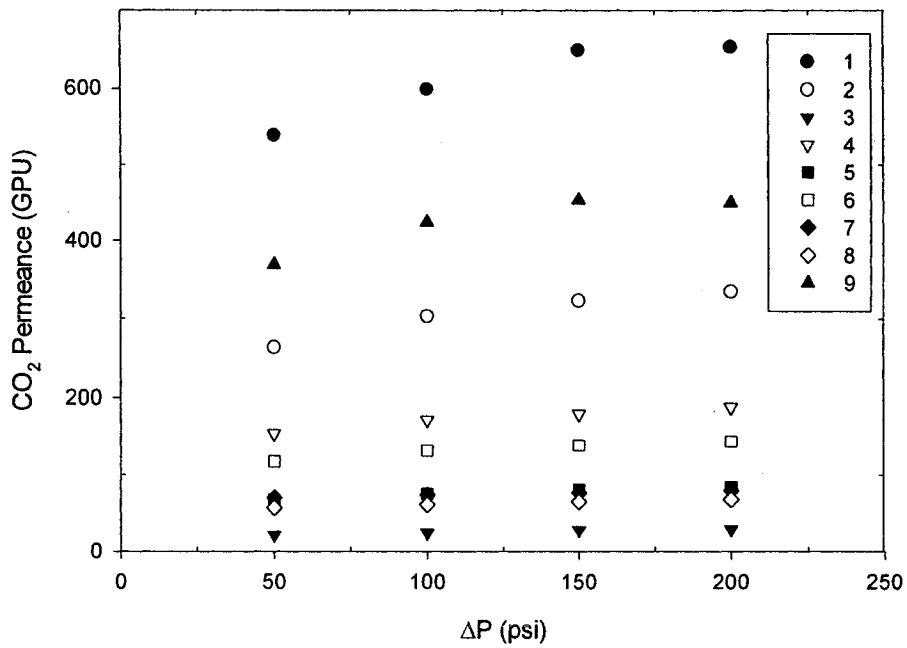

Fig. 8.3: CO_2 permeance of tested UF PES HW31 coupons.

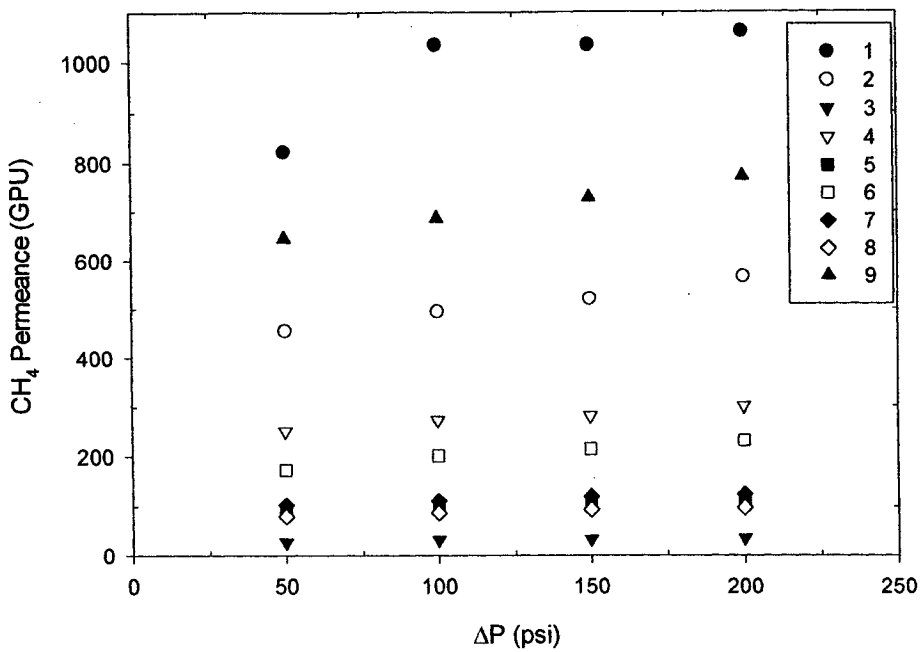

Fig. 8.4: CH_4 permeance of tested UF PES HW31 coupons.

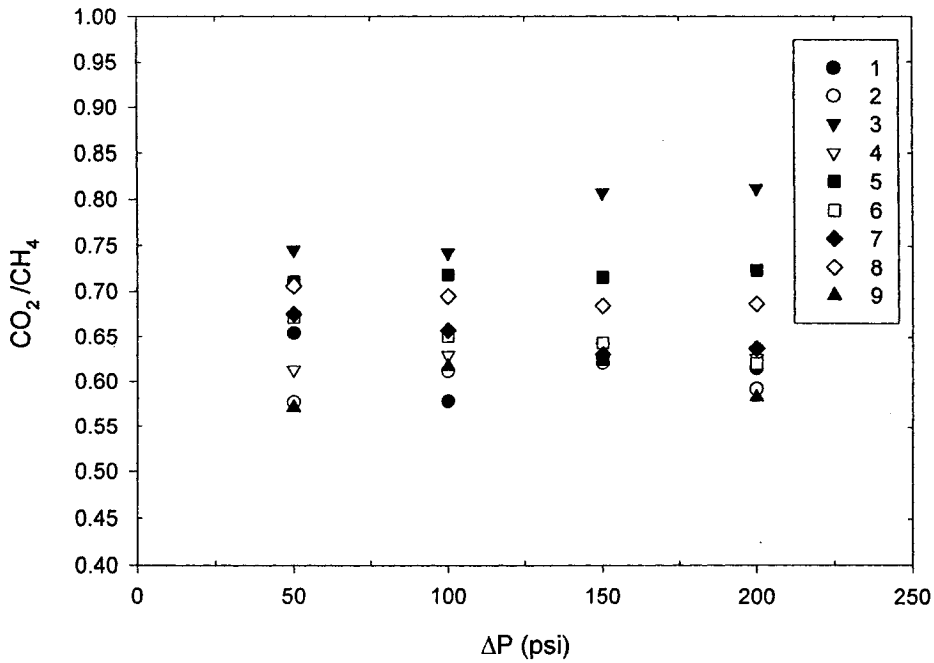

Fig. 8.5: CO_2/CH_4 permeance ratio of tested UF PES HW31 coupons.

As noticed in Fig. 8.5, CO_2 permeance is always less than that of CH_4 covering a CO_2/CH_4 ratio range from 0.55 to 0.81. For the expected pore size range, for the particular UF membrane, and the operating trans-membrane pressure; the pore flow mechanisms expected to dominate are Knudsen and Slip flow regimes. Knudsen and slip flow mechanisms would give a CO_2/CH_4 ratio equal to the inverse of the square root of their molecular weight ratio, i.e. 0.603, for the same operating trans-membrane pressure (see equations 5 and 6). The experimental CO_2/CH_4 ratio ranged from 0.55 to 0.81. This is attributed to, in addition to the surface flow resulting from the gas adsorbed on the pore wall, the solution-diffusion mechanism. Both the surface flow and the solution-diffusion mechanisms preferentially permeate CO_2 more than CH_4 as a result of: (i) CO_2 has higher solubility than CH_4 in PES polymer, and (ii) CO_2 has higher diffusivity in PES dense layer than CH_4. Therefore the permeance ratio of CO_2/CH_4 is expected to increase as the thickness of the dense PES layer decreases and the number of the pores decreases. However, increasing the number of pores and decreasing the dense layer thickness (assuming the pore length is equivalent to the dense layer thickness) will decrease the permeance ratio CO_2/CH_4.

8.4.2 Predicted Physical Characteristics of Tested UF Membrane Coupons

Table 8.3 lists the physical parameters of the tested UF coupons calculated from pure gas permeation. As explained in the theoretical part that the UF coupon characteristic parameters are determined based on the least sum of square errors. As well, Table 8.3 lists the total surface porosity of the tested coupons (no coating) and the expected porosity due to empty pores of the coupons after being coated with PPO polymer. For the later case, all pores that are larger than 42 nm, i.e. R_g = 21 nm, are considered plugged

due to polymer intrusion. Figures 8.6 and 8.7 show the plot of the differential (density function) and the integral (cumulative) distributions of the pore sizes obtained based on the values listed in Table 8.3 for some coupons (1, 2, 3, 6, and 9), just to avoid crowdedness. The values of $\bar{d}$ and σ listed in the last row of Table 8.3 are obtained from fitting the cumulative distribution of the pooled distributions for coupons 1 to 9. The distribution obtained from pooling coupons 1 to 9 still follows the log-normal distribution, Fig. 8.7.

Table 8.3: Physical parameters calculated from gas permeation data for the tested HW 31 coupons.

#	$\bar{d}$ (nm)	σ (nm)	N_t (10^{+9})	δ (10^{-6}m)	ε (10^{-4})	ε_e (10^{-4})	Error (%)
1	28.1	1.85	0.590	0.175	5.13	1.45	24.70
2	18.7	2.00	1.155	0.330	5.46	2.26	16.88
3	10.05	2.17	0.557	0.661	0.97	0.60	27.97
4	14.62	2.06	3.570	1.048	11.21	5.67	16.30
5	12.62	2.10	0.448	0.252	1.11	0.62	17.55
6	12.98	2.12	2.000	0.700	5.39	2.82	24.32
7	12.06	2.10	0.920	0.417	2.08	1.20	10.06
8	10.7	2.14	0.735	0.314	1.38	0.84	13.18
9	15.5	2.07	2.500	0.375	8.95	4.17	22.30
Pooled	19.7	2.12	1.386	0.475	8.60	2.67	-

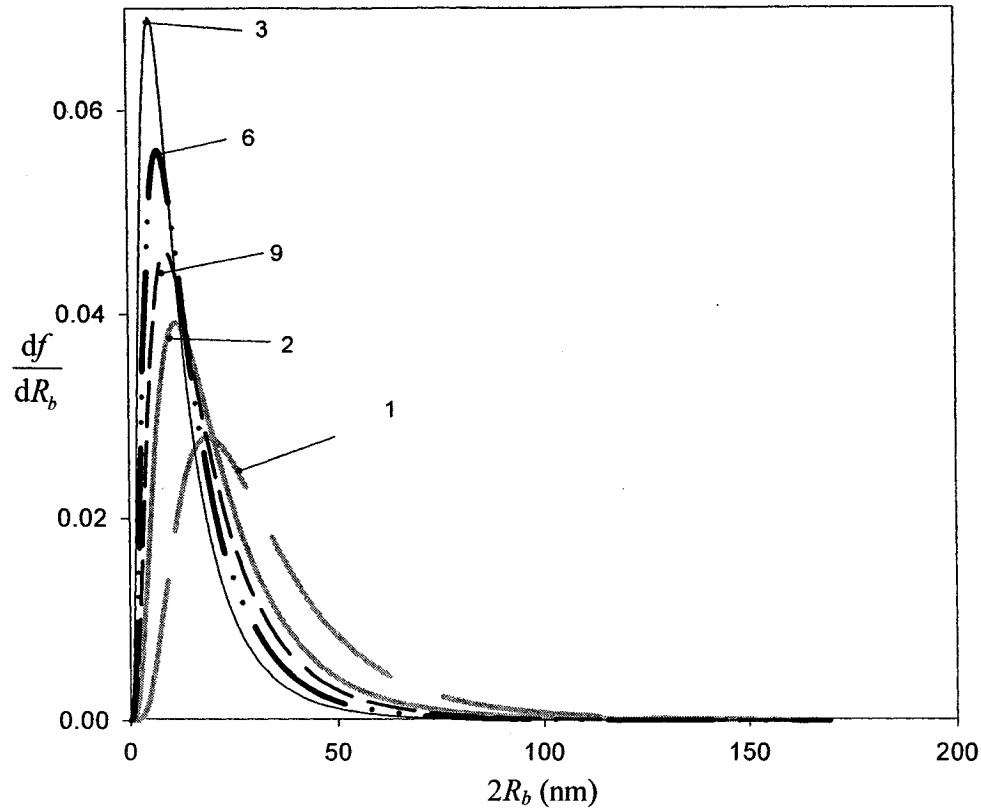

Fig. 8.6: Pore size distribution of tested HW31 coupons.

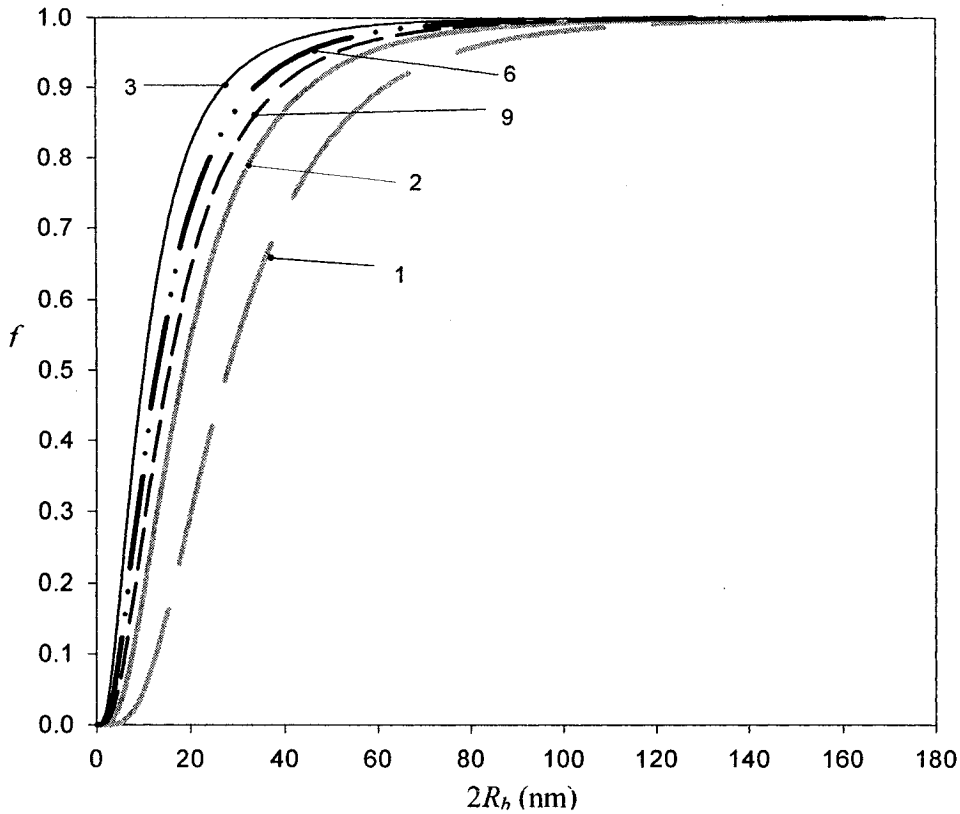

Fig. 8.7: Cumulative pore size distribution of tested HW31 coupons.

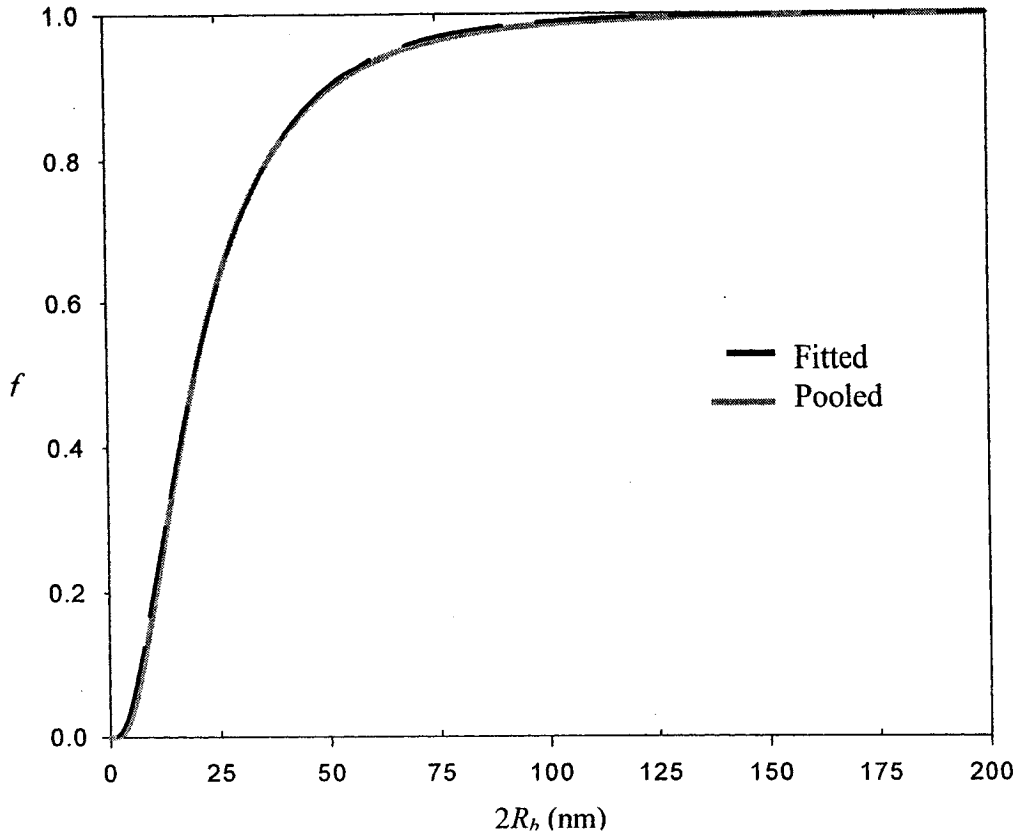

Fig. 8.8: Pore size distribution of pooled coupons.

8.4.3 TFC Performance

Figures 8.9 through 8.11 show the experimental performance of the TFC membranes prepared by coating PPO polymer on HW31 UF support substrates. The UF substrates used to prepare the TFC membranes were taken from the same membrane sheet from which coupons 1 to 9 were taken. As noticed in Figs. 8.9 and 8.10, decreasing the PPO concentration in the coating solution resulted generally in an increase in both CO_2 and CH_4 permeances. It is argued that the permeance of the TFC membranes is inversely proportional to the coating polymer concentration or the coated layer thickness. However, it is clearly noticed in Figs. 8.9 and 8.10 that the permeance of the gases is not inversely proportional to the coated thickness, represented by the coating polymer concentration, as

would be argued. Besides, there is a significant variability in the permeance of the gases and the their ratio. Part of this variability is associated with the coating step where identical and uniform coating thickness, even when the same PPO solution concentration was used, was almost unlikely. The major cause for the variability in the TFCs performance is associated with the high variability in the resistance of substrates toward the permeating gases.

This, as discussed previously, stems from the non-uniformity in the UF substrate's dense layer thickness, number of pores/area, and pores size distribution.

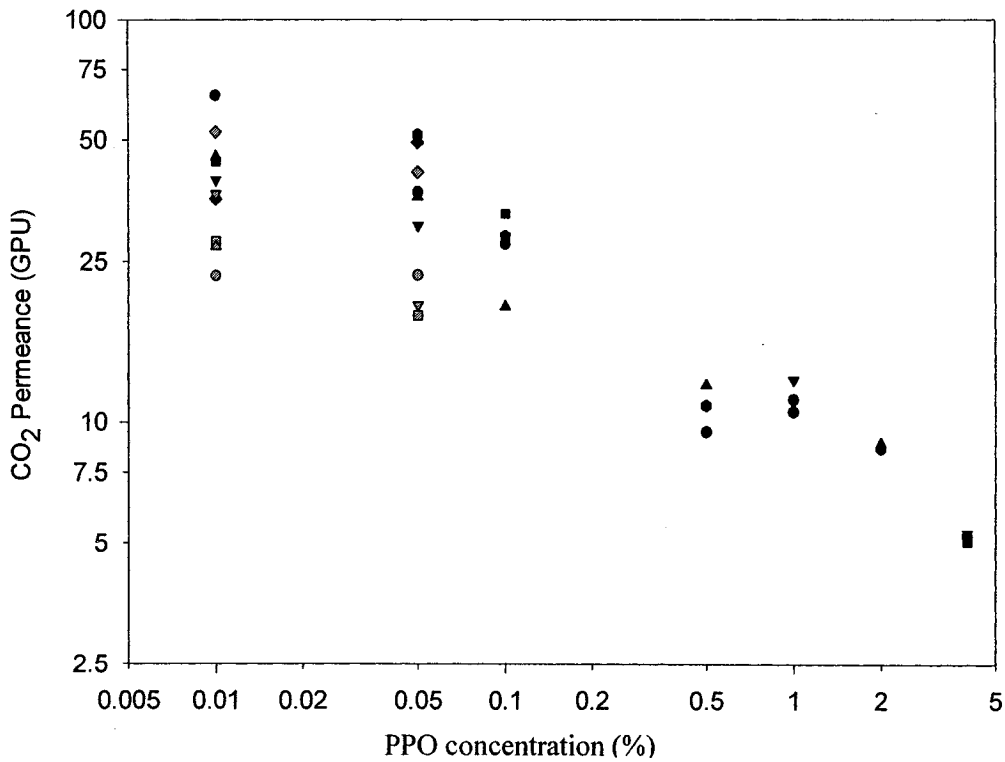

Fig. 8.9: Permeance of CO_2 in TFC membranes as a function of PPO concentration in coating solution.

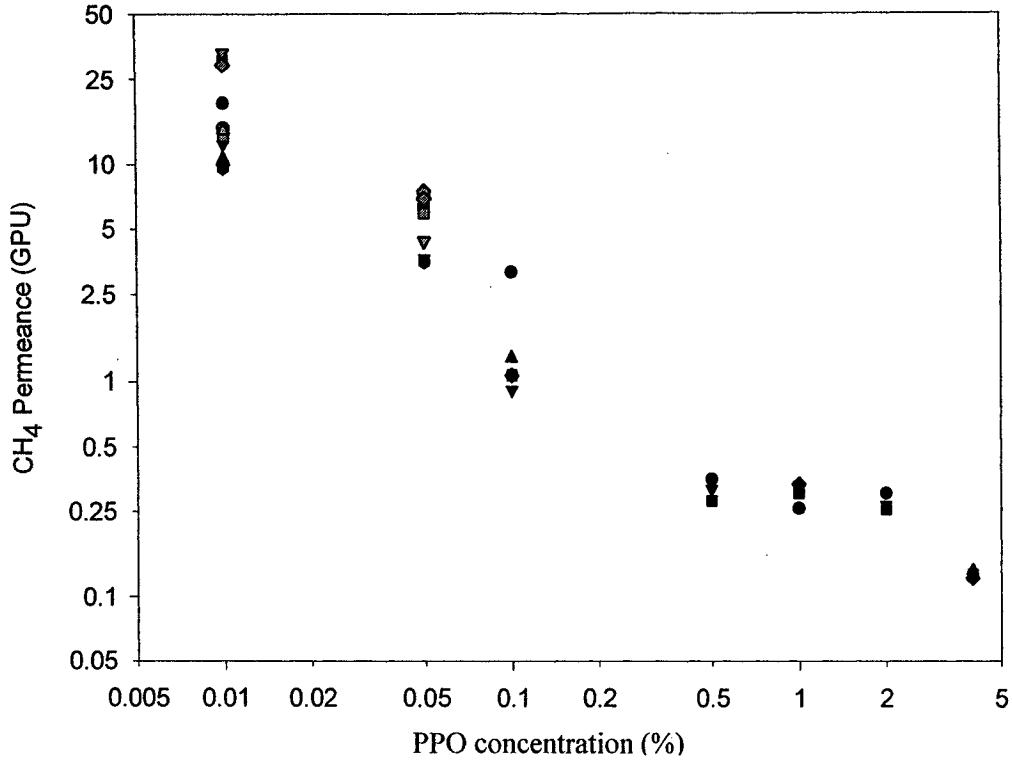

Fig. 8.10: Permeance of CH_4 in TFC membranes as a function of PPO concentration in coating solution.

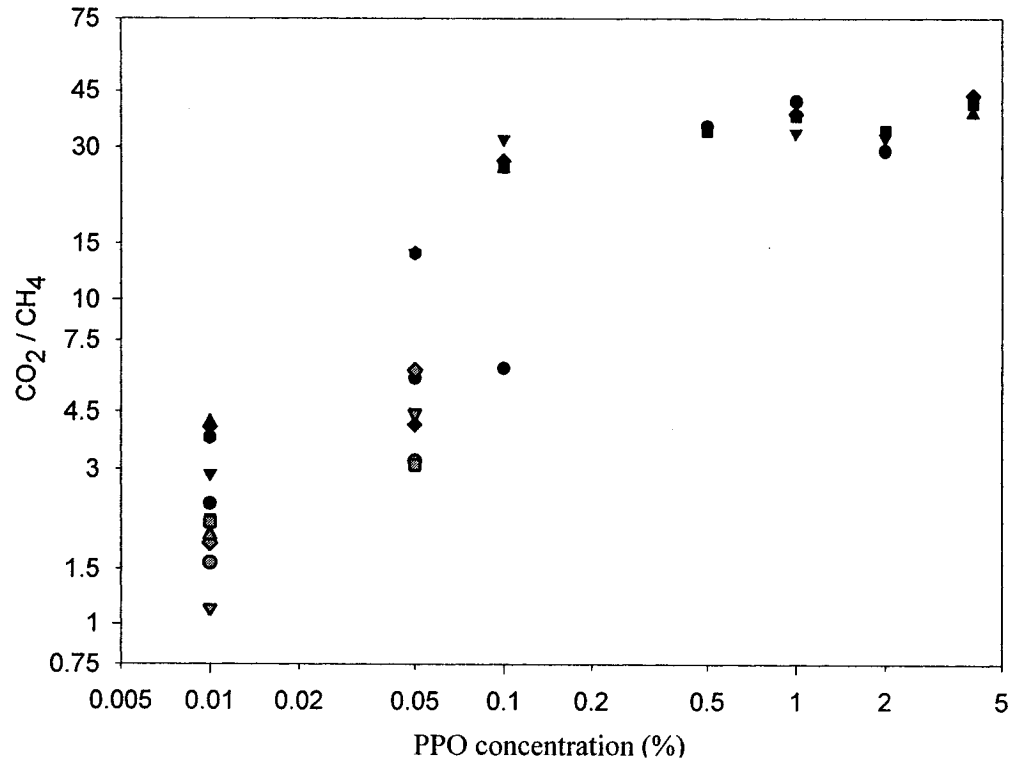

Fig. 8.11: Permeance ratio CO_2/CH_4 in TFC membranes as a function of PPO concentration in coating solution.

8.4.4 Prediction of Performance of TFC Membranes

Figure 8.12 presents the results of the computer simulation in comparison to the experimental data obtained for TFCs. These simulations are based on equations presented in the theoretical part and using the physical characteristics of the UF coupons given in Table 8.3 to calculate the resistance imposed by the UF substrate on the permeating gases. Referring to Figs. 8.3 and 8.4, UF coupon 9 shows one of the lowest resistances to gas permeation, while coupon 3 shows the highest resistances to gas permeation. Considering the fact that the porous support is more permeable to CH_4 than CO_2 as a result of the dominating pore flow mechanisms, then it is expected that the substrate with the higher resistance will undermine the performance of the coated layer, which is CO_2 selective. In other words, when a porous substrate is coated with a polymer like PPO that possesses high gas permeability, and the coating thickness is decreased, a point will be reached where the substrate starts to dominate or significantly contribute to the performance of TFC membranes. This explains the simulation results based on UF substrates 1 and 9. UF substrate 3 has the highest resistance to gas permeation, therefore it contributes significantly to the performance of the TFC even with thick coating layers (high polymer concentration). Therefore, the predicted performance curve based on UF substrate 3 has constituted a lower bound to the experimental data. On the other hand, UF substrate 9 (as well UF 1) has the lowest resistance and is expected as well to have the least contribution to the TFC performance; therefore predicted values for TFC membrane based on UF substrate 9 has constituted an upper bound to the experimental permeance and selectivity data. It can be concluded that the major source for the variability in the experimental performance of TFC membranes is the variability in the resistance of the

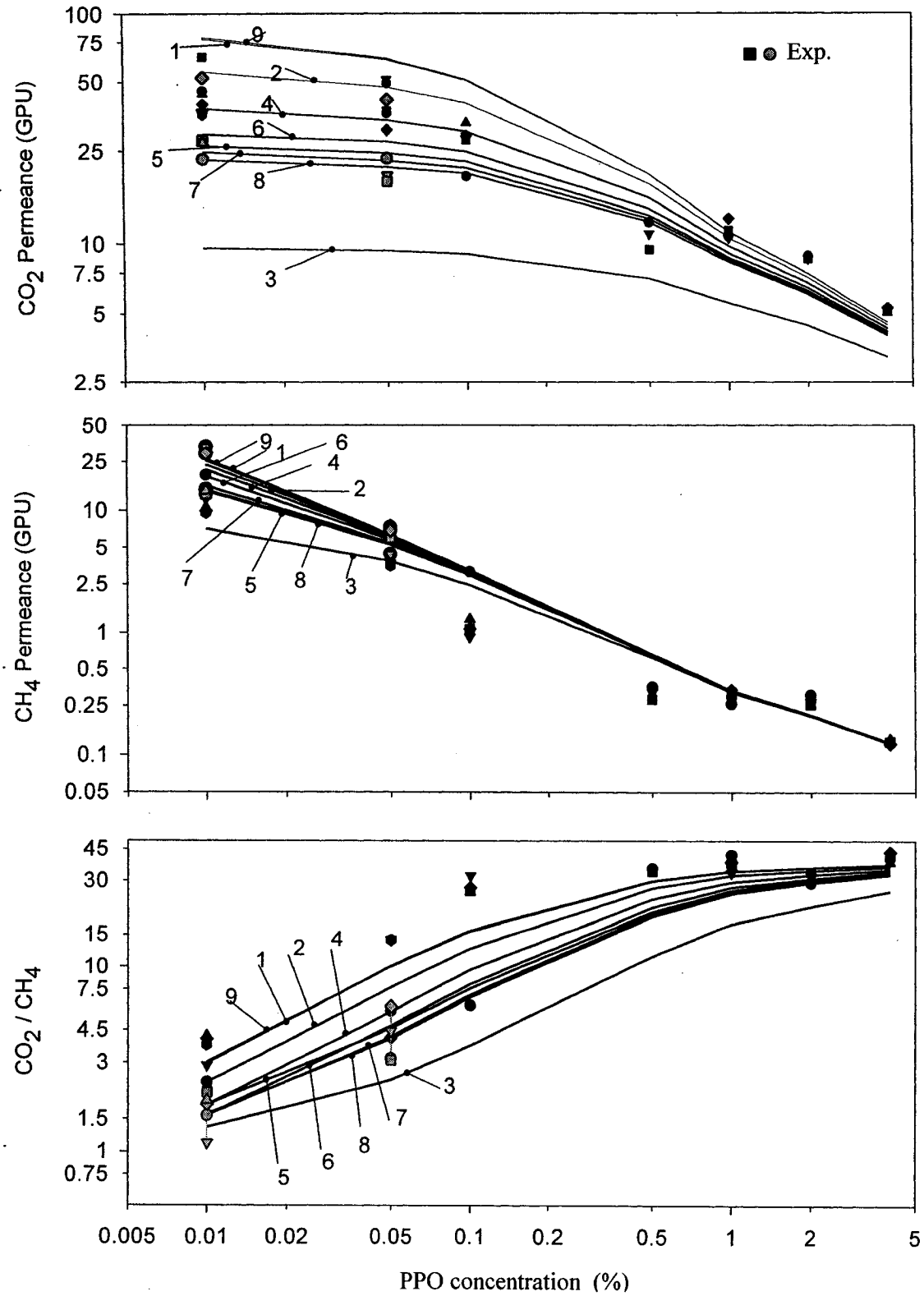

Fig. 8.12: Predicted performance of TFC membranes, based on physical parameters of UF membranes 1 to 9 shown in Table 3, in comparison to the experimental performance.

UF membranes used as supports. Part of the variability originates from pore plugging that is as well different from one support to another, as shown in Table 8.3.

It is important to optimize the physical characteristic parameters for the support substrate so that the performance of TFC membranes can be optimized. This can be clearly concluded by referring to Fig. 8.12; the permeance and the ideal selectivity of the TFC membrane based on UF coupon 9 has given equivalent or better results than UF coupon 1, although the latter has shown less resistance to gas permeation as seen in Figs. 8.3 and 8.4. Referring to Table 8.3, UF coupon 9 ranked 2nd in unplugged surface porosity and total number of pores after UF coupon 4, but it had much thinner dense layer thickness than UF coupon 4. Comparing UF coupons 9 and 1, coupon 9 had much better surface porosity and higher number of pores although UF coupon 1 had thinner dense layer and bigger pores. Therefore, it can be concluded that in order to maximize the TFC performance, it is needed to have thin dense layer thickness, high surface porosity available after coating.

To appreciate the impact of pore intrusion on the performance of a TFC; Figs. 8.13 and 8.14 show the theoretical performance of two TFC membranes, one has a support membrane with physical parameters corresponding to UF coupon 3, while the other one has a support membrane with physical characteristics corresponding to UF coupon 9. Figures 8.13 and 8.14 show the performance of the TFC membranes when (1) there is no pore intrusion or no pores plugging, (2) there is partial pore plugging (all pores with size larger than 42 nm are plugged), and (3) when all pores are plugged. In both Figs. 8.13 and 8.14, all experimental data seem to scatter in a range. The upper bound for the experimental data is best represented by UF coupon 9 based on partial plugging, when

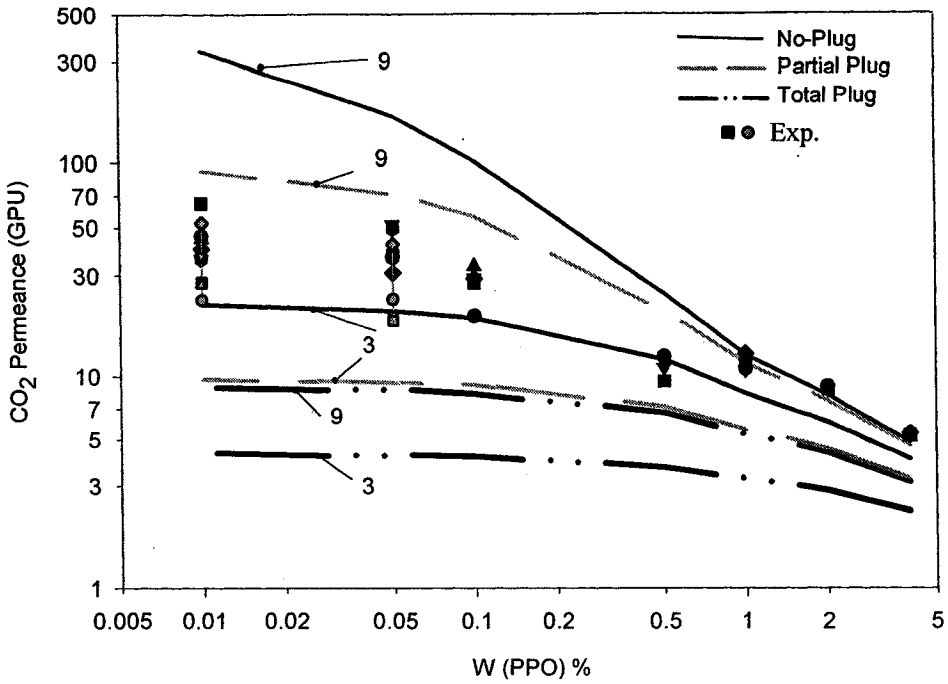

Fig. 8.13: Comparison of CO_2 permeance of TFC membranes based on UF supports 3 and 9.

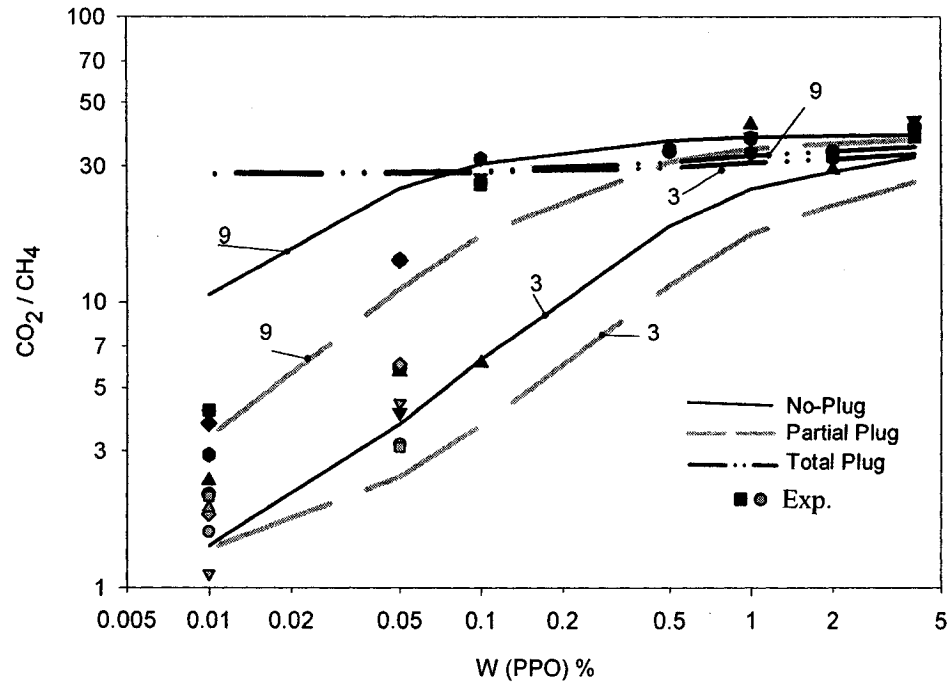

Fig. 8.14: Comparison of CO_2/CH_4 permeance ratio of TFC membranes based on UF supports 3 and 9.

PPO concentration is less than 1%, and no pore-plugging when PPO concentration is higher than 1.0%; while the lower bound for the experimental data is best represented by UF coupon 3 based on partial plugging when PPO concentration is lower than 1.0%, and no pore-plugging when PPO concentration is higher than 1.0%. This may imply that using high polymer concentration in the coating solution prevents pore intrusion by the coating polymer.

8.5 Conclusion

In this work, two simple models are proposed: one to simulate the transport of gases in UF porous membranes, and the second to simulate the transport of gases in TFCs having a porous UF support. The model describing the transport of gases in the porous support combines the solution-diffusion model to account for the gas transport in the polymer matrix of the dense layer, and the combination of the different pore flow mechanisms to describe transport in pores.

It is necessary to evaluate the variability in the resistance of the support toward gases. The support substrate, as a result of the dominating pore flow mechanisms, will compromise the performance of TFC membranes when it shows high resistance relative to that in the coating layer. In addition, the presence of pores that are susceptible to the coating polymer intrusion will worsen the performance of TFC membranes as a result of losing part of the surface porosity and increasing the resistance of the support against the more permeable gas.

An important need to optimize the performance of TFC membranes is to have a support substrate with as thin dense layer as possible, and able to maintain high surface porosity after coating.

The experimental performance of TFC membranes was presented best by the partial plugging of pores model, when low polymer concentration in the coating solution was used; while the unplugged pores model had best represented the experimental performance of TFC membranes when high polymer concentration was used in the coating solution.

8.6 References

[1] R. Kesting and A. Fritzche: "*Polymeric Gas Separation Membranes*", Wiley Interscience, NY (1993).

[2] D. R. Paul and Y. Yampol'skii: "*Polymeric Gas Separation Membranes*", CRC Press, Boca Raton, FL (1994).

[3] T. Matsuura: "*Synthetic Membranes and Membrane Separation Processes*", CRC Press, NY (1994).

[4] M. Rezac and W. Koros: *"Preparation of Polymer-Ceramic Composite Membranes with Thin defect-free Separating Layers"*, J. Appl. Polym. Sci., 46,(1992) 1927-1938.

[5] J. Nelson: "Composite membranes, their manufacture and use", US patent 4,822,382 (1989).

[6] K Kimmerle, T. Hofmann, and H. Strathmann: "Analysis of gas permeation through composite membranes", J. Membr. Sci., 61,(1991) 1.

[7] J. Koros and G. Fleming: "*Membrane-Based Gas Separation*", J. Membr. Sci., 83, (1993) 1.

[8] A.Michaels: "*Analysis and Prediction of Sieving Curves for Ultrafiltration Membranes: A Universal Correlation*", Sep. Sci. Tech., 15, (1980) 1305-1322.

[9] S. Singh, K. Khulbe, T. Matsuura, and P. Ramamurthy: "*Membrane Characterization by Solute Transport and Atomic Force Microscopy*", J. Membr. Sci., 142, (1998) 111-127.

[10] Y. Chen, A. Fouda, and T. Matsuura: "*A Study on Dry Cellulose Acetate Membrane for the Separation of Carbon Dioxide/Methane Gas Mixtures*", in "*Advances in Reverse Osmosis and Ultrafiltration*"; T. Matsuura and S. Sourirajan, Eds.; National Research Center of Canada: Ottawa, (1989) 259-274.

[11] F.Hamad, K.C. Khulbe, and T. Matsuura: "*Study on the interaction of methane gas with poly(phenylene oxide) membrane using infrared spectroscopic method*', J. Membr. Sci., 186, (2001) 281-284.

[12] P. Flory: "*Principles of Polymer Chemistry*", George Banta Company, Mensha, Wisconsin (1953).

[13] R. Perry, D. Green, and J. Maloney: "*Perry's Chemical Engineers' Handbook*", 7th ed., McGraw-Hill, New York (1997).

[14] V.T. Long, B.S. Minhas, T. Matsuura, and S. Sourirajan: "*Gas Chromatographic Method for the Measurement of Gas Sorption on Polymeric Materials*", J. of Colloidal and Interfacial Science, 125 (2), (1988) 478-483.

[15] F. Hamad, K.C. Khulbe, and T. Matsuura: "*Characterization of Gas Separation Membranes Prepared from Brominated Poly (phenylene oxide) by Infrared Spectroscopy*", Desalination, 148, (2002) 369–375.

8.7 Nomenclature

A Total membrane surface area, m^2.

A_m Area of the non-porous part of the support membrane surface area, m^2.

$\bar{C}$ Mean speed of gas molecules, m/s.

D_m Membrane diameter, m.

$\bar{d}$ Geometric mean pore size, m.

d_g Gas molecule diameter, m.

h Root mean-square end-to-end distance of the polymer coil, cm.

J_g Total gas flux, mol/(m^2 s).

k_H Henry's constant, mol/(m^3 Pa).

M Molecular weight of polymer, g/mol.

M_A Molecular weight of gas A, g/mol.

N_t Total number of pores.

$\bar{P}$ Average pressure across the porous substrate, Pa.

P_d Permeate side pressure, Pa.

P_m Pressure at interface between the coating layer and the porous support, Pa.

P_u Feed side pressure, Pa.

p_{gc} Permeability of gas in the coating layer polymer, mol m/(m^2 s Pa).

p_{gm} Permeability of gas in the support layer polymer, mol m/(m^2 s Pa).

p_{gp} Permeability of gas in the plugged support pores, mol m/(m^2 s Pa).

p_g^* Permeance of gas in the TFC membrane, mol/(m^2 s Pa).

Q Total gas flow through pores of the support (un-coated), mol/s.

Q_c Total gas flow through the coated layer, mol/s.

Q_{ep} Total gas flow through unplugged or empty pores of the coated support, mol/s.

Q_{sm} Total gas flow through the non-porous part of the support dense layer, mol/s.

Q_{pp} Total gas flow through the plugged pores of the coated support, mol/s.

Q_s Total gas flow through the support (coated), mol/s.

q_k Knudsen flow through a pore, mol/s.

q_s Slip flow through a pore, mol/s.

q_{sf} Surface flow through a pore, mol/s.

q_v Viscous flow through a pore, mol/s.

$\overline{q}_k$ Combined Knudsen flow and surface flow through a pore, mol/s.

$\overline{q}_s$ Combined slip flow and surface flow through a pore, mol/s.

$\overline{q}_v$ Combined viscous flow and surface flow through a pore, mol/s.

R Universal gas constant, 8.314 m^3 Pa/(mol K).

R_b Pore radius, m.

R_c Coating layer resistance to gas permeation, m^2 s Pa/mol.

R_{ep} Resistance of empty pores to gas permeation, m^2 s Pa/mol.

R_g Polymer coil radius of gyration, cm.

R_{sm} Resistance of the non-porous part of the porous support to gas permeation, (m^2 s Pa)/mol.

R_{pp} Plugged pores resistance to gas permeation, (m^2 s Pa)/mol.

R_T Total resistance to gas permeation through TFC, (m^2 s Pa)/mol.

ΔP Pressure difference, Pa.

V Hydrodynamic volume of polymer coil in solution, cm^3.

$\alpha_{1,2}$ Ideal gas selectivity.

δ Thickness of the dense layer of the support membrane, pore length, m.

δ_c Coating layer thickness, m.

ε Total surface porosity.

ε_{ep} Total surface porosity due to unplugged (empty) pores.

ε_{pp} Total surface porosity lost due to plugged pores.

Φ Frictional coefficient, 2.8×10^{21} dL/(mol cm^3).

η Gas viscosity, Pa s.

$[\eta]$ Intrinsic solution viscosity, dL/g.

λ Gas molecule mean free path for collision, m.

μ Surface viscosity of adsorbed gas layer, Pa s.

σ Geometric standard deviation of the log-normal distribution, nm.

Chapter 9

General Conclusions and Recommendation

9.1 Conclusions

High molecular weight Poly (phenylene oxide) having an intrinsic viscosity of 1.57 (dL/g) in chloroform was the focus of this research work. This research tackled different avenues in the membrane science.

- **PPO Membrane-Hydrocarbon Gas Interaction**

Gaseous hydrocarbons interact physically with PPO membranes to form unstable complexes that can be easily removed by purging the membranes with an inert gas such as helium. This interaction possesses kinetic characteristics; i.e. it depends on time and the gas partial pressure. Physical factors that contribute to the presence of irregularities in the polymer backbone in the membrane; such as the polymer molecular weight and the boiling point of the solvent used in preparing the casting solution, affect the extent of interaction of these gases with polymeric membranes.

- **Chemical Modification of PPO**

A synergistic effect was observed in the enhancement of PPO membrane performance in gas separation when PPO backbone was brominated and sulfonated simultaneously. The alteration in the performance of the membranes brought about by sulfonation and bromination was the result of the manipulation in the polymer backbone stiffness, membrane density, and membrane free volume fraction.

It was found that the change in the performance of cation exchanged sulfonated PPO was governed by the cross linking forces of cations, the steric hindrance effects due to the cationic sizes, membrane polarity due to the electronegativity of cations. These factors were correlated to the location in the periodic table of chemical elements. SPPO membranes in Mg-form possessed the highest separation efficiency, however it

possessed the lowest gas permeability with respect to all tested gases. On the other hand, SPPO in Al-form possessed the highest gas permeability among all tested cations, with less separation efficiency compared to the Mg-form.

- **Composite and Dense PPO Membranes**

Composite membranes prepared by coating a porous ultrafiltration PES membrane with a thin film of PPO solution in TCE was found to overwhelmingly surpass the separation efficiency of a dense PPO membrane for CO_2/CH_4 gas system, with a slight decrease ($\approx$13%) in the permeability of CO_2. The presence of the porous support membrane is believed to be responsible for this phenomenon; a part of the solvent percolated to the support membrane structure then slowly diffused back to the top surface. This caused the polymer to finely precipitate at the coated film/ support membrane interface. It is believed that compressive forces were developed at the bottom surface of the coated film as a result of the shrinkage of the swollen support. These forces were responsible for the compactness and fusion of the nodules, which consequently resulted in enhanced selectivity of the coated film. The compressive forces were strong enough to wrinkle the bottom surface of the coated layer.

- **Prediction of Composite Membranes Performance**

Simple models were proposed to simulate the transport of gases in ultrafiltration porous membranes and in thin film composite membranes. The model describing the transport of gases in porous membranes combined the solution-diffusion model to account for the gas transport in the polymer matrix of the dense layer, and the combination of the different pore flow mechanisms to describe transport in pores.

It is necessary to evaluate the variability in the resistance of the support toward gases.

The support substrate, as a result of the dominating pore flow mechanisms, will compromise the performance of TFC membranes when it shows high resistance relative to that in the coating layer. In addition, the presence of pores that are susceptible to the coating polymer intrusion will worsen the performance of TFC membranes as a result of losing part of the surface porosity and increasing the resistance of the support against the more permeable gas.

Optimizing the performance of the TFC is achieved by using a porous substrate membrane with a skin layer as thin as possible and by maintaining high surface porosity after coating.

An important need to optimize the performance of TFC membranes is to have a support substrate with as thin dense layer as possible, and able to maintain high surface porosity after coating.

The experimental performance of TFC membranes was predicted based on three scenarios: (i) the pores were totally plugged by the coated polymer, (ii) the pores were partially plugged by the coated polymer, and (iii) the pores were totally unplugged by the coated polymer. The partially- plugged pores model presented best the experimental performance data of the TFC membranes when low polymer concentrations in the coating solution were used; while the totally unplugged pores model presented best the experimental performance data of the TFC membranes when high polymer concentrations were used in the coating solution.

9.2 Recommendations

The following are recommendations formulated on the basis of the present work for future investigation:

- Investigate the possibility of using the change in IR spectra of PPO in the presence of methane as a technique for methane gas sensor.
- Reinvestigate the kinetics involved in the methane and PPO interaction including the desorption experiments. This will enable the acquisition of more precise values for reaction rate constants k_1 and k_2.
- Study the effect of exchanging the proton of the sulfonic groups of sulfonated brominated PPO membranes, particularly for those polymers which resulted in high gas permeability and high permeability ratio.
- Study the effect of controlling the solvent migration upon coating PPO-TCE solution on top of the PES support, and study the effect of controlling the swelling of the support membrane, on the performance of the composite PPO membrane and the morphology of the coated layer.
- Study the gas permeation, through porous membranes having consistent narrow pores size distributions, and through TFC membranes based on these porous membranes as supports. Using other techniques to characterize the size of the polymer coil in the coating solution, e.g. light scattering technique. This will permit a better insight about the size of the polymer coil, which is dependent on the concentration of the polymer in the solution, relative to the pore size.
- Study the performance of TFC membranes based on one of the sulfonated brominated PPO polymers that possessed both high gas permeability and permeability ratio, e.g. 60% brominated-32.9% sulfonated-PPO.